People's Democratic Republic of Algeria
Ministry of Higher Education and Scientific Research
KASDI MERBAH UINIVERSITY
Faculty of Applied Sciences
Department of Electrical Engineering

THESIS

Presented for the award of the degree of

DOCTORATE 3rd cycle

Domain: Science and Technology

Field: Electrotechnics

Specialty: Electrical Power Systems

Presented by:

HACHEMI Ahmed Tidjani

Management and Optimization of the Integration of Renewable Energy Sources in Distribution Power Systems

Publicly defended on 03/07/2024, before the jury composed of:

DJAFOUR Ahmed	Professor	Kasdi Merbah university	President
SADAOUI Fares	Associate Professor	Kasdi Merbah university	Supervisor
ARIF Salem	Professor	Amar Telidji University	Co-supervisor
LAROUCI Benyekhlef	Associate Professor	Kasdi Merbah university	Examiner
BOUREK Yacine	Associate Professor	Kasdi Merbah university	Examiner
OUBBATI Youcef	Associate Professor	Amar Telidji University	Examiner
SAIM Abdelhakim	Associate Professor	Nantes University	Invited

Academic Year 2023/2024

إدارة وتحسين تكامل مصادر الطاقة المتجددة في شبكات التوزيع الكهربائية

ملخص

في السنوات الأخيرة، شهدت عملية دمج مصادر الطاقة المتجددة في شبكات التوزيع زيادة كبيرة بسبب الاعتبارات التكنولوجية والمالية والبيئية. ومع ذلك، تنشأ تحديات من التقلبات الجوهرية في القدرات الناتجة عن مصادر الطاقة المتجددة ، وخاصة مولدات الطاقة الشمسية الفوتوفولتائية والرياح. هذه التحديات تستدعي التخطيط الدقيق، مع مراعاة الطلب على الطاقة، وسعر الطاقة، وتغيرات قدرة إنتاج مصادر الطاقة المتجددة .تقترح هذه الرسالة منهجيات فعّالة لتحديد الأحجام والمواقع المثلى لمصادر الطاقة المتجددة تحت ظروف احتمالية ومحددة باستخدام تقنيات التحسين المعقدة مثل خوارزمية تحسين الفظ المعدلة وخوارزمية تحسين الفظ القياسية . تشمل الوظائف الهدفية تحسين ملامح الجهد، وتقليل الفاقد الكلي للطاقة، وتقليل التكاليف، وتعزيز استقرار النظام. يتم تقدير احتمالية سرعة الرياح وإشعاع الشمس وطلب الطاقة ودرجة الحرارة وأسعار الشبكة باستخدام وظيفة توزيع احتمالات وايبول ووظيفة توزيع احتمالات العادية، بينما تقوم تقنيات المحاكاة بمونتي كارلو بالتقاط الغموض في النظام. تُظهر نتائج المحاكاة أن التخصيص المثلى لمصادر الطاقة المتجددة قد يؤدي إلى تقليل الفوارق الإجمالية، وتقليل الفاقد الكلي للطاقة، وتحسين ملامح الجهد، وتعزيز استقرار النظام. بالإضافة إلى ذلك، يتم تأكيد تفوق خوارزمية تحسين الفظ المعدلة على خوارزمية تحسين الفظ القياسية في حل مشاكل تخصيص مصادر الطاقة المتجددة في كلا السيناريوهين المحددين والاحتماليين.

كلمات مفتاحية

مصادر الطاقة المتجددة، شبكة التوزيع، خوارزمية تحسين الفظ المحسنة، التشغيل الأمثل، تقليل التكاليف، انحراف الجهد؛ استقرار الجهد، تقليل ضياعات الطاقة النشطة.

Management and Optimization of the Integration of Renewable Energy Sources in Distribution Power Systems

Abstract

In recent years, the integration of Renewable Energy Sources (RESs) into distribution networks has significantly increased due to technological, financial, and ecological considerations. However, challenges arise from the inherent fluctuations in the output powers of RESs, particularly photovoltaic and wind turbine generators. This uncertainty necessitates careful planning, considering load demand, energy pricing, and RESs output power variability. This thesis proposes effective methodologies for determining optimal RESs sizes and locations under both probabilistic and deterministic conditions, utilizing sophisticated optimization techniques such as the Modified Walrus Optimization Algorithm (MWaOA) and the Standard Walrus Optimization Algorithm (WaOA). Objective functions include improving voltage profiles, reducing total power loss, minimizing costs, and enhancing system stability. The likelihood of wind speed, solar irradiation, load demand, temperature, and network pricing is estimated using the Weibull Probability Distribution Function (WPDF) and the normal PDF, while Monte Carlo simulation techniques capture system uncertainty. Simulation results demonstrate that optimal RESs allocation can lead to reduced overall costs, minimized power losses, improved voltage profiles, and enhanced system stability. Additionally, the superiority of MWaOA over WaOA in resolving RESs allocation problems is confirmed in both deterministic and probabilistic scenarios.

Keywords

Renewable Energy Sources, Distribution Network, Improved Walrus Optimization Algorithm; Optimal Operation, Cost Reduction, Voltage Deviation, Voltage stability, Active Power Losses.

Gestion et optimisation de l'intégration des sources d'énergie renouvelable dans les réseaux de distribution électriques

Résumé

Ces dernières années, l'intégration des Sources en Énergie Renouvelable (RESs) dans les réseaux de distribution a considérablement augmenté en raison de considérations technologiques, financières et écologiques. Cependant, des défis se posent en raison des fluctuations inhérentes dans les puissances de sortie des RESs, en particulier des générateurs photovoltaïques et éoliens. Cette incertitude nécessite une planification minutieuse, en tenant compte de la demande de charge, de la tarification de l'énergie et de la variabilité de la puissance de sortie des RESs. Cette thèse propose des méthodologies efficaces pour déterminer les tailles et les emplacements optimaux des RESs dans des conditions probabilistes et déterministes, en utilisant des techniques d'optimisation sophistiquées telles que l'algorithme d'optimisation du morse modifié (MWaOA) et l'algorithme d'optimisation du morse standard (WaOA). Les fonctions objectifs comprennent l'amélioration des profils de tension, la réduction de la perte totale de puissance, la minimisation des coûts et l'amélioration de la stabilité du système. La probabilité de la vitesse du vent, de l'irradiation solaire, de la demande de charge, de la température et de la tarification du réseau est estimée en utilisant la fonction de distribution de probabilité de Weibull (PDF) et la PDF normale, tandis que les techniques de simulation de Monte Carlo capturent l'incertitude du système. Les résultats de la simulation montrent que l'allocation optimale des RESs peut entraîner une réduction des coûts globaux, des pertes de puissance minimales, des profils de tension améliorés et une stabilité accrue du système. De plus, la supériorité du MWaOA par rapport au WaOA dans la résolution des problèmes d'allocation des RESs est confirmée dans des scénarios déterministes et probabilistes.

Mots-clés

Sources d'énergie renouvelable, Réseau de distribution, Algorithme d'optimisation du morse amélioré, Fonctionnement optimal, Réduction des coûts, Déviation de tension, Stabilité de tension, Minimisation des pertes de puissance active.

Acknowledgments

First, I would like to thank God - ALLAH - for granting me the courage and patience throughout all these years of study.

I would like to express my gratitude to my thesis supervisor, Mr. Fares SADAOUI, Associate Professor at the University of Kasdi Merbah Ouargla, and my co-supervisor, Mr. Salem ARIF, Professor at Amar Telidji University of Laghouat, for providing me with the opportunity to pursue a doctoral thesis under their guidance. I also thank them for their valuable discussions, encouragement, wise advice, and suggestions. I am very grateful for the freedom and trust they have shown me throughout this work.

My thanks also go to all the members of the jury for the honor they have bestowed by agreeing to evaluate this work.

I would like to thank everyone who has assisted me, directly or indirectly, in developing and completing this thesis.

HACHEMI Ahmed Tidjani,

July, 2024

Dedication

To my parents, whose unwavering support and guidance have illuminated my path throughout my years of study.

To my brothers.

To my sister.

To my entire family.

To all my friends without exception.

I dedicate this modest work.

HACHEMI Ahmed Tidjani,

July, 2024

Contents

Chapter II: Techniques and Methods for Uncertainty Modeling in Power Systems

Chapter III: Enhancing Optimization: Walrus Optimization Algorithm

Abbreviations and Symbols list

Abbreviations list:

ARO	: Artificial Rabbits Optimization
BFS	: Backward/Forward Sweep
CDO	: Chernobyl Disaster Optimizer
DG	: Distributed Generation
DO	: Dandelion Optimizer
EDN	: Electric Distribution Network
FACTS	: Flexible Ac Transmission Systems
GWO	: Gray Wolf Optimization
IEA	: International Energy Agency
IGDT	: Information Gap Decision Theory
KCL	: Kirchhoff's Current Law
MCS	: Monte Carlo Simulation
MPP	: Maximum Power Point
MWaOA	: Modified Walrus Optimization Algorithm
OOP	: Optimal Operation Problem
PDF	: Probability Density Functions
PEV	: Plug-In Electric Vehicles
PV	: Photovoltaics
RESs	: Renewable Energy Sources
SBR	: Scenario Base Reduction
SCSO	: Sand Cat Swarm Optimization
SD	: Standard Deviation
TTAO	: Triangulation Topology Aggregation Optimizer
WaOA	: Walrus Optimization Algorithm
WT	: Wind Turbine
ZOA	: Zebra Optimization Algorithm
SCA	: Sine Cosine Algorithm

Symbols list:

A_{PV}	: Surface area utilized by the set of PV
D_{α}	: Load level factor
G_N	: Module's real irradiance nominal values

G_a : Module's real irradiance

G_s : Solar irradiance

G_{std} : Solar irradiation in a normal environment

I_L : Vector of injected currents at the terminal nodes

I_{Nsc} : PV module's nominal short-circuit current

I_{mpp} : Current at maximum power point

I_{sc}, : PV module's short-circuit current

K_i : Current temperature coefficient

K_v : Voltage temperature coefficient

N_p : Number of PV modules in parallel

N_s : Number of PV modules in series

P_{L0} : Nominal active powers

P_{Li} : Active power of the load at node i

P_r : Wind turbine's rated output power

P_{sr} : PV system's rated power

Q_{L0} : Nominal reactive powers

Q_{Li} : Reactive power of the load at node i

S_{Base} : Base power in MVA

S_{Li} : Complex power absorbed by the load at node i.

S_a : Average solar irradiation

T_N : Module's real temperature nominal values

T_a : Module's real temperature

T_c : Cell temperature

V_0 : Nominal voltage

V_{Base} : Base voltage in kv

V_{Noc} : PV module's nominal open-circuit voltage

V_i : Turbine's cut-in wind speed

V_i : Complex voltage at node i.

V_{mpp} : Voltage at maximum power point

V_o : Turbine's cut-out wind speed

V_{oc} : PV module's open-circuit voltage

V_r : Wind speed at which the turbine reaches its rated power output

X_c	: Particular irradiance point
Z_i	: Series impedance of branch i.
c_1, c_2, and c_3	: Constants
η_{PV}	: Conversion efficiency of the PV panels
η_r	: Efficiency of the PV panels
η_t	: Effectiveness of the maximum power point tracking equipment
$BIBC$	: Matrix of injected currents at nodes
FF	: Fill factor
G	: Solar irradiance
I	: Vector of branch currents
K	: Boltzmann constant
NB	: Number of buses in the distribution network
$NOCT$	: Nominal operating cell temperature
NS	: Number of PV/WT system
NT	: Number of branches in the distribution network.
T	: Module temperature
W	: Speed of the wind
Z	: Impedance Z in Ω
c , k	: Weibull PDF scale and shape parameters
n	: Density factor
pu	: Per-unit
q	: Electron's charge
ri	: End of branch i.
si	: Start of branch i.
Γ	: Gamma function
α , β	: Coefficients determine the nature of the load
γ	: Temperature coefficient of efficiency
μ	: Mean value
σ	: Standard deviation
φ , τ	: Beta distribution parameters

List of Figures

List of Tables

General Introduction

The demand for electricity worldwide has evolved permanently and rapidly due to population growth, economic activity development, household equipment rate evolution, modernization, and improved quality of life, among other factors. The electricity sector in most countries has undergone profound transformations [1]. The origins of these transformations lie in the deregulation and privatization of the energy market, leading to a complete restructuring of the electrical system. An electrical system can be divided into different phases, namely the generation phase, transmission phase, and distribution phase. The distribution phase is particularly significant as it represents the link between the transmission network and electricity consumers. The Electric Distribution Network (EDN) operates at voltages below 50 kV and features looped structures, albeit operated in an open-loop (radial configuration) [2, 3].

In recent years, researchers have paid particular attention to EDNs, which have become increasingly important due to the introduction of new sources of production onto these grids. These sources have endowed distribution networks with characteristics resembling those of transmission networks. Consequently, many studies previously conducted on transmission networks are now being applied to distribution networks. For example, optimal power flow studies, static and dynamic stability analysis, optimal placement of Flexible AC Transmission Systems (FACTS), optimization of reactive power flow using capacitor banks, load shedding analysis, state estimation problems, voltage control coordination, turbine commitment issues, and restoration problems are among the areas of research garnering significant interest [4].

The integration of decentralized production into EDNs aims to bring production closer to consumption points, thereby reducing the load on the transmission network, decreasing power transit through transmission lines, and consequently reducing energy costs. It also aims to relieve transformers at the source substations, improve the security of the EDN, and allow it to operate independently of the transmission network in case of contingencies. Integrating these sources also eliminates the monopolization of production. With the liberalization of the electricity market, this encourages competition among electricity producers, ensuring the provision of better quality service and price reduction [5, 6].

Decentralized renewable energy-based production has garnered significant attention from energy providers worldwide due to its benefits in preserving nature, reducing climate change caused by fossil fuels, and minimizing the consumption of finite resources [5]. Additionally,

the challenges associated with constructing overhead transmission lines or large power plants, which require substantial investments and lengthy implementation times, give an advantage to decentralized sources. These sources are easier to implement in a shorter timeframe and with limited investment.

The integration of decentralized renewable energy productions into distribution networks results in the electrical system behaving differently in terms of planning, design, operation, and management. Specifically, distribution networks are traditionally designed to evacuate energy by acting as passive systems (unidirectional electricity flow, from high voltage to low voltage). However, the integration of decentralized sources transforms them into active networks capable of participating in energy production (bidirectional electricity flow, from low voltage to high voltage and vice versa) [4]. This transformation brings about a change in the direction of energy flow along distribution lines, the possibility of exceeding voltage limits at injection points, exceeding the thermal limits of lines, malfunctioning of protections, and other challenges [6].

The integration of renewable energies into existing grids presents significant challenges, primarily due to the inherent uncertainty associated with these sources. Unlike conventional power generation, which can be reliably scheduled and dispatched, renewable energy generation depends on weather conditions such as sunlight, wind speed, and precipitation, which are inherently unpredictable. This uncertainty introduces variability and intermittency into the grid, making it difficult to ensure a stable and reliable power supply. Additionally, the location of renewable energy sources may not always align with demand centers, leading to transmission congestion and grid instability. Furthermore, the rapid growth of renewable energy installations can outpace grid infrastructure upgrades, exacerbating these challenges. Addressing these uncertainties requires advanced forecasting techniques, flexible grid management strategies, and investments in grid modernization to accommodate the unique characteristics of renewable energy generation.

The primary focus of this thesis is the advancement of EDN performance in the availability of Renewable Energy Sources (RESs) through the application of new algorithms and a novel objective function. Central to this endeavor is the utilization of a new algorithm grounded in the Levy flight mechanism, aimed at striking an optimal balance between exploration and exploitation to achieve targeted solutions effectively. A key aspect of this research involves developing a methodology for the optimal integration of Distributed Generation (DG), considering the hourly fluctuations in load demand and RESs sources.

Specifically, two types of RESs, namely photovoltaic and wind, are scrutinized, accounting for factors such as quantity, size, and power output characteristics. The integration process leverages both new and established metaheuristic algorithms in conjunction with a bespoke objective function, tailored to minimize power losses, enhance voltage profiles, and mitigate overall system costs while adhering to specified constraints across distribution systems of varied scales and complexities. Additionally, the study addresses the inherent uncertainty associated with load demand, pricing, environmental factors (temperature, wind speed, solar irradiance), and DG power output over a 24-hour period, offering insights into their collective impact on network dynamics throughout the designated timeframe. Through this comprehensive approach, the research aims to enhance the operational efficiency and resilience of distribution networks amidst the growing adoption of renewable energy sources.

Our research work in this thesis is divided into four chapters.

The first chapter emphasizes the growing adoption of DG technologies, particularly those based on renewable energy sources such as photovoltaics and wind turbines, reflecting a shift towards sustainability driven by environmental concerns and economic incentives. This chapter meticulously examines the impact of DG governance on distribution networks, focusing on its contribution to network resilience and reliability. Through the utilization of mathematical models, it delves into the intricate dynamics of DG systems, providing insights into their operation, optimization, and integration within contemporary energy networks. Additionally, the chapter reviews techniques for improving the status of DG, highlighting their profound implications for modern energy systems. Furthermore, the chapter discusses energy flow in distribution networks.

In chapter 2, we discussed models for managing parameter uncertainty in modern power systems, focusing on load demand, renewable generation, and electricity prices. We explored various methods, including probabilistic, possibilistic, and hybrid approaches, alongside robust optimization and interval analysis. Monte Carlo simulation emerged as a key technique, demonstrating practical significance in generating hourly scenarios for critical parameters. Additionally, we emphasized scenario-based reduction to enhance computational efficiency while maintaining accuracy. By introducing tools like probability distribution and optimal hourly scenarios, we underscored their value in assessing scenario likelihoods and identifying optimal conditions.

In chapter 3, we offer an overview of optimization techniques, discussing various state-of-the-art algorithms and their applications in solving optimization problems. Additionally, we introduce the Modified Walrus Optimization Algorithm (MWaOA), which integrates Levy flight to improve the solution search performance of the standard Walrus Optimization Algorithm (WAOA) method . The algorithm's performance is then evaluated across 23 benchmark functions and compared with several other state-of-the-art optimization algorithms.

Chapter 4 is dedicated to presenting findings and discussions regarding single- and multi-objective planning for the general manager. This chapter is divided into two parts. In the first part, we conduct a case study of a system operating in the absence of uncertainty, specifically examining a 24-hour period. Here, we explore the advantages of employing the Modified Walrus Optimization Algorithm (MWaOA) method over the traditional Walrus Optimization Algorithm (WaOA) in optimizing both single-objective and multi-objective functions. In the second part, we delve into a case study focusing on a specific system operating under conditions of uncertainty. Our analysis centers on a multi-objective function comprising key variables such as expected power losses, voltage deviation index, voltage stability index, and total annual expected cost. Specifically, we select the 12:00 PM hour as our focal point and conduct our investigation across 25 distinct scenarios. This deliberate choice allows us to probe the system's response to variable factors during a critical period of operation. The effectiveness of the methods presented in this chapter is evaluated through testing on various scenarios, including standard IEEE distribution networks like IEEE 33-Bus and IEEE 69-Bus.

Finally, we conclude our thesis with a summary and an exploration of future perspectives.

CHAPTER I

Distributed Generation and Power Flow Analysis

I.1. Introduction

The burgeoning adoption of distributed generation technologies within distribution networks serves as a tangible reflection of the remarkable advancements witnessed in renewable energy sources. This trend underscores a profound shift towards sustainability, driven by growing environmental consciousness and a concerted effort to mitigate the adverse effects of traditional energy generation on our planet. Moreover, the rapid proliferation of DG technologies is buoyed by compelling economic incentives, as stakeholders increasingly recognize the long-term cost savings and potential revenue streams afforded by decentralized energy production. As DG systems become increasingly integrated into distribution networks, they not only offer a pathway towards energy independence but also contribute significantly to enhancing grid resilience and reliability in the face of evolving energy landscapes and emerging challenges.

This chapter embarks on a thorough examination of DG, with a specific focus on renewable energy sources such as photovoltaics and wind turbines. Through the utilization of mathematical models, intricate electrical dynamics inherent within these systems are meticulously unraveled and analyzed. These models serve as indispensable tools, providing insights into the complex interplay of variables and parameters governing the performance, efficiency, and integration of DG units within contemporary energy networks. By delving into the intricacies of these mathematical frameworks, this exploration aims to elucidate the underlying principles and mechanisms driving the operation and optimization of renewable energy-based DG systems, thereby offering valuable insights for researchers, engineers, and practitioners in the field. As we delve into integration, we analyze impacts on power dynamics, voltage profiles, stability, costs, and emissions. The chapter culminates in a literature review of optimization techniques for DG placement. Analyzing power flow utilizing the Forward/Backward Sweep method in the presence of distributed generation offers a nuanced perspective for comprehending the profound implications of DG on modern networks, shedding light on its intricate role within contemporary power systems.

I.2. Distributed generation technologies

Distributed generation technologies can be categorized into conventional and renewable DG technologies. The conventional DG technologies such as fossil fuel-based generators, have

been widely deployed in distribution systems as backup generation or cogeneration without significant interaction with distribution networks. In recent years, the technological development in different fossil fuel-based DG technologies and distribution system automation has made DG one of the attractive options for distribution system reinforcement. On the other hand, the renewable DG technologies, such as wind generators, solar photovoltaics, clean-fuel based generators, are also seen to be increasingly employed in distribution networks due to environmental concerns and associated incentives. Different from fossil fuel-bassed DG technologies, which are capable of power output control, the power generation by renewable DG technologies is non-controllable.

A capacity factor, defined as a ratio of the average power output to the rated power output, is normally used to determine the equivalent generation capacity for renewable DG units. The capacity factor of renewable DG units is influenced by the availability of primary energy sources, such as wind and solar radiation, and is an important factor in selecting potential sites for these generators during the planning stage [7]. The power delivered by Distributed Generators can range from a few watts to several megawatts.Table I.1 provides a classification based on the power range [8].

Table I.1: Classification of distributed generators by power range

Categories	Power Range
Micro DG	~1 W to < 5 kW
Small DG	5 kW to < 5 MW
Medium DG	5 MW to < 50 MW
Large DG	50 MW to < 300 MW

I.2.1. Different types of renewable energy-based DG

Distributed Generators based on renewable energy harness power from replenishable sources such as the sun, wind, water, etc. Although these energy sources are unlimited, their intermittent nature is a primary limitation. In other words, the power output depends on the availability of the primary source.

The main advantage of renewable energy DGs is their low environmental impact and their positive contribution to diverse energy sources [9-12].

I.2.1.1. Photovoltaic solar energy

Solar energy is abundant, reliable, and inexhaustible. Photovoltaics (PV) are considered the most significant renewable energy source, leading to the highest number of installations. Photovoltaic panels directly capture and convert solar radiation into direct current through the properties of semiconductor materials. This energy source operates silently, has a long lifespan, zero emissions, and requires minimal maintenance and no fuel costs. However, it is weather-dependent, intermittent, and unavailable at night.

The advantages and disadvantages associated with solar PV based DG systems can be summarized in Table I.2.

Table I.2: Advantages and disadvantages of solar PV-based DG

Advantages	**Disadvantages**
No emissions	Non-firm power generation
No fuel cost since power is generated from sunlight	High capital investment on PV cells and ancillary equipment
No noise impact	Low efficiency
Capacity augmentation could be easy	Possible requiring large areas
Possible export of reactive power to the grid	Limitation of suitable locations depending on the availability of sunlight

I.2.1.2. Wind energy

Wind turbine (WT) generators harness the kinetic energy of the wind, transforming it into mechanical energy and then into electrical energy. Like solar energy, wind is abundant and inexhaustible. Wind turbines are emission-free and incur no fuel costs. However, they require a significant upfront investment and exhibit unpredictable and intermittent power generation. Besides the average wind speed, the key factors determining the feasibility of a wind turbine are the characteristics of the blades and the generator efficiency. The advantages and disadvantages associated with WT-based DG units are summarized in Table I.3 [13].

Table I.3: Advantages and disadvantages of WTG-based DG.

Advantages	Disadvantages
No emissions	Intermittent power generation
Low operation and maintenance cost	Low capacity factor
No fuel cost since the generator is powered by wind	Possible high noise level
Possible export of reactive power to the grid for network support	Difficult to predict power generation
	Not suitable for all locations due to the availability of wind

I.2.1.3. Hydropower

Hydropower operates on a principle similar to wind energy, using the potential and kinetic energy of water from rivers, lakes, or streams to drive a turbine that, in turn, rotates a generator, converting mechanical energy into electrical energy. Hydroelectricity is one of the most cost-effective methods of electricity production, consuming no water or fuel. The water passing through the turbine remains unaffected and available for other uses, with no emissions produced. The lifespan of a hydroelectric plant is long, with some operating for over 100 years [14].

I.2.1.4. Geothermal energy

Geothermal power plants utilize the heat from underground water reservoirs to generate electricity or for direct heating purposes. Hot water is pumped to the surface to pass through heat exchangers. The resulting steam drives a turbine, which powers a generator to produce electrical energy. Dry rock extraction technology is also employed, where cold water is pumped and heated in deep rock layers, and the resulting hot water is brought back to the surface. Geothermal plants offer the advantage of independence from weather conditions such as rain, sun, or wind [15].

I.2.1.5. Biomass

The primary concept of biomass is to use renewable organic fuels (wood, biogas, straw, and industrial and domestic organic waste) to produce electricity from generated heat. This type of power generation produces low emissions of greenhouse gases [16].

I.3. Modeling of photovoltaic and wind generators

In our study, we have considered PV and WT sources as Distributed Generators to be integrated into the distribution network. The photovoltaic system is capable of supplying active power, while the wind turbine can provide both active power and reactive power with a variable power factor.

I.3.1. Photovoltaic modeling

The modeling of a photovoltaic system involves representing its electrical behavior based on the characteristics of the solar cells and the overall configuration of the system. The fundamental elements considered in the photovoltaic model include the solar irradiance, temperature, and the characteristics of the photovoltaic modules. Here are some models commonly used to express the output power of a PV power unit:

- **MODEL 1**

This model illustrates how to calculate the power output from solar panels based on solar irradiance (G_s) and standard test conditions (G_{std}). It is used to determine how the power output changes with varying levels of solar irradiance.

$$P_{PV,\,\text{out}} = \begin{cases} P_{sr}\left(\dfrac{G_s^2}{G_{std} \times X_c}\right) & \text{for } 0 < G_s \leq X_c \\ P_{sr}\left(\dfrac{G_s}{G_{std}}\right) & \text{for } G_s \geq X_c \end{cases} \qquad \text{(I.1)}$$

where P_{sr} stands for the PV system's rated power. The solar irradiance at the place in question is denoted by G_s. The term G_{std} refers to the sun irradiation in a normal environment, which is around 1000 W/m^2. A particular irradiance point is represented by X_c , which is equal to 150 W/m^2 [17, 18].

- **MODEL 2**

This model is similar to the first one but uses a different approach to calculate the power output based on levels of solar irradiance and standard test conditions [19].

$$P_{PV,\,\text{out}} = \begin{cases} P_{sr}\left(\frac{G_s}{G_{std}}\right) & \text{for } 0 < G_s \leq G_{std} \\ P_{sr} & \text{for } G_s \geq G_{std} \end{cases} \quad \text{(I.2)}$$

- **MODEL 3**

This model depends on the number of solar panels , fill factor , open-circuit voltage , and short-circuit current to calculate the power output.

$$P_{PV,\,\text{out}} = N_s \times N_p \times FF \times V_{oc} \times I_{sc} \quad \text{(I.3)}$$

$$V_{oc} = \frac{V_{Noc}}{1 + c_2 \ln\left(\frac{G_N}{G_a}\right)} \left(\frac{T_N}{T}\right)^{c1} \quad \text{(I.4)}$$

$$I_{sc} = I_{Nsc}\left(\frac{G_a}{G_N}\right)^{c3} \quad \text{(I.5)}$$

$$FF = \left(1 - \frac{R_s}{\left(\frac{V_{oc}}{I_{sc}}\right)}\right)\left(\frac{\frac{V_{oc}}{nKT/q} - \ln\left(\frac{V_{oc}}{nKT/q} + 0.72\right)}{1 + \frac{V_{oc}}{nKT/q}}\right) \quad \text{(I.6)}$$

where N_s and N_p stand for the number of PV modules in series and parallel, respectively. The PV module's short-circuit current, open-circuit voltage, nominal open-circuit voltage, nominal short-circuit current, and fill factor are represented by the numbers I_{sc}, V_{oc}, V_{Noc}, I_{Nsc}, and FF, respectively. G_a represent the module's real irradiance, whereas G_N and T_N are its nominal values. Three constants are c_1, c_2, and c_3. The module temperature is indicated by T. The ideality factor is indicated by n. The electron's charge is denoted by q, and the Boltzmann constant is K [20].

- **MODEL 4**

This model explains how to calculate the power output from solar panels using the number of solar panels , fill factor , voltage , and current .

$$P_{PV,\,\text{out}} = N_s \times N_p \times FF \times V \times I \quad \text{(I.7)}$$

$$I = \frac{S_a}{S_{std}}[I_{sc} + K_i(T_c - 25)] \quad \text{(I.8)}$$

$$V = V_{oc} - K_v \times T_c \quad \text{(I.9)}$$

$$FF = \frac{V_{mpp} \times I_{mpp}}{V_{oc} \times I_{sc}} \quad \text{(I.10)}$$

where I_{mpp} is the current at maximum power point (MPP), V_{mpp} is the voltage at MPP, K_i is the current temperature coefficient, T_c is the cell temperature, and K_v is the voltage temperature coefficient, S_a and S_{std} represent the module's real and nominal irradiance. [21, 22].

- **MODEL 5**

This model depends on the area of the solar panels , efficiency, and solar irradiance to calculate the power output.

$$P_{PV} = A_{PV} \cdot \eta_{PV} \cdot I \quad \text{(I.11)}$$

$$\eta_{PV} = \eta_r \cdot \eta_t[1 - \gamma \cdot (T_c - T_r)] \quad \text{(I.12)}$$

$$T_c = T_a + \frac{I}{800} \cdot (NOCT - 20) \quad \text{(I.13)}$$

P_{PV} represents the power output from the solar panels, which depends on A_{PV} representing the area of the solar panels, η_{PV} representing the efficiency of the solar panels, and I representing the solar irradiance. The efficiency η_{PV} is calculated using η_r representing the efficiency of the cells under standard conditions, η_t representing the transmission efficiency, γ representing the temperature coefficient of efficiency, and the temperature difference between the cells in actual operation *Tc* and under standard conditions, which is *Tr* equal to 25°C. The cell temperature *Tc* is determined using *Ta* representing the ambient air temperature, and NOCT representing the Nominal Operating Cell Temperature.

We used model 5 in chapter 4 to represent the PV system due to its inclusion of temperature effects and its advantages over other models. This model accurately calculates the cell temperature, which significantly impacts the efficiency of the photovoltaic system. Additionally, it accounts for the temperature's effect on the efficiency of the solar panels, making it more precise and realistic in representing system performance under actual operating conditions.

I.3.2. Wind turbine modeling

Modeling a wind turbine involves creating a representation that captures its electrical behavior based on various factors, including wind speed, turbine characteristics, and power output.

The following models are frequently used to indicate a wind power unit's output power:

- **MODEL 1**

This model describes power P_w as a function of voltage V. Power is zero for $V < V_i$ and $V > V_o$, and increases linearly with voltage between V_i and V_r .

$$P_w(V) = \begin{cases} 0 & \text{for} \quad V < V_i \text{ and } V > V_o \\ P_r\left(\dfrac{V - V_i}{V_r - V_i}\right) & \text{for} \quad (V_i \le V \le V_r) \\ P_r & \text{for} \quad (V_r < V \le V_o) \end{cases} \tag{I.14}$$

where P_r is the wind turbine's rated output power. The turbine's cut-out and cut-in wind speeds are represented by the letters V_o, and V_i, respectively. V_r, represents the wind speed at which the turbine reaches its rated power output[23, 24].

- **MODEL 2**

In this model, power P_w as a function of voltage V is zero for $V < V_i$ and $V > V_o$. Between V_i and V_r , power increases cubically with voltage [25].

$$P_w(V) = \begin{cases} 0 & \text{for} \quad V < V_i \text{ and } V > V_o \\ P_r\left(\dfrac{V^3 - V_i^3}{V_r^3 - V_i^3}\right) & \text{for} \quad (V_i \le V \le V_r) \\ P_r & \text{for} \quad (V_r < V \le V_o) \end{cases} \tag{I.15}$$

- **MODEL 3**

This model defines power P_w as a function of voltage V. Power is zero for $V < V_i$ and $V > V_o$, and increases quadratically with voltage between V_i and V_r [26].

$$P_w(V) = \begin{cases} 0 & \text{for} \quad V < V_i \text{ and } V > V_o \\ P_r\left(\dfrac{V^2 - V_i^2}{V_r^2 - V_i^2}\right) & \text{for} \quad (V_i \le V \le V_r) \\ P_r & \text{for} \quad (V_r < V \le V_o) \end{cases} \tag{I.16}$$

We used model 1 in chapter 4 for wind turbine modeling. We chose this model because it is the easiest to model, thanks to its linear relationship between output power and voltage within the operational range , which aligns perfectly with the characteristics observed in our wind turbine system.

I.4. Integration of DG into the distribution network

The incorporation of DG into a modern electrical system helps consumers meet their load requirements with reasonable quality and continuity. Integrating renewable energies at strategic locations within the EDN can offer numerous advantages, such as minimizing losses, improving voltage, and enhancing overall system reliability and efficiency. Generally, these benefits can be categorized into three main areas: technical, economic, and environmental [8, 27-29].

I.4.1. Technical advantages

I.4.1.1. Minimization of power/energy losses

Unlike transmission networks, distribution networks have a high R/X ratio, leading to significant power losses that can result in voltage instability. Studies have indicated that 13% of the total power generated is wasted in line losses at the distribution level [30]. According to

the literature, the optimal location and size of DG are crucial factors in reducing electrical losses. Well-integrated DG can significantly decrease electrical losses. However, improper planning of DG can lead to excessive power losses. Various researchers have developed different methods to address the optimal integration of DG into the EDN with minimal power losses, considering it as the objective function. Formulations have been made assuming that the summation of the total power injected at all nodes could represent network losses [31]. Most research has focused solely on total active losses in distribution networks [32, 33], while daily, monthly, and annual energy losses have been chosen as functions to minimize [34-36].

I.4.1.2. Voltage profile improvement and voltage stability

One of the objectives of integrating DG into the EDN is to enhance voltage profile and stability. Some researchers focused solely on improving the voltage profile [37, 38] or voltage stability [37] as the objective function, while most considered reducing losses simultaneously with improving the profile or stability of the voltage [19, 38, 39].

I.4.2. Economic advantages

The incorporation of DG into the distribution network is economically beneficial for both electricity suppliers and consumers. Optimally placed DGs are well-suited to significantly reduce losses, thereby reducing costs. They also allow for a reduction in the costs of transport and distribution expansion, as they are placed near customers. Additionally, they reduce the overall cost by delaying the need to invest in new transport and distribution infrastructure. According to the International Energy Agency (IEA), cost savings in transport and distribution can reach 30% of electricity costs with DG. Industries may install their own DG to partially meet their energy demand, reducing purchases from the grid [28, 40, 41].

I.4.3. Environmental advantages

The primary technologies of decentralized production are associated with renewable sources, making it possible to produce clean energy [28]. According to published literature, 80% of all pollution worldwide is caused by the combustion of fossil fuels [40]. Numerous researchers have confirmed that DG, primarily based on renewable energies, can reduce carbon emissions by around 40% [28]. The main environmental advantages of DG are that they are low-noise, with minimal emissions and cleaner energy [8].

I.5. Literature survey on the integration of DG into the network and the contribution of this work

Optimization Techniques and Algorithms play a pivotal role in the efficient design and operation of energy systems, particularly in the context of EDN systems and DG integration. This review delves into various optimization methodologies proposed in recent literature, highlighting their contributions towards achieving optimal system configurations and addressing uncertainties. The authors of [42] employed a method to verify the suggested optimal configuration and component sizes of the hybrid micro-grid energy system , taking into account the economic and environmental aspects of the system. In [43], a solution called the Success History-based Adaptive Differential Evolution algorithm was presented for optimal allocation of the DGs considering the uncertain conditions. In [44], a scenario-based approach has been used to deal with cost, load and renewable based uncertainties. The authors of [45] proposed a two-stage adaptable optimization process to achieve low-carbon operation while taking into account the uncertainties. The best cost for the worst-case scenario can be obtained using balanced economics. The Coronavirus herd immunity optimizer was utilized in [46] to improve power plant economic, environmental and technical performance. The Artificial Hummingbird Algorithm was introduced by M. S. Abid and H. J. Apon in [47], which is an effective algorithm for addressing the problem of RESs planning optimization with multiple objectives. The authors of [48] proposed a genetic algorithm for determining the optimal size for solar and wind turbines in a grid-connected residential building's distribution system. To reduce total emissions, costs and power loss, the particle swarm algorithm and improved grey wolf algorithm were used in [49].

Now, we will explore research studies that have addressed the challenge of ensuring grid stability amidst the integration of renewable energy sources, particularly photovoltaics. The authors of [50] examine several technological challenges related to the stability issues associated with extensive PV penetration into the power grid. Frequency regulation, active power reduction, reactive power injection, and storing energy are only a few examples. In [51], ramp-rate control algorithms have been used with Energy Storage Systems to minimize power fluctuations to the grid. In [52], the technical challenges, such as frequency disturbances and voltage limit violations, arise as a result of large-scale and intensive PV system penetration into the power network, as well as the resulting stability issues. The impact of large-scale PV system integration on the grid is also considered, along with possible solutions. In [53], a solution called

search-based dragonfly algorithm was presented for optimal allocation of the PV considering the load and PV uncertainties.

Numerous research endeavors have addressed the optimization of sizing and placement for DG within EDNs, utilizing a diverse array of algorithms and methodologies. These efforts are geared towards minimizing power losses, costs, emissions, and improving voltage profiles, stability, and reliability, while contending with inherent uncertainties within the system. Notable among these approaches is the bilayer optimization technique suggested by the authors of [32] specifically tailored for optimizing the placement of battery energy storage systems and solar photovoltaics within EDNs. In [54], a solution called strength Pareto evolutionary algorithm 2 was presented for tackling the DG and capacitor placement problem with load uncertainty. In [55], the authors employed the Success history-based adaptive differential evolution with epsilon constraint handling technique and Monte Carlo Simulation to allocate the DG sizes and sites. The authors of [56] used the crow search algorithm to determine the optimal location and size of DG. The authors of [57] suggested a bilayer optimization technique to achieve optimal battery energy storage systems and to determine the solar photovoltaic locations in a distribution system. PSO, modified SCA [58], and other approaches have been utilized to define the optimal size and site of DGs in radial distribution systems, while taking system uncertainties into account. In [59], a unique ant lion optimizer is used that reduces energy costs, reduces losses and voltage deviation, and enhances dependability. The Dragonfly Algorithm was suggested by the authors in [60] to improve voltage profile and reduce the power loss in electrical EDNs. In [61], the authors propose an algorithm for DG allocation planning based on using the probabilistic uncertainty modeling method. In [62], a modified differential evolution algorithm was proposed for optimal DG allocation.

In distribution systems, numerous metaheuristic strategies are employed to solve the distributed generators allocation problem. The authors in [63] suggested an improved adaptive genetic algorithm for resolving the optimal DG allocation problem. In [64], an efficient method has been presented for the optimal planning of accommodating the integration of plug-in electric vehicles (PEV) along with renewable DGs under uncertainties of the system. The author in [65] proposed a stochastic model for optimizing the investment of the DGs under uncertain conditions in EDNs. The authors in [66] offered a genetic algorithm along with the Monte Carlo method for solving the optimal DG integration problem under the uncertainties of RER generation. The cost of energy losses and DGs have been considered in the model. The

Particle Swarm Optimization algorithm was applied to optimize two objective functions, represented by the sum of active power losses, voltage deviation, and Max-I relay tripping time for IEEE 33 and 69 EDNs [67]. The Invasive Weed Optimization algorithm was implemented and tested on IEEE 33-bus and IEEE 69-bus distribtion networks for different load models with objective functions based on minimizing active power losses, system operational cost, and improving the voltage stability index of the network buses [68]. The Dragonfly Algorithm was utilized and applied to IEEE 15-bus, 33-bus, and 69-bus networks to improve voltage profiles of buses by minimizing voltage deviation (VD), regulation, voltage stability, active power losses, and operational cost of the studied systems [69].

Monte Carlo simulation was employed in [70] for optimum DG allocation. Esmaeili et al. presented a multi-objective framework for optimizing the DG allocation and reconfiguration of the EDN using the Big Bang–Big Crunch algorithm [71]. In [72], a probabilistic planning method was suggested based on mixed integer nonlinear programming and has been implemented to assign energy loss reduction with optimal integration of RESs in a rural distribution system. The authors in. [73] propose a planning strategy for a hybrid solar-wind generation system with hydrogen energy storage using a novel multi-objective optimization algorithm to minimize the following three objective functions: loss of load expected, annualized cost of the system, and loss of energy expected. The authors of [74] used the GA optimization algorithm to solve the problem of optimal DG allocation in EDNs while considering economic and technological goals. The authors in [75] applied the Crisscross Optimization Algorithm and Monte Carlo Simulation to assign the rating and location of DG in the distribution system, aiming to reduce the power losses and costs.

The topic of optimal DG sizing was addressed and solved in [76] by reaching the objectives of minimizing DG costs and maximizing network load ability. In [77], using a scenario synthesis approach, optimal power siting and sizing for an active distribution system, considering demand response and the optimal integration of wind turbines, as well as system uncertainties, were determined using a cuckoo search algorithm. The Adaptive Genetic Algorithm was applied to the IEEE 69-bus standard network and the practical Indian 52-bus network, considering tap changer control, with the aim of minimizing the objective function based on active power losses and maximum bus voltage [78].The Symbiotic Organism Search algorithm, incorporating a loss sensitivity factor, was applied to minimize active power losses in the studied EDNs, namely IEEE 33-bus, 69-bus, and 118-bus [79]. The Bat Algorithm was

implemented on the IEEE 33-bus standard network to minimize the objective function based on active power losses [80]. In [81], the Binary Particle Swarm Optimization algorithm was applied to minimize active power losses, which were considered as the objective function of the study, for the practical EDN of Cairo's 59-bus system. The Novel Cuckoo Search algorithm with genetically replaced nests was employed to optimize the multi-objective function represented by technical parameters: active power losses, voltage stability index, and voltage deviation for IEEE 33-bus and IEEE 119-bus standard EDNs [82]. The Population-Based Incremental Learning algorithm was applied to the IEEE 33-bus and IEEE 69-bus standard networks to reduce active power losses and square error in bus voltage profiles of the studied systems [83].The Ant Lion Optimization algorithm was applied to IEEE 15-bus, 33-bus, 69-bus, and 85-bus standard networks to reduce active power losses, which were considered as the objective function for the study [84]. The Salp Swarm Algorithm was applied to IEEE 33-bus and 69-bus standard systems with the aim of minimizing the multi-objective function, which simultaneously minimizes active power losses, voltage deviation, and improves bus voltage stability [85]. In [86], the Spider Monkey Optimization algorithm was used to minimize the voltage deviation problem as an objective function for the IEEE 33-bus, 69-bus, and the practical Indian 85-bus EDNs. The Wind Driven Optimization algorithm was applied to maximize the voltage stability index for the IEEE 30-bus and 118-bus standard networks [87]. The Modified Crow Search Algorithm was applied to the IEEE 33-bus standard network to reduce the multi-objective function based on active power losses and total voltage deviations [88]. The Moth Flame Optimization algorithm was used to optimize the placement of Distributed Photovoltaic Generation to minimize active power losses, which werre considered as the objective function for IEEE 33-bus, 69-bus, and 118-bus EDNs [89]. The Genetic Algorithm was applied to regulate voltage and reduce active power losses in IEEE 33-bus and 69-bus EDNs [90]. The Adaptive Dissipative PSO algorithm was applied to the IEEE 33-bus and 69-bus EDNs with the aim of minimizing active power losses [91]. The Genetic Moth Swarm Algorithm was applied to the IEEE 33-bus and 69-bus standard networks to minimize active power losses as an objective function [92]. The authors in [93] was applied the Adaptive Modified Whale Optimization Algorithm to the IEEE 33-bus and 69-bus networks to optimize the objective function based on active power losses and voltage stability index. In [94], The Elephant Herding Optimization algorithm was applied to the IEEE 15-bus, 33-bus, and 69-bus networks to optimize the considered objective functions: improving voltage profiles and stability, minimizing active power losses, and reducing the operating cost of the studied

systems. In [95], the Fine-tuned PSO algorithm was used to reduce active power losses with the reconfiguration of IEEE 33-bus and IEEE 69-bus networks. The Enhanced Coyote Optimization Algorithm was also applied and tested on IEEE 33-bus, 69-bus, and 85-bus EDNs to optimize objective functions based on minimizing active power losses, operational cost, and improving voltage stability of bus systems [96]. The Adaptive Quantum Evolutionary Algorithm was applied to minimize active power losses and voltage deviation as objective functions, depending on the load model for IEEE 85-bus and 118-bus networks [97]. The Sine Cosine Algorithm was applied to the IEEE 33-bus and 69-bus standard networks to optimize a multi-objective function, simultaneously minimizing total active power losses, annual energy loss costs, gas pollutant emissions, and maximizing the voltage stability index of bus systems [33]. The authors in [98] was applied and tested the Harris Hawk Optimization algorithm on the IEEE 33-bus and IEEE 69-bus networks to optimize power losses, voltage profiles by minimizing voltage deviation, annual energy savings, and reducing greenhouse gas emissions.

The primary goals of this work are to fill up the aforementioned research gaps, which may be summed up as follows:

1. This study proposes a modified walrus optimization algorithm (MWaOA) specifically designed to solve the optimal planning problem involving renewable energy resources within distribution networks .
2. Investigating the synergies between RESs (WTs and PVs), thereby enhancing grid stability and reducing reliance on expensive grid energy purchases.
3. The effectiveness and reliability of the MWaOA algorithm are rigorously demonstrated through extensive statistical comparisons with established optimization techniques.
4. Rigorous uncertainty analysis to account for the stochastic nature of key parameters including load demand, solar irradiation, wind speed, temperature, and energy pricing. This facilitates the robust optimization of the distribution grid operation.

I.6. Power flow in distribution networks

The electrical distribution network is characterized by changes in load demand, which influence power losses in branches and the voltage profile at network nodes. Various power flow calculation methods are employed by researchers in the literature. These methods can be divided into two categories: Newtonian methods [99-102] and forward/backward sweeping methods [103, 104]. The first type of methods is generally used to solve power flow problems

in transmission networks. Among these methods, the Newton-Raphson method and the fast decoupled method have proven their efficiency in addressing this issue. The application of these methods in EDNs has, in the majority of cases, proven to be unsuccessful, mainly due to distinctive characteristics compared to transmission networks [105]. On the other hand, the second type of methods is based on backward sweeping for branch current calculation and forward sweeping for node voltage calculation [106, 107]. This type of methods is specifically designed for solving power flow problems in EDNs.

I.6.1. The per-unit

The per-unit (pu) system is a system of reduced quantities that allows for a consistent consideration of relative magnitudes of certain parameters independently of voltage and power levels [108]. For a base power (S_{Base}) in MVA, a base voltage (V_{Base}) in kV, and an impedance Z in Ω, the normalized impedance (Z_{pu}) is obtained by:

$$Z_{pu} = Z \frac{S_{\text{Base}}}{V_{\text{Base}}^2} \tag{I.17}$$

The normalized active and reactive load powers are obtained, respectively, using formulas (I.18) and (I.19):

$$P_{pu} = \frac{P}{S_{\text{Base}} \times 10^3} \tag{I.18}$$

$$Q_{pu} = \frac{Q}{S_{\text{Base}} \times 10^3} \tag{I.19}$$

I.6.2. Modeling of network branches and loads

I.6.2.1. Branch modeling

The radial distribution network is composed of a set of branches. Each branch in this network is modeled as a series combination of resistance and pure inductance. The impedance of any branch i in this network (see Figure I. 1) is written as follows:

$$Z_i = R_i + jX_i \tag{I.20}$$

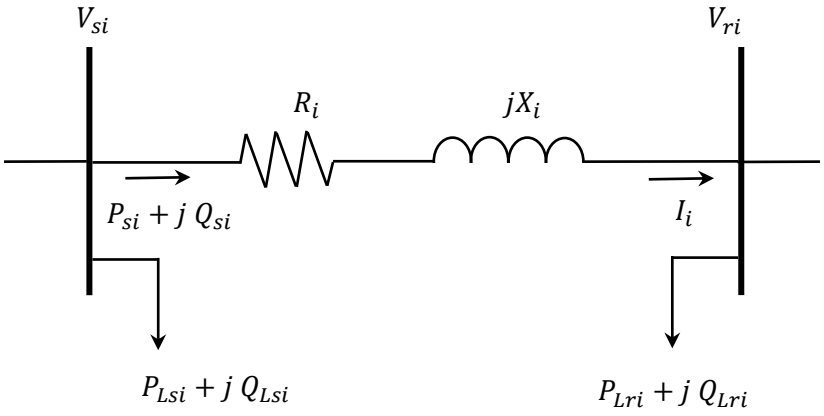

Figure I.1: Representation of two nodes in the radial EDN.

I.6.2.2. Load modeling

Load is the most uncertain parameter in the distribution electrical network; it is constantly variable. Over a year, the load can vary significantly from season to season, day to day, and hour to hour. It is the most sensitive parameter that can influence the solution to the EDN planning problem. Most researchers in the literature assume a constant load model in their EDN planning studies. Decisions and results based on this assumption are not technically feasible for real distribution systems where the load is not constant. In this study, to achieve an effective analysis, two types of loads will be considered:

I.6.3. Periodic constant load model

This load model is characterized by relatively constant electrical energy consumption during certain time intervals, with a variation that depends very little on weather conditions. The energy demand is fairly stable from day to day and season to season. The level of consumption can change significantly from one to three times at most during the day. Large consumers and many industrial customers belong to this load model. Mathematically, the active and reactive powers during each level of demand α are calculated respectively by equations (I.21) and (I.22):

$$P_{L\alpha} = P_{L0} \times D_{\alpha} \quad \text{(I.21)}$$

$$Q_{L\alpha} = Q_{L0} \times D_{\alpha} \quad \text{(I.22)}$$

Where, P_{L0} and Q_{L0} are the nominal active and reactive powers, D_{α} is the load level factor.

I.6.4. Static load model

The static model represents the characteristics of loads in steady-state conditions. It generally describes the relationship between active and reactive power with the voltage level over a specified period of time. In this load model, active and reactive powers are represented in exponential form. This model is also used to approximate the dynamic characteristics of loads. The load model is expressed by the following equations [109]:

$$P_{Li} = P_{L0}\left(\frac{V_i}{V_0}\right)^{\alpha} \quad \text{(I.23)}$$

$$Q_{Li} = Q_{L0}\left(\frac{V_i}{V_0}\right)^{\beta} \quad \text{(I.24)}$$

Where, V_0 is the nominal voltage,P_{Li} and Q_{Li} are the active and reactive power of the load at node i for a voltage equal to V_i.The coefficients α and β determine the nature of the load.

The values of the coefficients α and β depend on the aggregated characteristics of the load components. When both coefficients α and β are equal to 0, the load behaves like a constant power load, which means the power does not vary when the voltage changes. On the other hand, if the coefficients are equal to 1, the load behaves like a constant current load, where the power varies proportionally with the voltage. If the coefficients are equal to 2, the load behaves like a constant impedance load, where the power varies proportionally with the square of the voltage.

I.7. Power flow calculation in distribution network

Power flow calculations, or load distribution calculations, in an electric network planning problem, are crucial for determining energy losses for any network states that may arise and ensuring that these states satisfy the network's operational constraints.

In the context of electric network planning, power flow calculations are a repetitive and essential task, especially when using optimization methods, as will be employed later in this work. The use of a fast and accurate power flow calculation method is vital to accomplish this task.

However, electric distribution networks have certain typical characteristics that differ from transmission networks. They are characterized by [110]:

- Generally radial or weakly meshed structure,
- High resistance-to-reactance ratio ,
- Large number of branches and nodes,
- Unbalanced loads.

Various algorithms have been developed in the literature [111, 112], specifically designed to solve the power flow problem in electric distribution networks. The most common algorithm is the Backward/Forward Sweep Algorithm [113], which will be explained in the following section.

I.7.1. Backward/forward sweep algorithm

Over the past decades, various methods based on the Backward/Forward Sweep (BFS) Algorithm have been developed in several studies reported in the literature [114-116]. This was done to accelerate the power flow calculation in EDNs and achieve good convergence by avoiding the simultaneous solution of systems of equations and the use of large matrices. Unlike common methods such as Gauss-Seidel and Newton-Raphson, the sweep algorithm has the advantage of requiring less computational effort and time.

In this section, we will explain the iterative algorithm principle of the Backward/Forward Sweep method. This algorithm calculates the current on each branch and the voltage for each node. At each iteration, two sweeps are executed:

- Backward Sweep: Determines the currents in the branches of the network using the first Kirchhoff's law.
- Forward Sweep: Calculates the node voltages by computing voltage drops along the branches.

The BFS algorithm is characterized by its simplicity, speed, and accuracy. It operates in three steps.

Step 1: Calculation of Injection Currents

After reading the data from the EDN and initializing all node voltages, the injected current at each node is calculated based on the power absorbed by the connected load and the voltage at that node. For a node i, the injected current can be expressed as follows:

$$I_{Li} = \frac{S_{Li}^*}{V_i^*} \tag{I.25}$$

Where, S_{Li}^* is the complex power absorbed by the load at node i.V_i^* is the complex voltage at node i.

Step 2: Backward Sweep

During the second step, a backward sweep is performed in a descending manner from the terminal nodes of the network towards the source node (source substation) to calculate the branch currents by summing the currents at different nodes of the network. The branch currents are calculated using the formula (I.26):

$$[I] = [BIBC][I_L] \tag{I.26}$$

Where, I represents the vector of branch currents. $BIBC$ is the matrix of injected currents at nodes (Bus Injection Branch Current), which is an upper triangular matrix containing only 0 and 1 values. I_L denotes the vector of injected currents at the terminal nodes of the network.

Construction of the BIBC Matrix [117, 118]:

5. Identification of Nodes and Branches: Begin by identifying all nodes and branches within the electrical network. Nodes represent points of connection, while branches denote conductive elements such as transmission lines and transformers.
6. Assignment of Node Indices: Assign unique indices to each node within the network. These indices will serve to identify the rows and columns of the BIBC matrix.
7. Formulation of Kirchhoff's Current Law (KCL) Equations: Write KCL equations for each node in the network, expressing the sum of currents entering and leaving the node as zero for a stable system.
8. Matrix Representation of KCL Equations: Represent the KCL equations in matrix form to create the BIBC matrix. This matrix is square with dimensions corresponding to the number of nodes in the network.
9. Determination of Matrix Elements: Populate the elements of the BIBC matrix based on the network's connectivity.
    - If there exists a direct path or connection from node i to node j, assign a value of 1 to the corresponding element in the BIBC matrix.
    - If no direct connection exists between nodes i and j, assign a value of 0.
10. Structuring the BIBC Matrix: The BIBC matrix typically exhibits an upper triangular structure due to the directional flow of currents in the network.

Step 3: Forward Sweep

During the third step, a forward sweep is performed in an ascending manner from the source node towards the terminal nodes of the network to calculate the voltage for each node by computing the voltage drop on each branch.

$$V_{ri} = V_{si} - Z_i \cdot I_i, \qquad i = 1,2, \dots, NT \tag{I.27}$$

Where, si and ri are the start and end of branch i, Z_i is the series impedance of branch i, NT is the number of branches in the EDN.

I.7.1.1. Convergence criterion

The three steps of the algorithm are repeated until convergence. The differences in node voltages between the previous and current iterations are used as the convergence criterion to stop the iterative calculation.

$$\max\left(\left|V_i^{k+1} - V_i^k\right|\right) < \varepsilon, i = 1,2, \dots, NB \tag{I.28}$$

Where ε represents the desired precision and NB is the total number of network buses.

The active power losses at each branch i are calculated using the equation (I.29):

$$P_{\text{Loss},i} = R_i \cdot \frac{P_i^2 + Q_i^2}{|V_i|^2} \tag{I.29}$$

The total active power losses in the branches of the EDN are calculated by the equation (I.30):

$$P_{T,\text{Loss}} = \sum_{i=1}^{NT} P_{\text{Loss},i} = \sum_{i=1}^{NT} R_i \cdot \frac{P_i^2 + Q_i^2}{|V_i|^2} \tag{I.30}$$

The reactive power losses at the branch i are calculated using the equation (I.31):

$$Q_{\text{Loss},i} = X_i \cdot \frac{P_i^2 + Q_i^2}{|V_i|^2} \tag{I.31}$$

The total reactive power losses in the lines of the EDN are calculated by the equation (I.32):

$$Q_{T,\text{Loss}} = \sum_{i=1}^{NT} Q_{\text{Loss},i} = \sum_{i=1}^{NT} X_i \cdot \frac{P_i^2 + Q_i^2}{|V_i|^2} \tag{I.32}$$

I.7.2. Steps of the backward/forward sweep method

Step 1: Input network data: Enter data such as linedata (start node, end node, resistances, and reactances of branches) and busdata (active and reactive powers of loads). Initialize node voltages [1pu] and define the desired tolerance value.

Step 2: Calculate injection currents at all nodes.

Step 3: Calculate branch currents using backward sweep .

Step 4: Calculate node voltages using forward sweep .

Step 5: Test voltage convergence for consecutive iterations. If voltage convergence is achieved, proceed to the next step. Otherwise, go back to Step 2.

Step 6: Calculate active and reactive power losses for all branches, and total active and reactive power losses for the network .

Step 7: Display node voltages, active and reactive power losses of branches, and total active and reactive power losses of the network.

I.8. Conclusion

This chapter provides a comprehensive overview of distributed generation (DG) technologies and their integration into modern EDNs. DG units based on renewable energy sources like solar PV, wind turbines, and hydro power can offer many technical, economic, and environmental benefits.

The chapter discusses mathematical models for representing the electrical behavior of PV and wind turbine generators, which are the most dominant DG sources. Accurate modeling is crucial for assessing the impacts of integrating these intermittent energy resources.

When optimally sized and placed, DG units can reduce power losses, enhance voltage profiles, and improve stability and reliability of distribution systems. However, improper planning can also lead to adverse effects. This highlights the significance of optimization techniques for determining the best locations and capacities for DG allocation.

The chapter also spotlights an efficient power flow calculation method known as the Backward/Forward Sweep algorithm. Its simplicity, speed, and robustness in solving load flow problems makes it well-suited for distribution systems. Repeated load flow analyses are indispensable when employing optimization to identify optimal DG placement strategies.

CHAPTER II

Techniques and Methods for Uncertainty Modeling in Power Systems

II.1. Introduction

These days, there are many opportunities for operation and control in power systems due to their development and the emergence of new and advanced energy concepts like smart grids, energy storage systems for renewable energy sources, microgrids, and nanogrids. However, there are also many challenges associated with the planning, investment, scheduling, and operation of modern power system networks. This makes it difficult to accurately describe deterministic states of parameters in power networks due to the increase in uncertainty associated with high penetration of renewable energy sources, or others that could expose the systems to potential risks. Uncertainty in energy systems is thus a persistent problem, especially in modern renewable energy systems. Therefore, from the standpoints of operation and management, making accurate selections is essential to weighing options, projecting expenses, anticipating income, and securely and consistently reducing potential dangers. The easiest approach is to have enough information at hand to assist in making the best choice within a reasonable amount of time; nevertheless, uncertainty is synonymous with the lack of verified information. As a result, to manage uncertainty, decision-making techniques have been studied in a variety of contexts to examine potential risks and outcomes of all scenarios some of which may be impossible and to accurately quantify the practical significance of the sources of uncertainty to better understand how uncertainties will affect the performance of power systems [119-121].

II.2. Uncertainty modeling methods

The literature presents a variety of uncertainty modeling techniques, which may be divided into six primary categories [122]:

1- Probabilistic approaches [123]: A problem's input parameters are randomly chosen, and a Probability Density Functions (PDF) is found for each of them. The widely used probabilistic approaches, also known as uncertainty modeling methods, can be divided into two categories: numerical and analytical. The former include methods based on scenario analysis, linearization, and PDF approximation; the latter include Monte Carlo Simulation (MCS), sequential MCS, Markov Chain MCS, pseudo sequential MCS, and nonsequential MCS methods.

2- Possibilistic approach [124]: It is based on fuzzy sets, where a membership function is used to represent the input parameters.

3- Hybrid possibilistic-probabilistic approaches [125]: There is a combination of probabilistic and possibilistic input parameters. The fuzzy-scenario and fuzzy-MCS approaches are the ones most frequently used in this category.

4- Information gap decision theory [126]: The Information Gap Decision Theory (IGDT) method, whose two main characteristics are robustness and opportuneness, describes how much the unknown parameter may move while guaranteeing the decision maker's minimal income.

5- Robust optimization [127]: The judgments that are made are determined by solving a problem with the worst-case circumstances of an unclear dataset in mind.

6- Interval analysis [128] : It is expected that the input parameters come from a predetermined range.

In Figure II.1 an overview is presented, showcasing the various methodologies employed in the literature for modeling uncertainty in electric power systems. This visual representation provides a concise glimpse into the diverse methods utilized to address uncertainties within the realm of electric power systems, setting the stage for a comprehensive understanding of the modeling approaches discussed in the literature.

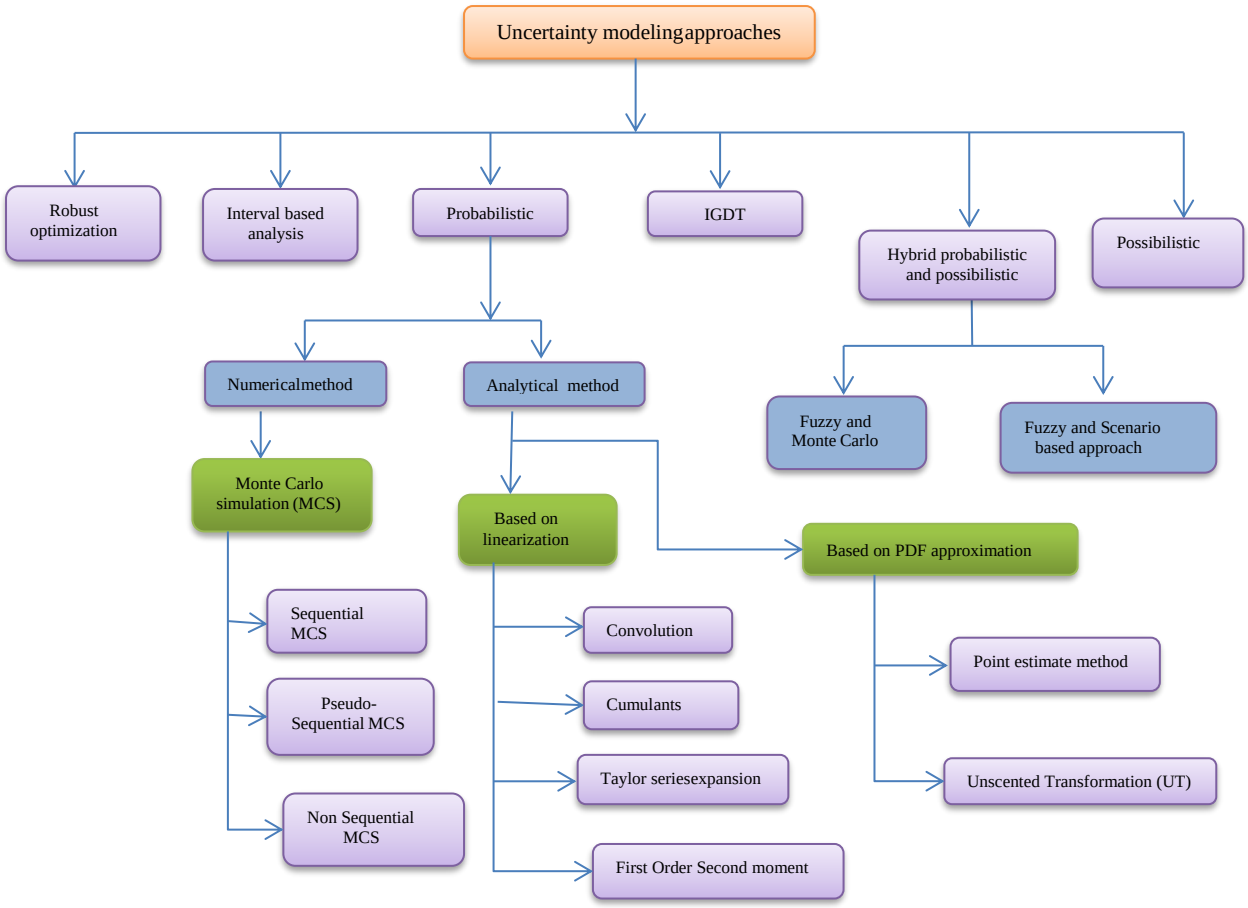

Figure II.1: Methods used in the literature for modeling uncertainty in electric power systems

II.3. Probability density functions

Uncertainty representation within our analysis hinges on Probability Density Functions (PDF), which serve as crucial tools for capturing the probabilistic nature inherent in various parameters [129] . In the subsequent sub-sections, we conduct an in-depth exploration of the selected PDFs for pivotal parameters, including solar irradiance, wind speed, load demand, price, and temperature. This meticulous elucidation of the probabilistic representation for each parameter aims to establish a robust foundation for our analyses, facilitating a comprehensive comprehension of the inherent uncertainties embedded in our modeling framework. The chosen PDFs for each parameter are outlined as follows:

II.3.1. Probabilistic model of solar radiation

The following is how the sun irradiance fluctuations have been modelled using the Beta probability density functions [130, 131]:

$$f_b(G) = \begin{cases} \dfrac{\Gamma(\varphi+\tau)}{\Gamma(\varphi)\Gamma(\tau)} G^{(\varphi-1)}(1-G)^{(\tau-1)} & 0 \le G \le 1; \varphi, \tau \ge 0 \\ 0 & \textit{otherwise} \end{cases} \quad \text{(II.1)}$$

where τ and φ can be calculated using the following equations . Γ represents the gamma function, and G is the variable of the function, representing solar irradiance.

$$\tau = (1-\mu) \times \left(\frac{\mu \times (1+\mu)}{\sigma^2} - 1 \right) \quad \text{(II.2)}$$

$$\varphi = \frac{\mu \times \tau}{1-\mu} \quad \text{(II. 3)}$$

where the average value μ is obtained from prior data. σ represents the standard deviation.

II.3.2. Probabilistic model of wind speed

The wind speed uncertainty can be modeled using the Weibull PDF [132]:

$$F(W) = \left(\frac{k}{c}\right)\left(\frac{W}{c}\right)^{k-1} exp\left[-\left(\frac{W}{c}\right)^{k}\right] \quad \text{(II.4)}$$

where W is the wind speed. The scale and shape parameters of the Weibull PDF are noted by k and c, respectively.

II.3.3. Probabilistic model of load demand

The uncertainty in load demand can be modeled using the normal PDF as follows [130, 133]:

$$f_n(L) = \frac{1}{\sigma_L \sqrt{2\pi}} exp\left[-\frac{(L-\mu_L)^2}{2\sigma_L^2}\right] \quad \text{(II.5)}$$

Where μ_L is the load average value and σ_L is the standard deviation.

II.3.4. Probabilistic model of price

The electricity cost is an accurate random characteristic due to its uncertainty value derived from the power grid. In this study, the normal PDF is employed to simulate the probabilistic nature of the electricity price [134, 135]:

$$f(P) = \frac{1}{\sigma_P \sqrt{2\pi}} exp\left[-\frac{(P - \mu_P)^2}{2{\sigma_P}^2}\right] \quad \text{(II.6)}$$

Where μ_P is the load average value and σ_P is the standard deviation.

II.3.5. Probabilistic model of temperature

The ambient temperature is continually varying and its probabilistic nature is defined as follows referring to the normal probability distribution [136, 137]:

$$f(T) = \frac{1}{\sigma_T \sqrt{2\pi}} exp\left[-\frac{(T - \mu_T)^2}{2{\sigma_T}^2}\right] \quad \text{(II.7)}$$

where μ_T is the average temperature and σ_T is the standard deviation.

II.4. Monte Carlo Simulations (MCS)

Monte Carlo methods constitute a diverse category of computational algorithms that leverage the process of repeated random sampling to derive numerical results. Widely applied in mathematical problem-solving contexts, they prove especially valuable when traditional mathematical methods encounter challenges or impracticalities. The fundamental premise underlying Monte Carlo methods involves the generation of multiple random samples, guided by a probability distribution function (PDF) that encapsulates the behavior of specific parameters. The PDF serves as a mathematical representation detailing the likelihood of different outcomes or values for a given variable. In the context of Monte Carlo simulations, this implies that the uncertainty introduced through the iterative sampling adheres to a predefined probability distribution, offering a means to capture and model the inherent probabilistic nature of the phenomena under investigation. By integrating probability

distributions into the Monte Carlo framework, these methods provide a powerful tool for tackling complex problems, offering insights into scenarios where deterministic mathematical solutions are challenging to attain. This approach not only facilitates a more realistic representation of uncertainty but also enhances the robustness and versatility of the computational analysis, making Monte Carlo methods an invaluable resource in various scientific, engineering, and financial applications [135, 138, 139].

II.4.1. Main merits of monte carlo methods

The main merits of employing MCS as a computational strategy are instrumental in enhancing its utility across diverse domains. This section succinctly outlines the primary advantages associated with MCS [140, 141]:

1. Ease of use and adaptability: MCS is known for its straightforward implementation and adaptability, making it accessible across various fields.
2. Effective problem solving: MCS excels in solving complex, non-convex, and non-differentiable problems, providing effective solutions where traditional methods may fall short.
3. Applicability to systems with many uncertain variables: MCS is well-suited for systems with numerous uncertain variables, allowing for the modeling and simulation of complex systems with inherent variability.
4. Compatibility with all probability distribution formats: MCS seamlessly integrates with all Probability Distribution Function (PDF) formats, ensuring accurate representation of a wide array of uncertainties.

   The representation of MCS is as follows:

$\boldsymbol{for}\ i = 1{:}n$
$Generate\ sample\ X, using\ PDF\ of\ uncertain\ decision\ variables.$
$Calculate\ y\ =\ f(X, Z)$
$\boldsymbol{End\ for}$

This structure aligns with the fundamental concept of Monte Carlo Simulation, where random samples X are drawn from probability distributions, and the model or function of interest y is evaluated for each sample. This process allows for statistical analysis and the

exploration of uncertainties associated with the input parameters, including any additional parameters Z that may affect the model's behavior [130].

$$\mu = \frac{\sum_{i=1}^{n} y}{n} \tag{II.8}$$

The mean, denoted as μ, is calculated by summing up all individual data points y and dividing the total by the number of data points n. This formula provides a measure of central tendency, representing the average value of the dataset.

$$\sigma = \sqrt{\frac{\sum_{i=1}^{i=n} (y - \mu)^2}{n}} \tag{II 9}$$

The standard deviation, denoted as σ, measures the amount of variation or dispersion in a set of values. It is calculated by taking the square root of the average of the squared differences between each data point y and the mean μ. A higher standard deviation indicates greater variability in the dataset.

The expressions represent formulas for calculating the mean and standard deviation of a set of data points. The results, conveying information about uncertain parameters from collected data, are visually presented in Figures II.2 through II.6, illustrating both the means and standard deviations.

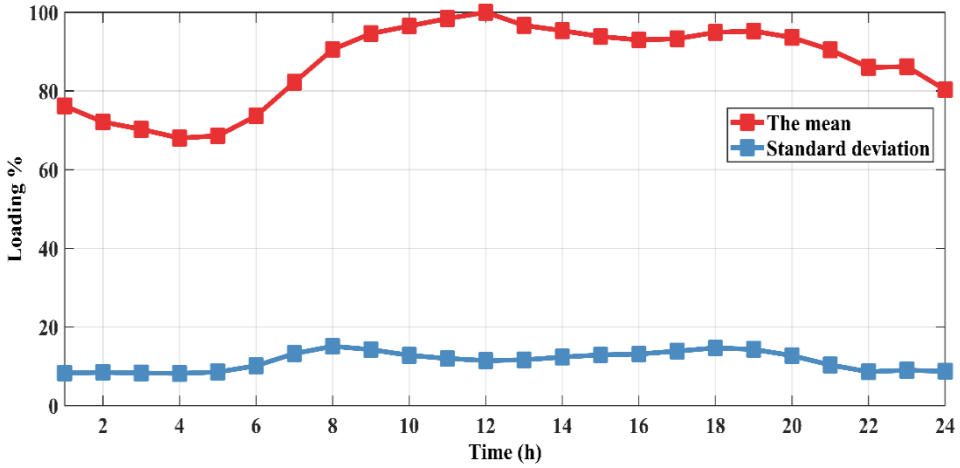

Figure II.2: The mean and the standard deviation values of load demand.

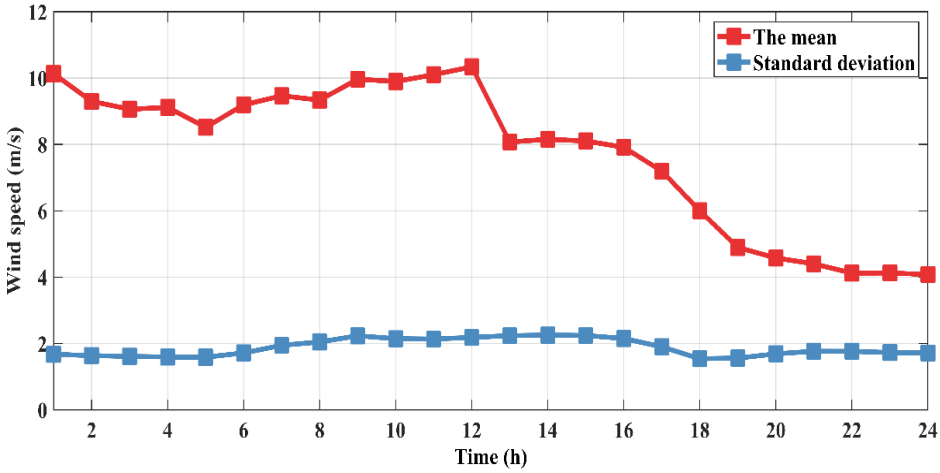

Figure II.3: The mean and the standard deviation values of wind speed.

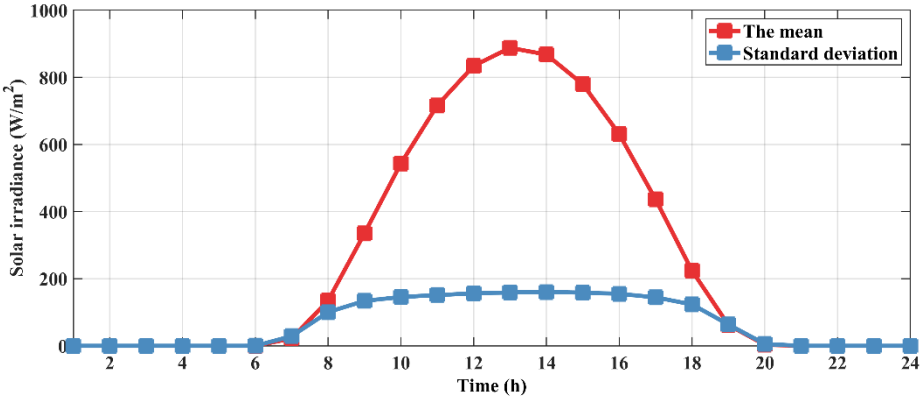

Figure II.4: The mean and the standard deviation values of solar irradiance.

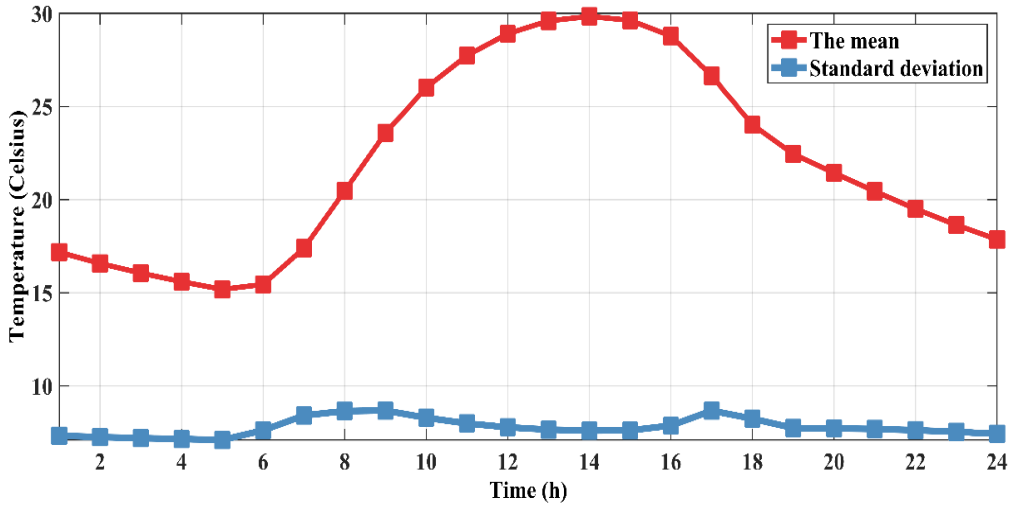

Figure II.5: The mean and the standard deviation values of temperature.

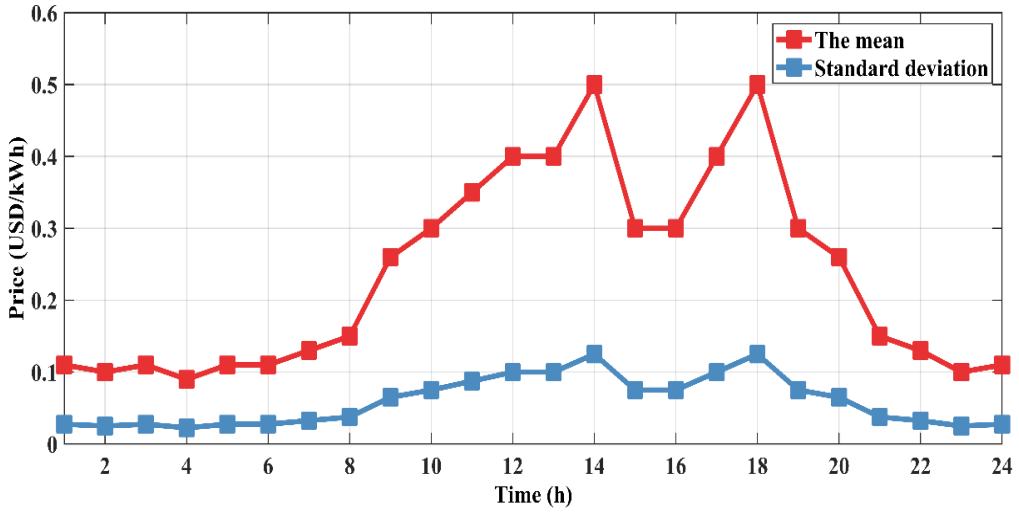

Figure II.6: The mean and the standard deviation values of price.

II.4.2. Hourly scenarios: Monte Carlo simulations results

Using the parameters of the probability density function (PDF) of the variables wind speed, temperature, solar irradiance, load, and price, whichare calculated using the gathered data, Monte Carlo simulations generate 1000 data points for each variable. Figures II.7 through II.11 illustrate the generated scenarios for these parameters on an hourly basis throughout the day.

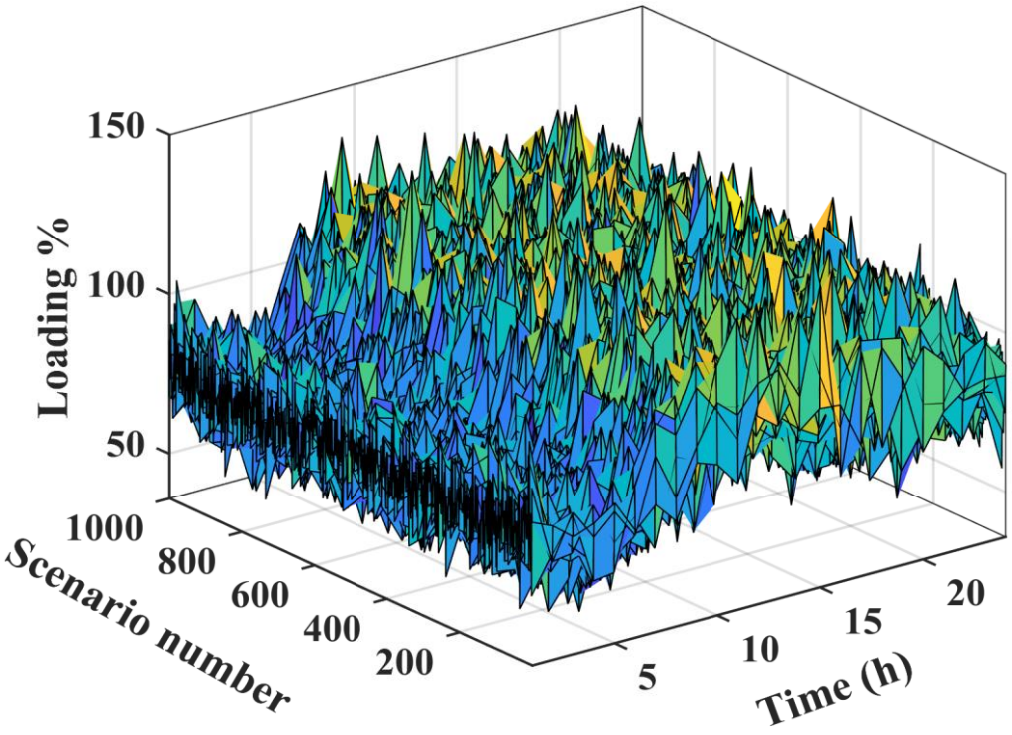

Figure II.7: The scenarios generated by MCS for loading.

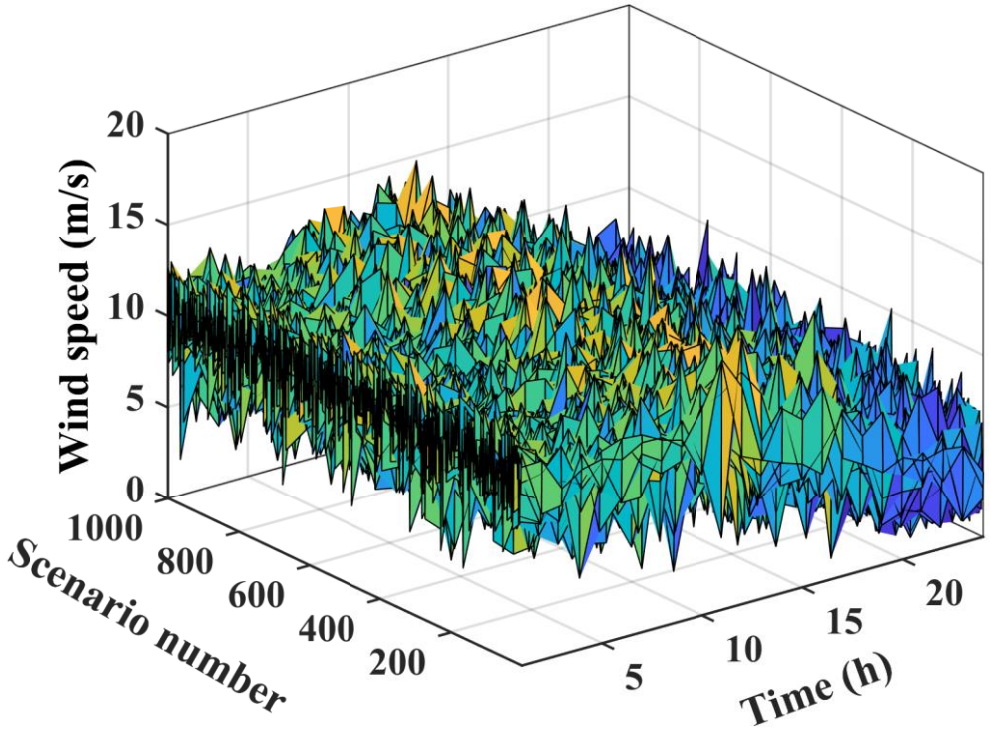

Figure II.8: The scenarios generated by MCS for wind speed.

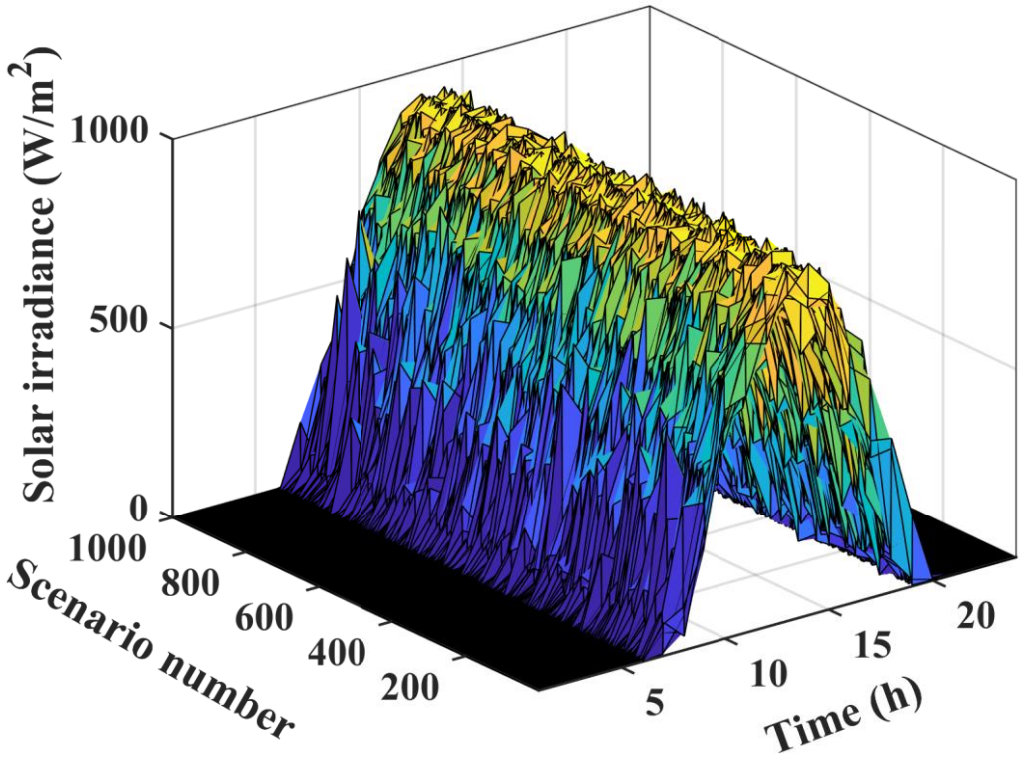

Figure II.9: The scenarios generated by MCS for solar irradiance.

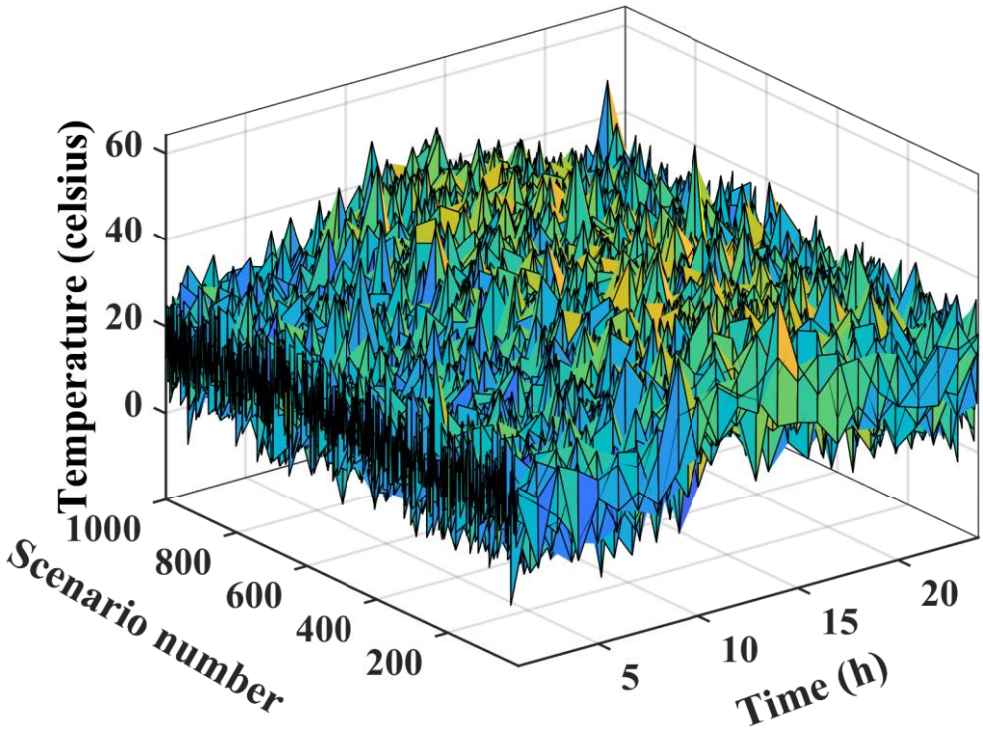

Figure II.10: The scenarios generated by MCS for temperature.

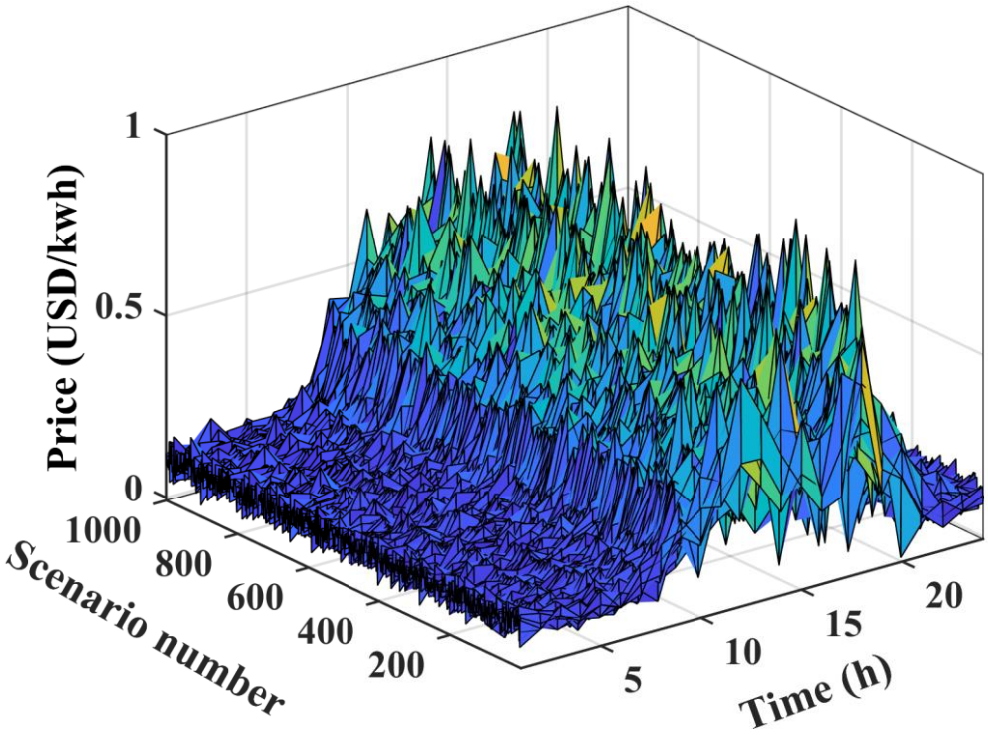

Figure II.11: The scenarios generated by MCS for price.

II.5. The scenario base reduction method

Within the domain of complex systems research, Monte Carlo Simulation has become a cornerstone technique for quantifying uncertainty and making informed decisions. However, the inherent strength of MCS, its ability to generate a myriad of potential future scenarios, can become a weakness when dealing with computationally demanding problems. This is where Scenario Base Reduction (SBR) emerges as a critical tool, strategically reducing the scenario base while preserving vital system characteristics [142 ,136] .

The primary objective of SBR is to strike a delicate balance between computational efficiency and solution accuracy. By minimizing the number of scenarios analyzed, SBR alleviates the computational burden associated with solving problems like the Optimal Operation Problem (OOP) within the MCS framework. This translates to faster simulations, improved resource utilization, and ultimately, the ability to explore a wider range of scenarios within the same timeframe.

The SBR methodology encompasses a systematic approach to scenario reduction. This typically involves three key phases:

1. Scenario generation: The initial stage involves employing MCS to generate a diverse set of scenarios, each representing a potential realization of the system under study. This stage accounts for various uncertainties and fluctuations inherent to the system.

2. Scenario analysis and ranking: SBR algorithms assess each scenario and assign a relative importance based on its contribution to understanding the system's behavior. This analysis often involves metrics like distance measures, sensitivity analysis, or information entropy.

3. Scenario reduction: Based on the assigned rankings, SBR strategically removes scenarios that offer minimal information gain or redundancy while preserving the essential statistical representation of the system. This can be achieved through various techniques, including clustering, distance-based pruning, or dominance-based approaches. However, it's important to recognize that the specific implementation of SBR can vary depending on the complexities of the system and the desired level of accuracy.

II.5.1. Hourly scenarios: scenario base reduction results

In this section, we present and analyze the outcomes derived from the systematic application of SBR methodology. Our objective has been to effectively reduce the initial set of scenarios to 25 key scenarios, a process designed not only to streamline computational demands but also to enhance the interpretability of results. This reduction facilitates a more focused analysis of critical hourly scenarios, contributing to a deeper understanding of the system dynamics.

The depicted Figures II.12 through II.16 encapsulate the outcomes of a Monte Carlo simulation framework empowered by SBR techniques. This comprehensive analysis focuses on key parameters loading, wind speed, solar irradiance, temperature, and price over a 24-hour period. The utilization of SBR is integral to refining and streamlining the scenarios, optimizing computational efficiency without compromising the accuracy of the simulation.

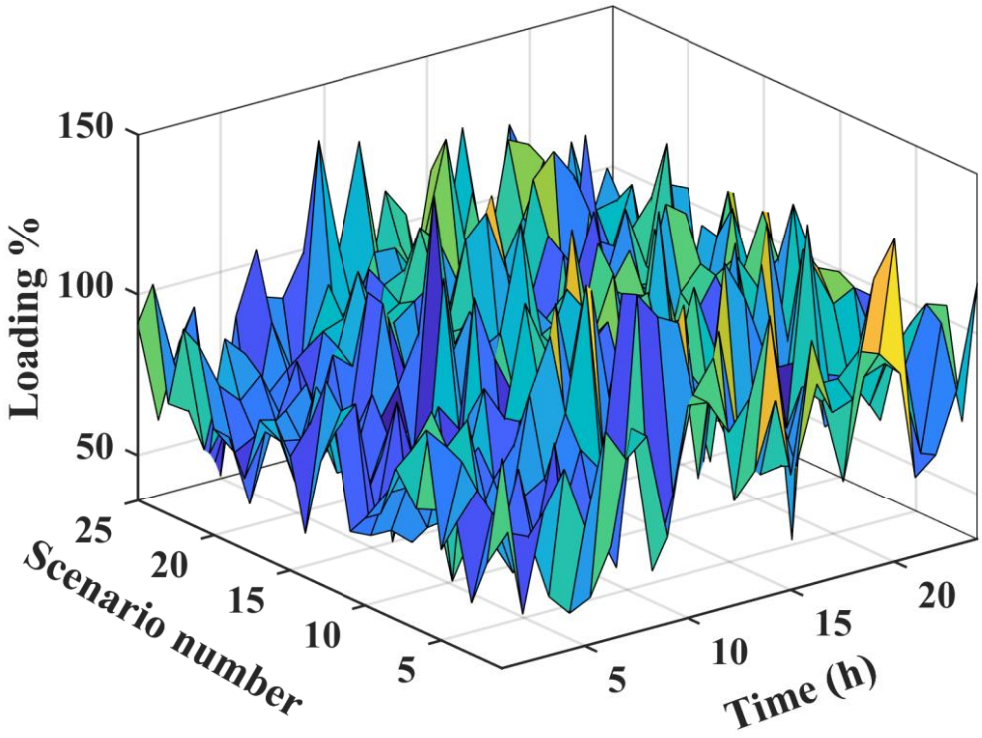

Figure II.12: The obtained scenarios by SBR for loading.

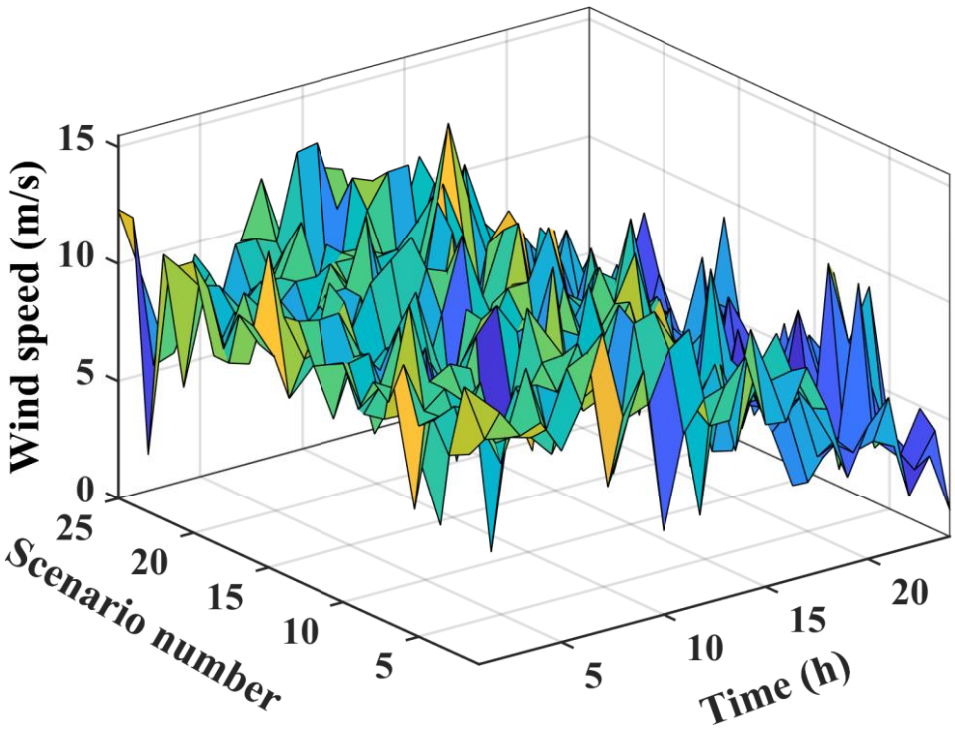

Figure II.13: The obtained scenarios by SBR for wind speed.

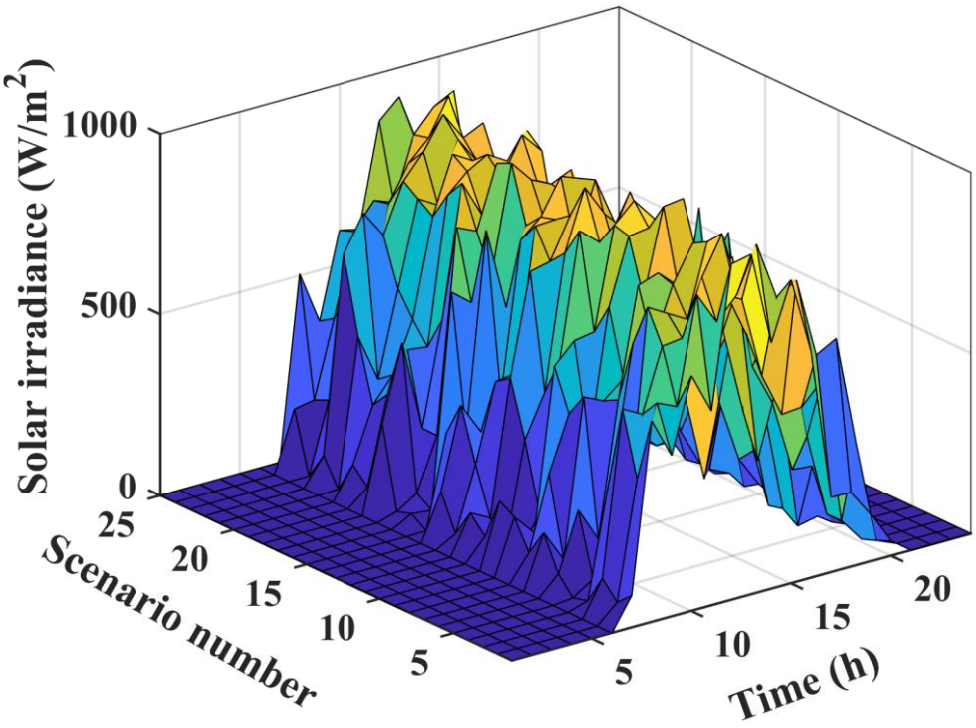

Figure II.14: The obtained scenarios by SBR for solar irradiance.

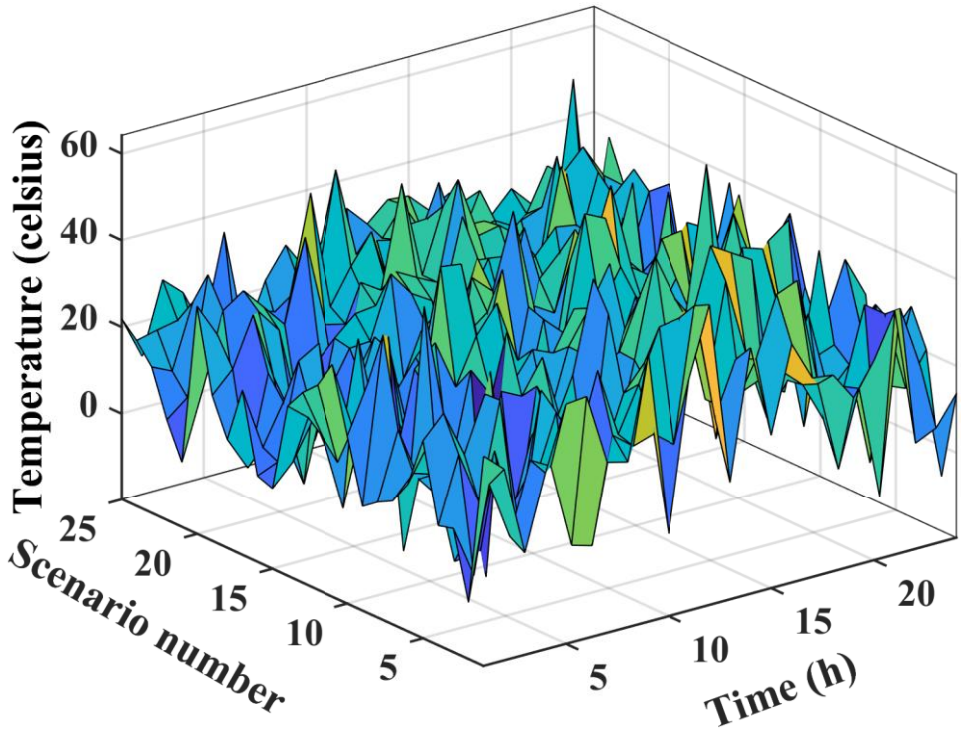

Figure II.15: The obtained scenarios by SBR for temperature.

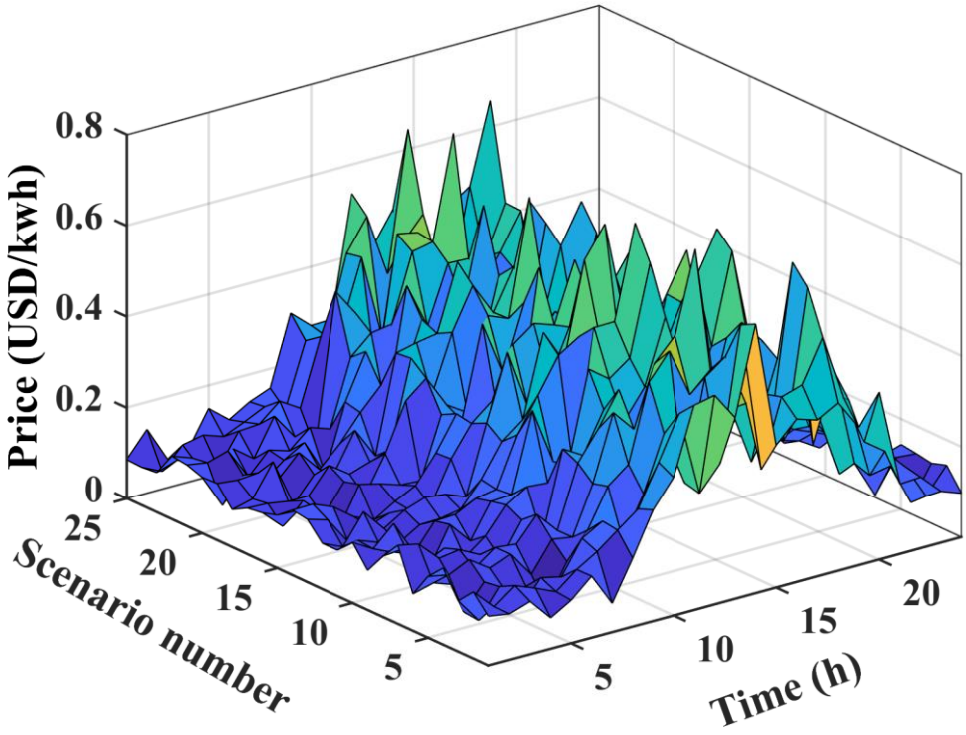

Figure II.16: The obtained scenarios by SBR for price.

The scenarios, post-SBR, reveal a focused and nuanced exploration of loading, wind speed, solar irradiance, temperature, and price dynamics. Notably, the reduction in scenarios does not compromise the variability essential for capturing uncertainties in each parameter. This streamlined approach ensures a more efficient computational analysis while maintaining a high level of representativeness.

These results hold significant implications for decision-makers in the energy sector. The refined scenarios empower them with a practical and efficient tool for strategic decision-making in power system planning and operation.

In the end, SBR plays a pivotal role in enabling efficient and insightful analysis within the MCS framework for complex systems. By effectively reducing the scenario base, SBR fosters faster simulations, enhances resource utilization, and allows for a broader exploration of possible futures. As research in computational optimization and uncertainty quantification continues to evolve, SBR will undoubtedly remain a crucial tool for navigating the intricacies of complex systems and making informed decisions under the ever-present veil of uncertainty.

II.6. Probability distribution

Understanding and quantifying the likelihood of different scenarios occurring within a specified time frame is a crucial aspect of effective uncertainty modeling in power systems. The probability distribution, which represents the probabilities associated with each scenario, plays a pivotal role in providing a comprehensive overview of the system's anticipated states throughout the 24-hour period [143].

This distribution is visually portrayed through a set of discrete time intervals, each encapsulating the probability of specific scenarios transpiring during the corresponding hour.

Interpreting the peaks and troughs in the probability distribution is key to uncovering temporal patterns in system behavior. Peaks indicate moments when specific scenarios are more likely, while troughs represent periods of reduced likelihood. This temporal insight is invaluable for anticipating variations in demand, renewable energy generation, and market conditions. Strategically, decision-makers leverage the probability distribution to allocate resources and prioritize attention based on the expected impact of different events. The quantification of scenario likelihoods facilitates risk assessment, aids in operational planning, and informs the development of adaptive strategies.

In essence, the probability distribution serves as a compass for decision-makers navigating the dynamic landscape of the power system. By offering a quantifiable guide, it empowers stakeholders to make informed choices, adapt to uncertainties, and optimize operational and strategic plans in response to the ever-changing nature of the energy sector.

Figures II.17 through II.21 elucidate the probability distribution associated with each scenario at 12:00 PM, providing a comprehensive overview of the system's anticipated states throughout this hour.

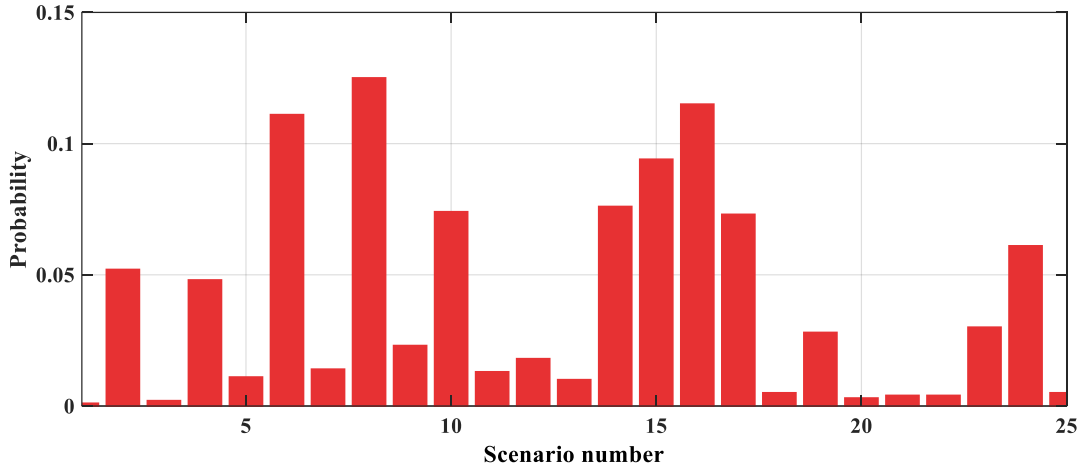

Figure II.17: The probability of loading.

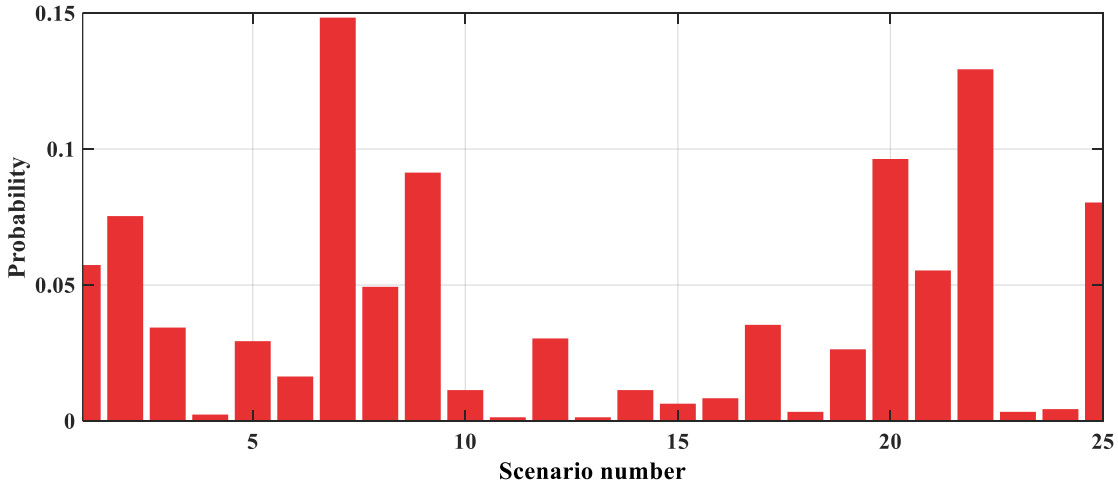

Figure II.18: The probability of wind speed.

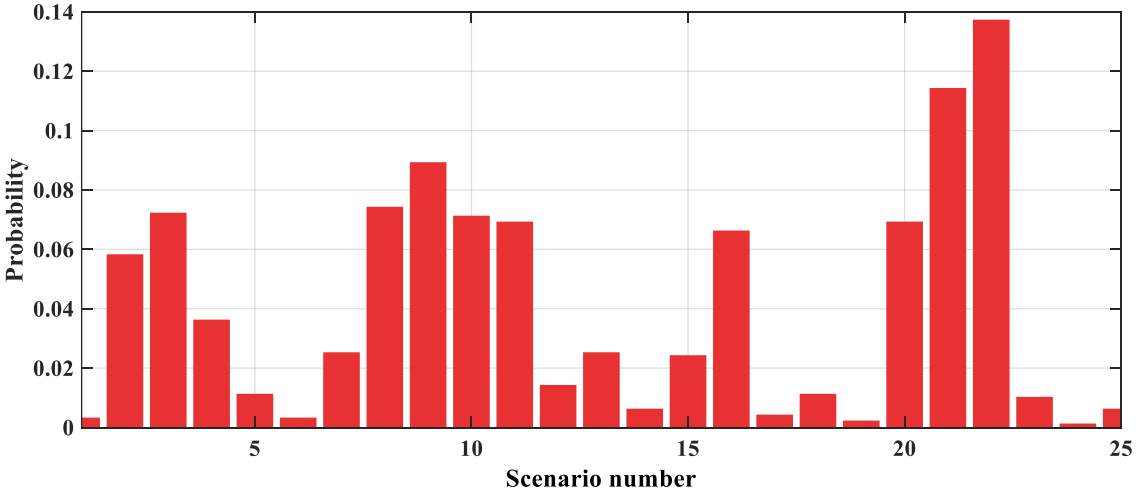

Figure II.19: The probability of solar irradiance.

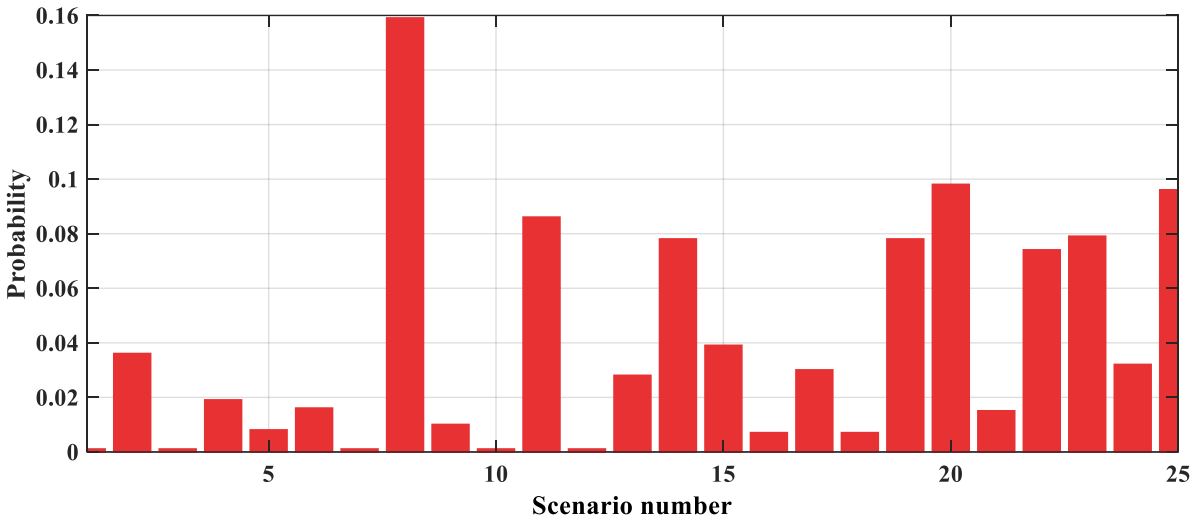

Figure II.20: The probability of temperature.

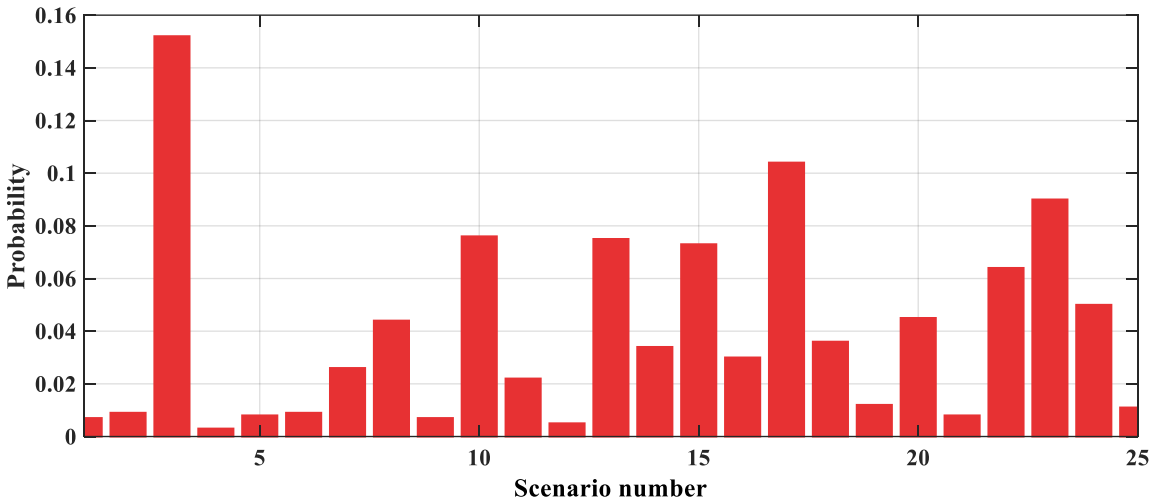

Figure II.21: The probability of price.

II.7. Hourly optimal scenario

The concept of the Optimal Scenario for a specific parameter is fundamental in uncertainty modeling within power systems. It involves the strategic selection of a configuration derived from reduced scenarios and their associated probabilities, intending to depict the most favorable conditions for a particular parameter over a 24-hour period. This scenario plays a crucial role in providing decision-makers with insights into optimal operating states, facilitating tasks such as load forecasting, resource allocation, and risk management. The equation governing the determination of the Optimal Scenario is as follows:

$$HOS(h) = \sum_{i=1}^{N_{sce}} SBR(i,h) \times probability(i,h) \qquad h = 1,2,\dots,24 \qquad \text{(II.10)}$$

This equation signifies that for each hour h, each reduced scenario for the parameter is multiplied by its corresponding probabilit**y,** and the results are summed over all 25 keys scenarios. The outcome is a comprehensive representation of the optimal state for that specific parameter.

Where, $SBR(i,h)$ is the i^{th} reduced scenario for the parameter at time h, and $probability$(i, h) is the associated probability for the the i^{th} reduced scenario at the same time.

II.8. Conclusion

This chapter comprehensively addressed models for handling parameter uncertainty in modern power systems, encompassing aspects like load demand, renewable generation, and electricity prices. Exploring diverse approaches such as probabilistic, possibilistic, hybrid methods, information gap decision theory, robust optimization, and interval analysis, the chapter offered a versatile toolkit for uncertainty management. Monte Carlo simulation emerged as a key technique, lauded for its user-friendly nature, effectiveness in tackling complex problems, and compatibility with probability distributions. The application of Monte Carlo simulation in generating hourly scenarios for critical parameters was elucidated, emphasizing its practical significance. Additionally, the chapter highlighted scenario-based reduction as a means to enhance computational efficiency while preserving accuracy. Introducing tools like the probability distribution and optimal hourly scenario, it underscored their value in assessing scenario likelihoods and identifying optimal conditions. This comprehensive exploration equips decision-makers with essential insights and strategies for navigating uncertainty in modern power system planning and operations, fostering informed decision-making and strategic planning amid evolving challenges.

CHAPTER III

Enhancing Optimization: Walrus Optimization Algorithm

III.1. Introduction

The communities of computer science and operations research have endeavored to solve complex real-world problems. While addressing large-scale problems, there is a need to find a feasible solution and improve it to converge towards the optimal global solution. However, exact solutions are challenging to find due to limited resources and the inherent complexity of most optimization problems. Metaheuristics can overcome this difficulty by offering approximate solutions. A metaheuristic algorithm is a search procedure designed to find a good solution to a complex optimization problem that is difficult to solve optimally [144]. It is imperative to find a quasi-optimal solution based on imperfect or incomplete information in this real-world with limited resources (e.g., computing power and time). The emergence of metaheuristics to solve such optimization problems is one of the most notable achievements in recent decades. There are challenges that warrant attention to develop better solutions compared to traditional approaches. Various metaheuristic algorithms are described by authors that are quite extensive in various applications to solve nonlinear and non-convex optimization problems. Thus, metaheuristics can often find good solutions with less computational effort than iterative methods and simple greedy heuristics [145].

In this chapter, we will delve into the introduction of a refined optimization approach known as the Modified Walrus Optimization Algorithm (MWaOA), designed to address complex optimization problems with increased efficiency. Specifically, we will enhance the standard Walrus Optimization Algorithm (WaOA) by integrating the Levy flight mechanism, aiming to improve the delicate balance between exploration and exploitation during the search process. The chapter unfolds with a comprehensive assessment of the MWaOA's performance, employing a suite of 23 benchmark functions. This evaluation involves a thorough comparison against various state-of-the-art metaheuristic algorithms, providing valuable insights into the algorithm's effectiveness. Our analysis will spans statistical findings related to the final solutions, convergence plots that visually depict optimization trajectories, and boxplots illustrating result distributions across independent runs.

III.2. Design methodology

Optimization is often reduced to mathematical resolution techniques, to which the failures encountered are subsequently attributed. However, as with most problems to be solved,

optimization must be the subject of a systematic approach that includes four phases, summarized in Figure III.1. The phases can be chained sequentially, but iterations and feedback are often essential [2, 146].

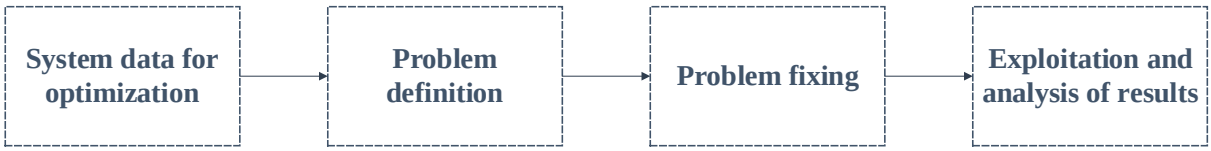

Figure III.1: Optimization problem resolution process.

III.3. Formulation of the optimization problem

The formulation of the optimization problem is foundational in the design process as it critically influences the success of subsequent stages. However, it is a complex task as the choice of design variables is seldom unique, and current computational capabilities can only handle a limited number of variables. The design problem, as outlined in the specifications, must be translated into an equivalent mathematical problem. This is the most intricate step in the design process since, like the selection of design variables, the formulation of a problem is seldom unique, especially when defining the functions characterizing the system's performance. Precisely, it involves the definition of [147]:

III.3.1. Objective function

The objective function is a crucial element in defining the goal of an optimization problem, and it can manifest in two fundamental forms: either as a cost to minimize (such as manufacturing cost, consumption, operational cost, or development time) or as a performance metric to maximize (including profit, efficiency, or transmission factor). The selection of the objective function is pivotal in shaping the optimization problem, influencing not only the definition of the problem itself but also the modeling approach used to compute it. When dealing with a single objective, the choice of the objective function is straightforward. For instance, in situations where the aim is to determine the characteristics of a device producing specified performance values, the objective function can be formulated as the disparity between the actual and specified performance values. However, in many optimization scenarios, there is a need to accommodate multiple objectives, some of which may be conflicting, adding a layer of complexity to the optimization process [2]. This necessitates thoughtful consideration of the

objectives and the incorporation of a well-defined objective function, a critical component in steering the optimization algorithm towards achieving a well-balanced and satisfactory solution.

III.3.2. Design parameters

The design parameters or variables are controlled factors that influence the performance of the system. They can take various forms, such as geometric dimensions, material properties, structural choices, etc. These parameters may be quantitative or qualitative, continuous or discrete. The choice and number of parameters also significantly impact the definition of the optimization problem. While it might be advantageous to vary a large number of factors to expand the search space, this approach would lengthen the optimization process. Designers may introduce constraints to ensure, for example, a suitable geometric shape, validate the chosen modeling approach, and guarantee the proper functioning of the system, among other considerations [2].

III.3.3. Constraints related to manufacturing or device utilization

Constraints related to manufacturing or device utilization encompass various limitations imposed by the production process or the intended use of the device. These constraints often revolve around practical considerations, such as material availability, production capabilities, operational conditions, or safety requirements. For instance, manufacturing constraints may involve limitations on available materials, production techniques, or manufacturing tolerances, influencing the design choices. On the other hand, device utilization constraints could include operating temperature ranges, environmental conditions, or regulatory standards that the device must adhere to during its usage. Integrating these constraints into the optimization process ensures that the final solution aligns with real-world feasibility and practicality, optimizing the design within the bounds of operational and manufacturing necessities [148].

III.3.4. Constraints introduced by the designer

Constraints introduced by the designer represent a crucial aspect of the optimization process, adding a layer of customization and expertise to the problem formulation. These constraints are imposed based on the designer's insights, experience, and specific requirements beyond the initial specifications. They serve as a means for the designer to guide the

optimization algorithm towards solutions that align with their expertise and knowledge of the problem domain. These constraints could involve design preferences, ethical considerations, or unique insights that the designer deems essential for the success and applicability of the final solution. By introducing these constraints, designers not only contribute their expertise to the optimization process but also play a pivotal role in shaping the solution space to meet broader objectives and contextual considerations [150 ,149].

The complexity arises not only from the multitude of choices in design variables and constraints but also from the interconnectedness of these elements. Achieving a balance between conflicting objectives and constraints is a delicate task that requires careful consideration. Furthermore, the designer must navigate the challenge of reconciling real-world complexities with the mathematical abstraction necessary for optimization. The success of subsequent optimization algorithms hinges on the precision and accuracy with which the optimization problem is formulated, making it a critical aspect of the overall design process.

III.4. Optimization methods

Optimization is a branch of mathematics that seeks to model, analyze, and solve problems analytically or numerically, involving the minimization or maximization of a function over a given set. Optimization problems in electrical engineering pose several challenges related to user requirements, the characteristics of the problem at hand, and computation time. Many studies rely on exact solution methods to obtain a solution with guaranteed optimality. However, in certain situations, the emphasis may shift towards obtaining high-quality solutions without the guarantee of optimality but with the advantage of reduced computation time [151, 152]. Various methods for solving problems of different complexities have been proposed. As a result, a wide variety and notable differences in principles, strategies, and performances have been observed. This diversity has led to the classification of optimization methods into two categories: conventional methods and metaheuristic methods.

III.4.1. Conventional methods

Conventional methods for optimization have long been the workhorses of problem-solving, often categorized into two groups:

III.4.1.1. Analytical techniques

Analytical techniques represent the system with a set of numerical equations for which the solution is calculated directly. These methods offer the advantages of short computation times and ease of implementation while ensuring problem convergence [41, 153]. However, their precision and computational efficiency may be impacted by the size and complexity of the problem.

III.4.1.2. Deterministic techniques

Deterministic techniques constitute a class of mathematical optimization methods based on the iterative improvement of the initial solution. Numerous deterministic methods exist in the literature, primarily falling into two broad categories: Linear Programming and Non-Linear Programming. Weaknesses of these techniques include sensitivity to the number of decision variables, significant computation time, and susceptibility to getting trapped in a local optimum [154].

III.4.2. Metaheuristic methods

The term "metaheuristic" was coined by F. Glover in 1986, derived from the combination of two Greek words: "meta," meaning "beyond or at a higher level," and "heuristic," meaning "to find or discover" [155]. Metaheuristics constitute a family of optimization algorithms, also known as approximation algorithms, designed to solve challenging optimization problems arising from operations research for which no classical, more efficient method is known. They offer a solution to optimization problems regularly encountered by engineers and decision-makers. Metaheuristics are typically iterative stochastic algorithms that progress towards an optimum by sampling an objective function.

The execution of metaheuristics unfolds in three phases: Diversification, Intensification, and Memorization**.** Diversification ensures thorough coverage of the solution space and identifies "promising" areas [156]. Intensification delves deeper into the search within each localized promising area, and Memorization supports learning, enabling the algorithm to consider only areas where the optimum is likely to be found and retain past results to guide optimization in subsequent iterations. Metaheuristics iteratively and alternately progress between diversification, intensification, and learning phases. The original phase is often chosen

randomly, and the algorithm continues until a stopping criterion is met. Metaheuristics are often inspired by natural systems, whether in physics (as in simulated annealing), evolutionary biology (as in genetic algorithms), or ethology (as in walrus optimization algorithm or particle swarm optimization).

III.5. The algorithm of walrus optimization

WaOA is an algorithm that draws inspiration from nature and mimics walrus behavior in its quest for food. WaOA is capable of efficiently exploring the search space and identifying better solutions by first randomly initializing the population of walruses and then rearranging them in accordance with their fitness values [157]. A walrus image is shown in Figure III.2.

Figure III.2: Walrus photo.

III.5.1. Mathematical principle of the WaOA method

The search for the best position by the WaOA algorithm is structured into the following three steps:

III.5.1.1. Algorithm initialization

Walruses constitute the search members of the WaOA population-based metaheuristic algorithm. Each walrus in WaOA represents r a potential solution for the optimization problem. However, the potential values for the problem variables are determined by the location of each walrus within the search space. Consequently, each walrus is represented as a vector, and the

so-called population matrix is used to numerically represent the walrus population. When WaOA is initially implemented, the walrus populations are ramdomly initialized. Equation (III.1) is employed to determine this WaOA population matrix.

$$X = \begin{bmatrix} X_1 \\ \vdots \\ X_i \\ \vdots \\ X_N \end{bmatrix}_{N\times m} = \begin{bmatrix} x_{1,1} & \cdots & x_{1,j} & \cdots & x_{1,m} \\ \vdots & \ddots & \vdots & \cdots & \vdots \\ x_{i,1} & \cdots & x_{i,j} & \cdots & x_{i,m} \\ \vdots & \ddots & \vdots & \cdots & \vdots \\ x_{N,1} & \cdots & x_{N,j} & \cdots & x_{N,m} \end{bmatrix}_{N\times m} \quad \text{(III.1)}$$

where N is the number of walruses, m is the number of decision variables, X_i is the ith walrus (candidate solution), and $x_{i,j}$ is the value of the jth choice variable recommended by the ith walrus.

III.5.1.2. Feeding strategy (exploration phase)

Each walrus' location is updated by migrating towards the most powerful walrus, which represents the most effective solution discovered thus far. As per Equations (III.2) and (III.3), the feeding behavior of the walruses serves as the basis for the mathematical depiction of how to update their locations.

$$x_{i,j}^{P_1} = x_{i,j} + rand_{i,j} \cdot \left(SW_j - I_{i,j} \cdot x_{i,j}\right) \quad \text{(III.2)}$$

$$X_i = \begin{cases} X_i^{P_1}, & F_i^{P_1} < F_i, \\ X_i, & else, \end{cases} \quad \text{(III.3)}$$

For every walrus i^{th}, new placements $x_{i,j}^{P_1}$ are produced in the first WaOA phase according to the feeding strategy. The new position's j^{th} dimension is $x_{i,j}^{P_1}$. The new position of the walruses is $x_{i,j}$, which reflects the location of particle i in dimension j, after calculating the function of goal $F_i^{P_1}$ at this new location. On the other hand, X_i is a vector that includes the location in every dimension. With $\text{rand}_{i,j}$, randomization is introduced by producing numbers between 0 and 1. The most powerful walrus that directs motion is SW . In order to expedite the exploration phase, $I_{i,j}$ are randomly selected integers of 1 or 2. Wider jumps are produced

by $I_{i,j}$= 2 as opposed to 1 for regular steps. This widens the search field, making it easier to locate new, promising regions and break free from local optima. In conclusion, a randomized method biased towards the best solution to date is used in the first phase to update positions. Large steps every now and then improve worldwide exploration to stay out of trouble.

III.5.1.3. Migration

Each walrus updates its position by moving towards the location of a different walrus chosen at random. WaOA employs this migratory process to guide the walruses as they explore the search space and help them find advantageous areas. Equations (III.4) and (III.5) provide the formal expression of this behavioral process.

$$x_{i,j}^{P_2} = \begin{cases} x_{i,j} + rand_{i,j} \cdot \left(x_{k,j} - I_{i,j} \cdot x_{i,j}\right), & F_k < F_i, \\ x_{i,j} + rand_{i,j} \cdot \left(x_{i,j} - x_{k,j}\right), & else\ , \end{cases} \quad \text{(III.4)}$$

$$X_i = \begin{cases} X_i^{P_2}, & F_i^{P_2} < F_i, \\ X_i, & else, \end{cases} \quad \text{(III.5)}$$

The freshly created location of the i^{th} walrus, obtained from the second phase, is represented by $x_{i,j}^{P_2}$. The symbol for its location on the j^{th} dimension is $x_{i,j}^{P_2}$. The value of its objective function is $F_i^{P_2}$. X_k denotes the position of the chosen walrus to which the i^{th} walrus is migrated, where k ∈ {1, 2... N} and k ≠ i. The location of the k^{th} walrus on the j^{th} dimension is represented by $x_{k,j}$, and its objective function value is indicated by F_k.

III.5.1.4. Fighting and getting away from predators (exploitation phase)

WaOA enhances its food-finding capabilities by imitating walrus behavior in its native habitat. WaOA can enhance search space exploration and solution generation by modeling the way walruses change posture in response to threats. The method creates a virtual neighborhood around each walrus and uses Equations (III.6) and (III.7) to randomly generate new places within this range. Equation (III.8) states that if the objective function is improved with this new position, it replaces the previous one. WaOA's efficacy in local search and landscape adaption is improved by this behavior simulation.

$$x_{i,j}^{P_3} = x_{i,j} + \left(lb_{local,j}^{t} + \left(ub_{local,j}^{t} - \ rand \ \cdot lb_{local,j}^{t}\right)\right) \quad \text{(III.6)}$$

$$\text{Local bounds} : \begin{cases} lb_{local,j}^{t} = \dfrac{lb_j}{t}, \\ ub_{local,j}^{t} = \dfrac{ub_j}{t}, \end{cases} \quad \text{(III.7)}$$

$$X_i = \begin{cases} X_i^{P_3}, & F_i^{P_3} < F_i, \\ X_i, & else, \end{cases} \quad \text{(III.8)}$$

Here, the newly formed location of the i^{th} walrus utilizing the third phase is denoted as $x_{i,j}^{P_3}$. The coordinates $x_{i,j}^{P_3}$ indicate where it is on the j^{th} dimension. The value of its objective function is denoted by $F_i^{P_3}$. The iteration cycle is represented by t. The lower and upper bounds of the j^{th} parameter are represented by the symbols lb_j and b_j , respectively. Furthermore, the locally allowed lower and upper limits for the j^{th} parameter are represented by the symbols $lb_{local,j}^{t}$ and $ub_{local,j}^{t}$, respectively, simulating localized exploration close to possible solutions.

III.6. Modified walrus optimization algorithm by levy flight

The rapid evolution within engineering and scientific domains presents a growing set of challenges for optimization algorithms tasked with solving intricate problems. In response, there is a burgeoning focus on enhancing algorithms to cope with evolving complexities. This emphasis on algorithm improvement has become a pivotal research area, aimed at elevating the efficiency and adaptability of algorithms [158, 159]**.**

One notable stride in this ongoing journey of algorithm enhancement involves the assimilation of levy flight. Levy flight, a stochastic process characterized by occasional extensive jumps, draws inspiration from the flight patterns observed in certain animals. This integration seeks to introduce a more robust exploration mechanism into optimization algorithms. The distinct characteristics of levy flight, particularly its capacity to explore larger solution spaces through occasional substantial steps, render it a valuable addition to algorithms aiming to strike a balance between exploration and exploitation [160].

In our specific case, modifications were implemented within the Walrus Optimization Algorithm (WOA), originally designed to emulate the cooperative hunting behavior of walruses. The integration of levy flight into WOA serves the purpose of further amplifying its exploration capabilities while addressing limitations linked to premature convergence and constrained exploration. By permitting occasional significant leaps in the solution space, levy flight facilitates the escape from local optima and fosters a more thorough search for optimal solutions.

This decision to integrate levy flight into the walrus optimization algorithm aligns seamlessly with the overarching goal of staying at the forefront of algorithmic advancements. It signifies a strategic move to leverage the advantages of nature-inspired strategies, ultimately enhancing the algorithm's overall performance, adaptability, and efficiency in addressing complex optimization challenges.

The specific modification involves bolstering the exploration phase of the WaOA technique. This is achieved by updating the locations of the walrus agents around the best solution using the Levy Flight distribution, as outlined in equation (III.9). This modification strategically enhances the algorithm's ability to exploit promising regions, contributing to its effectiveness in finding optimal solutions.

$$x_{i,j}(t+1) = r_3 \text{Best}\,(t) - r_4 x_{(i,j)}(t) + C_1 \cdot L_F \cdot \left(x_{(r,j)}(t) - x_{(i,j)}(t)\right) \qquad \text{(III.9)}$$

where r_3 and r_4 refer to random values in the rang [0, 1]. $x_{(i,j)}(t)$ and $\text{Best}\,(t)$ represent the current location of the Walrus and the best location, respectively. The position $x_{(r,j)}(t)$ is chosen randomly among the positions of the walrus agents, different from $x_{(i,j)}(t)$. $C_1 = 2r_4(1 - T/T_{\max})$ represents an operator that measures the intensity of the Levy flight. L_F is the Levy flight function which can be measured as follows:

$$L_F = 0.05 \times \frac{u \times \sigma}{|v|^{1/\beta}} \qquad \text{(III.10)}$$

In which

$$\sigma = \left(\frac{\Gamma(1+\beta) \times \sin(\pi\beta/2)}{\Gamma((1+\beta)/2) \times \beta \times 2^{(\beta-1)/2}} \right)^{1/\beta} \quad \text{(III.11)}$$

where, u and v denote random values that can be obtained from the normal distribution. β refers to a constant that is 1.5.

The flowchart of MWaOA algorithm is shown in Figure III.3.

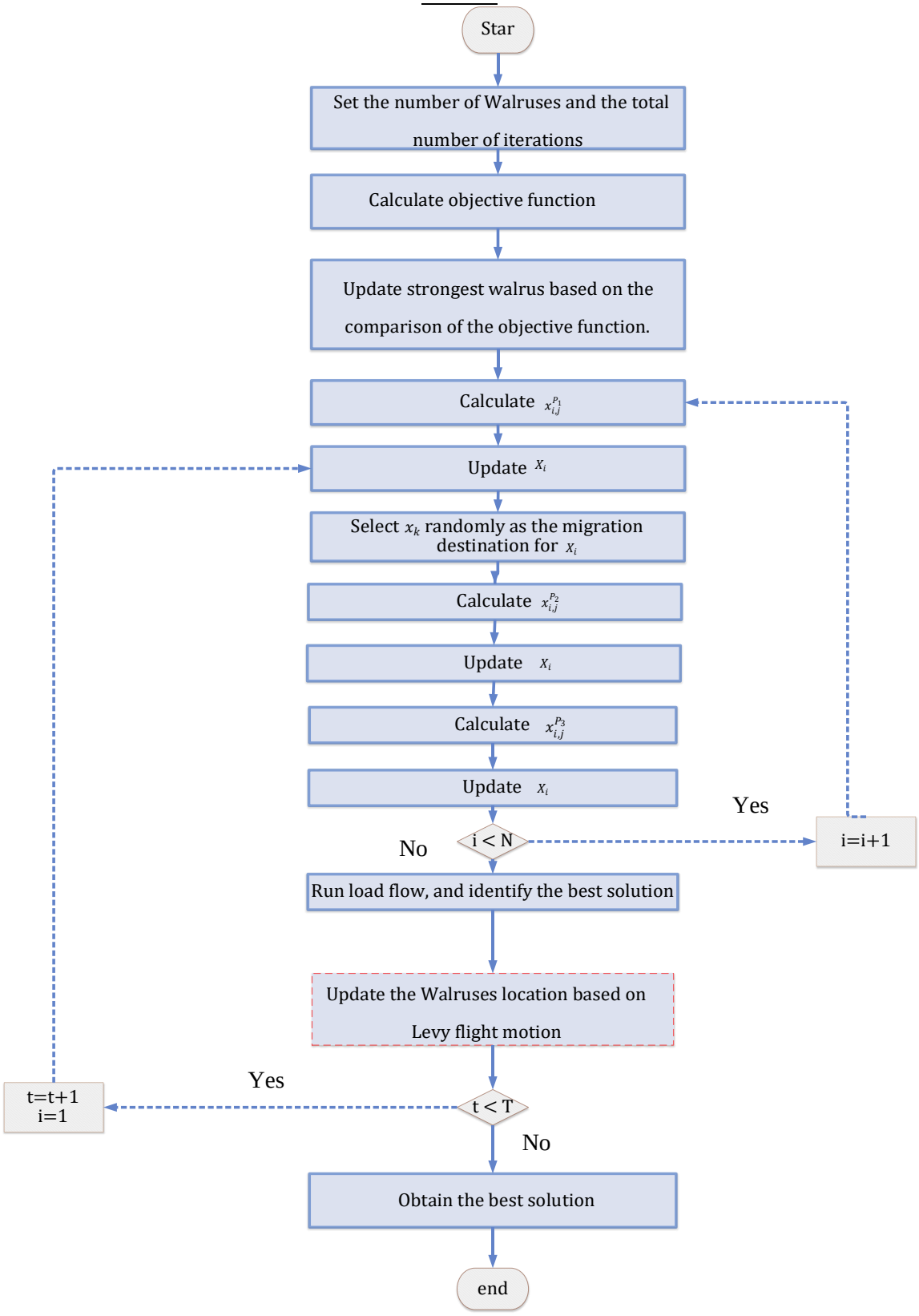

Figure III.3: The flowchart of the MWaOA.

III.7. Simulation results

The effectiveness of the suggested Modified Walrus Optimization Algorithm (MWaOA) was assessed by contrasting it with a number of well-known optimization techniques. These included Sand Cat Swarm Optimization (SCSO) [161], Triangulation Topology Aggregation Optimizer (TTAO) [162], Zebra Optimization Algorithm (ZOA) [163], Gray Wolf Optimization (GWO) [164], Sine Cosine Algorithm (SCA) [165], Artificial Rabbits Optimization (ARO) [166], Dandelion Optimizer (DO)[167] , and standard walrus behavior (WaOA) [157]. Every method was developed using MATLAB 2021a and executed on a PC equipped with an Intel i7 2.5 GHz CPU and 6 GB RAM. The purpose of the comparative study was to evaluate the suggested MWaOA's performance in comparison to the most advanced optimization methods available today.

III.7.1. Examining the MWaOA method using a selection of frequently used test functions

In this work, we analyze the 23 classic functions listed in Tables III.1, III.2, and III.3 [168] [169] [170], using the suggested MWaOA technique. Table III. 4 serves as the basis for setting the parameters in all scenarios to guarantee uniformity. After conducting the experiment thirty times, the findings are recorded. A schematic design of the partial pictures of 23 common reference test functions is shown in Figure III.4.

Table III.1: Unimodal functions.

Dimensions	F_{min}	Range	Function
30	0	[-100, 100]	$f_1(x) = \sum_{j=1}^{n} x_j^2$
30	0	[-10, 10]	$f_2(x) = \sum_{j=1}^{n} \lvert x_j \rvert + \prod_{j=1}^{n} \lvert x_j \rvert$
30	0	[-100, 100]	$f_3(x) = \sum_{j=1}^{n} \left(\sum_{i-1}^{j} x_i \right)^2$
30	0	[-100, 100]	$f_4(x) = max \quad \lvert x_j \rvert, 1 \le j \le n$
30	0	[-30, 30]	$f_5(x) = \sum_{j=1}^{n-1} \left[100 \left(x_{j+1} - x_j^2 \right)^2 + \left(x_j - 1 \right)^2 \right]]$
30	0	[-100, 100]	$f_6(x) = \sum_{j=1}^{n} \left([x_j + 0.5] \right)^2$
30	0	[-1.28, 1.28]	$f_7(x) = \sum_{j=1}^{n} j x_j^4 + random(0,1)$

Table III.2: Multimodal functions.

Dimensions	F_{min}	Range	Function
30	-12.56	[-500, 500]	$f_8(x) = \sum_{j=1}^{n} -x_j \sin\left(\sqrt{\lvert x_j \rvert}\right)$
30	0	[-5.12, 5.12]	$f_9(x) = \sum_{j=1}^{n} \left[x_j^2 - 10\cos(2\pi x_j) + 10\right]$
30	0	[-32, 32]	$f_{10}(x) = -20\exp\left(-0.2\sqrt{\frac{1}{n}\sum_{j=1}^{n} x_j^2}\right) - \exp\left(\frac{1}{n}\sum_{j=1}^{n}\cos(2\pi x_j) + 20 + e\right)$
30	0	[-600, 600]	$f_{11}(x) = \frac{1}{4000}\sum_{j=1}^{n} x_j^2 - \prod_{j=1}^{n} cos\left(\frac{x_j}{\sqrt{j}}\right) + 1$
30	0	[-50, 50]	$f_{12}(x) = \frac{\pi}{n}\left\{10\sin(\pi x_1) + \sum_{j=1}^{n-1}(x_j - 1)^2\left[1 + 10\,sin^2(\pi z x_{j+1})\right] + (x_n - 1)^2\right\} + \sum_{j=1}^{n} u(x_j, 10, 100, 4)$
30	0	[-50, 50]	$f_{13}(x) = 0.1\left\{sin^2(3\pi x_1) + \sum_{j=1}^{n}(x_j - 1)^2\left[1 + sin^2(3\pi x_j + 1)\right] + (x_n - 1)^2[1 + sin^2(2\pi x_n)]\right\} + \sum_{j=1}^{n} u(x_j, 5, 100, 4)$ $u(x_j, v, s, h) = \begin{cases} s(x_j - v)^h & x_j > v \\ 0 & -v < x_j < v \\ s(-x_j - v)^h & x_j < -v \end{cases}$

Table III.3: Fixed-dimension multimodal benchmark functions.

Dimensions	F_{min}	Range	Function
2	1	[-65.536, 65.536]	$f_{14}(x) = \left(\frac{1}{500} + \sum_{i=1}^{25}\frac{1}{i + \sum_{j=1}^{2}(x_j - a_{ji})^6}\right)^{-1}$
4	0.00030	[-5, 5]	$f_{15}(x) = \sum_{j=1}^{11}\left[a_j - \frac{x_j(b_j^2 + b_j x_2)}{b_j^2 + b_j x_{3+} x_4}\right]^2$
2	-1.0316	[-5, 5]	$f_{16}(x) = 4x_1^2 - 2.1x_1^4 + \frac{1}{3}x_1^6 + x_1x_2 - 4x_2^2 + 4x_2^4$
2	0.398	[-5, 5]	$f_{17}(x) = \left(x_2 - \frac{5.1}{4\pi^2}x_1^2 + \frac{5}{\pi}x_1 - 6\right)^2 + 10\left(1 - \frac{1}{8\pi}\right)\cos x_1 + 10$
2	3	[-2, 2]	$f_{18}(x) = [1 + (x_1 + x_2 + 1)^2(19 - 14x_1 + 3x_1^2 - 14x_2 + 6x_1x_2 + 3x_2^2)] * [30 + (2x_1 - 3x_2)^2(18 - 32x_1 + 12x_1^2 + 48x_2 - 36x_1x_2 + 27x_2^2)]$
3	-3.86	[1, 3]	$f_{19}(x) = -\sum_{j=1}^{4} c_j\, exp\left(-\sum_{i=1}^{3} a_{ji}\left(x_i - p_{ji}\right)^2\right)$
6	-3.32	[0, 1]	$f_{20}(x) = -\sum_{j=1}^{4} c_j\, exp\left(-\sum_{i=1}^{6} a_{ji}\left(x_i - p_{ji}\right)^2\right)$
4	-10.1532	[0, 10]	$f_{21}(x) = -\sum_{j=1}^{5}\left[(x - a_j)(x - a_j)^T + c_j\right]^{-1}$
4	-10.4028	[0, 10]	$f_{22}(x) = -\sum_{j=1}^{7}\left[(x - a_j)(x - a_j)^T + c_j\right]^{-1}$
4	-10.5363	[0, 10]	$f_{23}(x) = -\sum_{j=1}^{10}\left[(x - a_j)(x - a_j)^T + c_j\right]^{-1}$

Table III.4: The optimization algorithms' chosen parameters.

Algorithms	Parameter	Value
SCSO [161]	Sensitivity range (rg)	[2,0]
	Phases control range (R)	$[-2rg, 2rg]$
	Maximum iteration	300
	Populations	30
TTAO [162]	r_0	[0,1]
	r_1	[0,1]
	r_2	[0,1]
	r_3	[0,1]
	r_4	[0,1]
	Maximum iteration	300
	Populations	30
DO [167]	α	[0,1]
	k	[0,1]
	Populations	300
	Maximum iteration	30
SCA [165]	r	[0,1]
	Maximum iteration	300
	Populations	30
GWO [164]	r_1	[0,1]
	r_2	[0,1]
	Maximum iteration	300
	Populations	30
ZOA [163]	Maximum iteration	300
	Populations	30
ARO [166]	Maximum iteration	300
	Populations	30
WaOA [157]	Maximum iteration	300
	Populations	30
MWaOA	Maximum iteration	300
	Populations	30

III.7.1.1 Examination of statistical results

The suggested MWaOA is compared to various optimization techniques in this section, such as the traditional WaOA, ARO, GWO, DO, TTAO, ZOA, SCA, and SCSO. Table III.5 presents statistical findings for each algorithm technique, including the mean, worst, standard deviation (SD), and best.

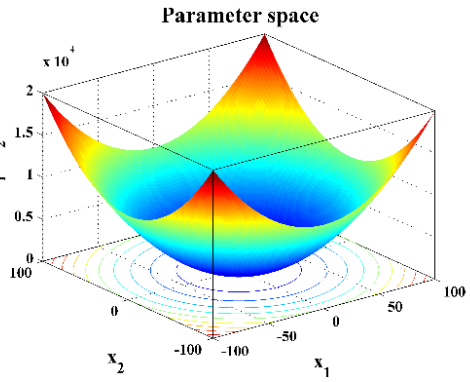
Parameter space
x 10^4
F1(x_1 , x_2)
x_2
x_1

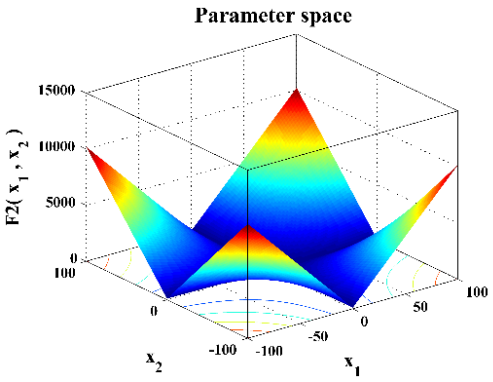
Parameter space
F2(x_1 , x_2)
x_2
x_1

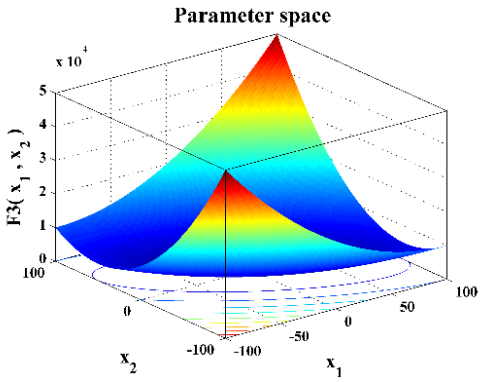
Parameter space
x 10^4
F3(x_1 , x_2)
x_2
x_1

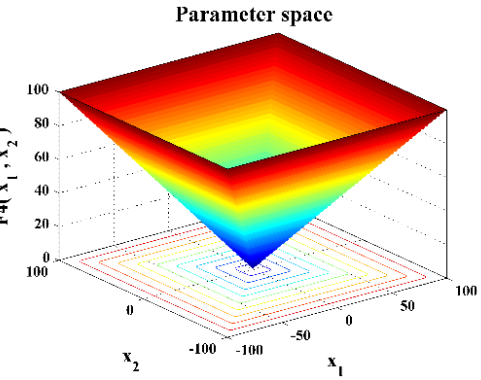
Parameter space
F4(x_1 , x_2)
x_2
x_1

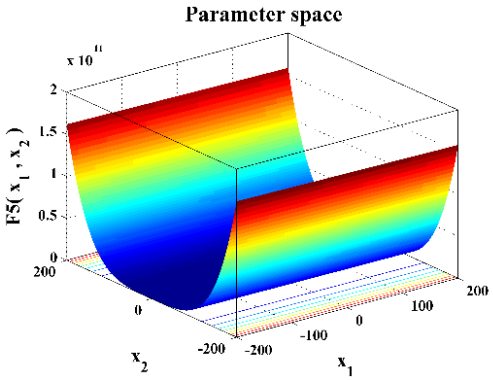
Parameter space
x 10^11
F5(x_1 , x_2)
x_2
x_1

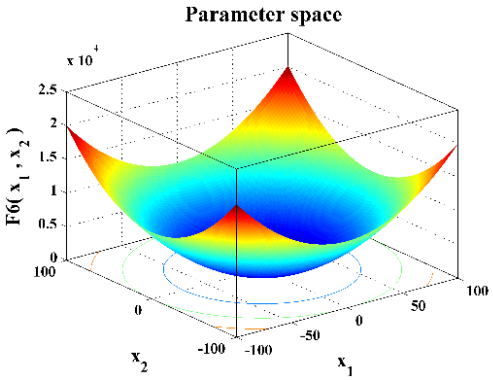
Parameter space
x 10^4
F6(x_1 , x_2)
x_2
x_1

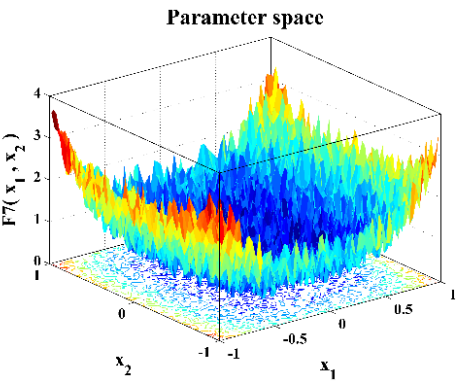
Parameter space
F7(x_1 , x_2)
x_2
x_1

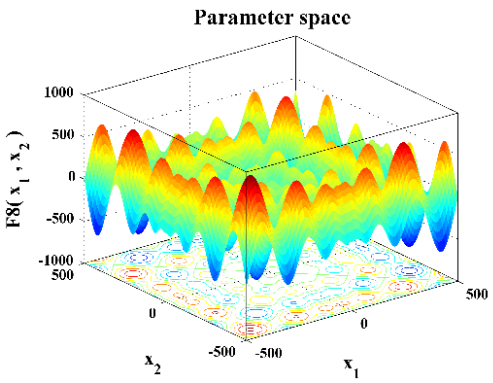
Parameter space
F8(x_1 , x_2)
x_2
x_1

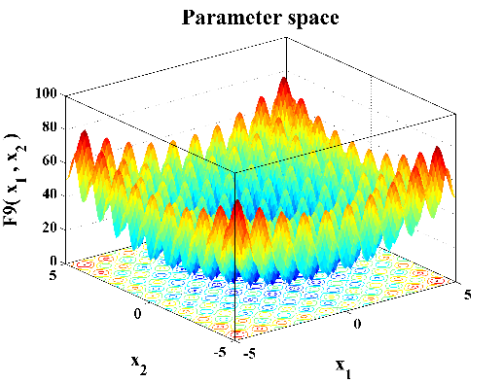
Parameter space
F9(x_1 , x_2)
x_2
x_1

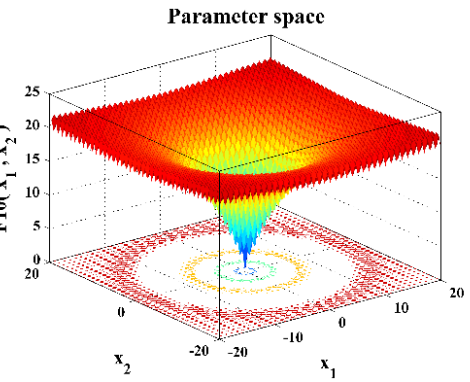
Parameter space
F10(x_1 , x_2)
x_2
x_1

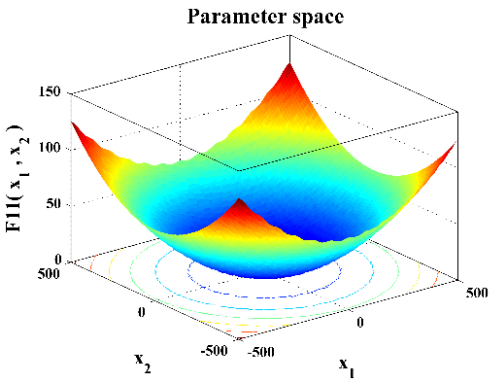
Parameter space
F11(x_1 , x_2)
x_2
x_1

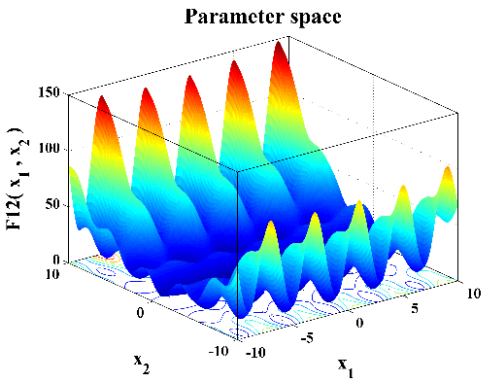
Parameter space
F12(x_1 , x_2)
x_2
x_1

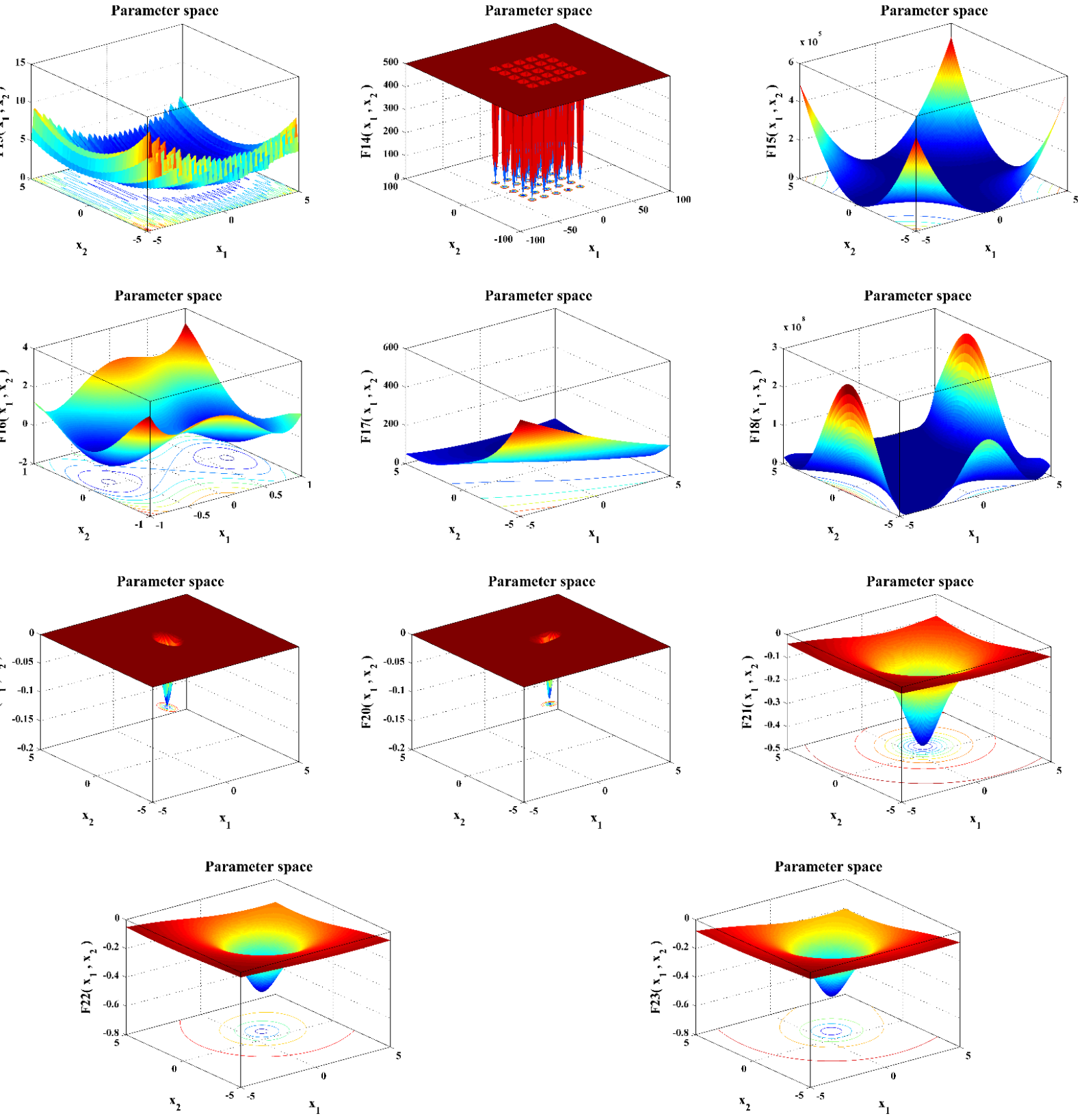

Figure III.4: Schematic diagram of partial images of 23 standard reference test functions.

Table III.5: Analytical results of several optimization techniques on the benchmark functions.

Fun.	Algorithms	Average	Best	Worst	SD
F1	TTAO	4,743490584	2,186719159	7,812885752	1,936006317
	ZOA	5,05E-148	2,66E-154	3,03E-147	1,24E-147
	SCA	218,438701	3,699481988	859,5647287	326,8358795
	ARO	2,22E-36	1,27E-38	5,22E-36	2,29E-36
	SCSO	4,97E-69	9,72E-73	2,09E-68	8,56E-69
	DO	0,001309467	0,000384983	0,00341229	0,001062139
	GWO	3,40E-15	4,70E-16	8,94E-15	3,27E-15
	WaOA	7,32E-169	1,16E-172	3,99E-168	0
	MWaOA	**0**	**0**	**0**	**0**
F2	TTAO	9,424183092	1,644455705	20,60803944	5,15997673
	ZOA	2,76E-77	1,86E-82	4,18E-76	9,41E-77
	SCA	0,326322096	0,038167436	1,053365013	0,29018973
	ARO	2,08E-19	3,71E-23	2,59E-18	5,99E-19
	SCSO	7,37E-35	6,45E-38	1,42E-33	3,17E-34
	DO	0,011268072	0,003916718	0,01781139	0,003234138
	GWO	1,48E-09	2,97E-10	5,43E-09	1,14E-09
	WaOA	1,74E-85	2,09E-89	2,89E-84	6,40E-85
	MWaOA	**3,87E-236**	**5,91E-241**	**5,99E-235**	**0**
F3	TTAO	1454,892	712,3401	2340,812	431,1617
	ZOA	6,46E-85	9,64E-101	1,29E-83	2,89E-84
	SCA	13328,9	4183,185	25045,26	5868,258
	ARO	5,77E-22	6,96E-31	1,03E-20	2,29E-21
	SCSO	4,21E-56	1,12E-65	8,40E-55	1,88E-55
	DO	161,0223	3,0728	623,1615	131,7561
	GWO	7,67E-02	3,82E-04	5,86E-01	1,61E-01
	WaOA	1,88E-125	8,29E-134	3,03E-124	6,77E-125
	MWaOA	**0,00E+00**	**0,00E+00**	**0,00E+00**	**0**
F4	TTAO	17,09088	10,73851	29,97114	5,485492
	ZOA	7,86E-67	1,67E-71	1,07E-65	2,53E-66
	SCA	44,79608	27,83024	69,81073	12,56874
	ARO	6,32E-14	8,10E-19	2,93E-13	8,72E-14
	SCSO	5,28E-29	9,82E-35	5,94E-28	1,47E-28
	DO	4,832629	0,651916	15,49904	3,79969
	GWO	8,49E-04	1,47E-04	2,26E-03	6,68E-04
	WaOA	1,55E-80	2,46E-83	1,21E-79	3,29E-80
	MWaOA	**2,59E-232**	**2,47E-240**	**2,34E-231**	**0**
F5	TTAO	3554,884	914,5005	20597,15	4219,463
	ZOA	2,86E+01	2,80E+01	2,89E+01	2,98E-01
	SCA	191189,7	3571,064	843823,9	237536,5
	ARO	3,89E+00	5,46E-02	2,72E+01	8,07E+00
	SCSO	2,81E+01	2,62E+01	2,88E+01	7,36E-01
	DO	35,48766	25,08149	92,6144	20,31688
	GWO	2,69E+01	2,61E+01	2,79E+01	5,65E-01
	WaOA	0,00E+00	0,00E+00	0,00E+00	0,00E+00
	MWaOA	**0,00E+00**	**0,00E+00**	**0,00E+00**	**0**
F6	TTAO	3,948525	1,365282	12,48421	2,529383
	ZOA	3,13E+00	1,48E+00	4,74E+00	8,12E-01
	SCA	125,0794	12,52875	546,5877	147,5893
	ARO	2,26E-02	4,06E-03	7,28E-02	1,56E-02

	SCSO	2,07E+00	1,03E+00	3,47E+00	6,00E-01
	DO	0,000237	7,78E-05	0,00052	0,000116
	GWO	1,02E+00	2,58E-01	2,00E+00	3,99E-01
	WaOA	0,00E+00	0,00E+00	0,00E+00	0,00E+00
	MWaOA	**0,00E+00**	**0,00E+00**	**0,00E+00**	**0**
F7	TTAO	0,47237	0,223985	0,853949	0,177411
	ZOA	1,83E-04	3,33E-05	5,24E-04	1,35E-04
	SCA	0,305572	0,024549	0,790963	0,219393
	ARO	1,08E-03	9,07E-05	2,91E-03	8,05E-04
	SCSO	3,70E-04	1,61E-05	1,31E-03	4,07E-04
	DO	0,033625	1,50E-02	0,068954	0,014127
	GWO	4,35E-03	1,11E-03	8,80E-03	2,10E-03
	WaOA	9,04E-05	8,44E-06	2,35E-04	5,77E-05
	MWaOA	**4,33E-05**	**2,58E-06**	**1,10E-04**	**2,94E-05**
F8	TTAO	-7602,92	-8521,21	-6889,56	422,3522
	ZOA	-6,31E+03	-7,31E+03	-4,90E+03	5,82E+02
	SCA	-3560,45	-3956,55	-3181,6	212,1354
	ARO	-9,58E+03	-1,04E+04	-8,75E+03	4,80E+02
	SCSO	-6,51E+03	-7,54E+03	-5,28E+03	6,71E+02
	DO	-7808,14	-9,92E+03	-6310,28	863,9655
	GWO	-5,50E+03	-6,71E+03	-2,64E+03	1,04E+03
	WaOA	-8,48E+03	-9,02E+03	-6,62E+03	5,77E+02
	MWaOA	**-1,98E+05**	**-2,39E+06**	**-7,36E+03**	**5,31E+05**
F9	TTAO	72,36106	36,96365	100,6566	19,19289
	ZOA	3,53E+00	0,00E+00	7,06E+01	1,58E+01
	SCA	68,37239	5,638867	173,4022	45,86052
	ARO	0,00E+00	0,00E+00	0,00E+00	0,00E+00
	SCSO	0,00E+00	0,00E+00	0,00E+00	0,00E+00
	DO	29,37103	8,11E+00	73,89074	16,29224
	GWO	1,02E+01	2,77E-11	4,59E+01	9,72E+00
	WaOA	0,00E+00	0,00E+00	0,00E+00	0,00E+00
	MWaOA	**0,00E+00**	**0,00E+00**	**0,00E+00**	**0,00E+00**
F10	TTAO	6,521846	3,635202	8,627524	1,487937
	ZOA	8,88E-16	8,88E-16	8,88E-16	0,00E+00
	SCA	14,63171	0,537291	20,31696	7,816035
	ARO	1,24E-15	8,88E-16	4,44E-15	1,09E-15
	SCSO	8,88E-16	8,88E-16	8,88E-16	0,00E+00
	DO	0,083329	3,84E-03	1,523692	0,33904
	GWO	1,38E-08	3,96E-09	4,34E-08	9,38E-09
	WaOA	2,31E-15	8,88E-16	4,44E-15	1,79E-15
	MWaOA	**8,88E-16**	**8,88E-16**	**8,88E-16**	**0,00E+00**
F11	TTAO	0,329282	0,119308	0,57801	0,129054
	ZOA	0,00E+00	0,00E+00	0,00E+00	0,00E+00
	SCA	3,622114	0,467573	16,96208	4,14095
	ARO	0,00E+00	0,00E+00	0,00E+00	0,00E+00
	SCSO	0,00E+00	0,00E+00	0,00E+00	0,00E+00
	DO	0,018158	8,21E-04	0,047488	0,015158
	GWO	6,01E-03	4,11E-15	2,65E-02	1,08E-02
	WaOA	0,00E+00	0,00E+00	0,00E+00	0,00E+00
	MWaOA	**0,00E+00**	**0,00E+00**	**0,00E+00**	**0,00E+00**
F12	TTAO	21,97507	5,99451	97,12421	20,65217
	ZOA	2,34E-01	4,99E-02	5,00E-01	1,06E-01

	SCA	108344,3	6,107985	849753,6	235337,3
	ARO	1,51E-03	2,22E-04	5,37E-03	1,48E-03
	SCSO	1,10E-01	5,09E-02	2,18E-01	4,86E-02
	DO	0,17853	6,16E-06	1,666394	0,436488
	GWO	6,30E-02	2,29E-02	2,03E-01	4,16E-02
	WaOA	1,57E-32	1,57E-32	1,57E-32	2,81E-48
	MWaOA	**1,57E-32**	**1,57E-32**	**1,57E-32**	**2,81E-48**
F13	TTAO	69,94719	14,06542	156,813	35,34528
	ZOA	2,25E+00	1,69E+00	2,88E+00	3,23E-01
	SCA	4568193	9805,383	56074535	12385981
	ARO	1,86E-02	4,35E-04	1,08E-01	2,58E-02
	SCSO	2,48E+00	1,14E+00	2,89E+00	3,86E-01
	DO	0,002541	7,27E-05	0,011408	0,004516
	GWO	8,07E-01	3,08E-01	1,38E+00	2,91E-01
	WaOA	1,35E-32	1,35E-32	1,35E-32	2,81E-48
	MWaOA	**1,35E-32**	**1,35E-32**	**1,35E-32**	**2,81E-48**
F14	TTAO	1,886771	0,998004	5,928845	1,807386
	ZOA	1,84E+00	9,98E-01	5,93E+00	1,12E+00
	SCA	2,232872	0,998007	10,76318	2,217235
	ARO	9,98E-01	9,98E-01	9,98E-01	1,61E-16
	SCSO	3,12E+00	9,98E-01	1,08E+01	2,77E+00
	DO	1,047705	9,98E-01	1,992031	0,222271
	GWO	5,21E+00	9,98E-01	1,08E+01	3,96E+00
	WaOA	1,05E+00	9,98E-01	1,99E+00	2,22E-01
	MWaOA	**1,05E+00**	**9,98E-01**	**1,99E+00**	**2,22E-01**
F15	TTAO	0,001109	0,000479	0,002164	0,000592
	ZOA	3,66E-04	3,08E-04	6,01E-04	1,16E-04
	SCA	0,001205	0,000763	0,00159	0,000345
	ARO	3,21E-04	3,08E-04	3,45E-04	1,73E-05
	SCSO	3,46E-04	3,08E-04	5,23E-04	8,68E-05
	DO	0,004146	3,07E-04	0,020363	0,007955
	GWO	7,09E-03	4,00E-04	2,04E-02	1,03E-02
	WaOA	4,60E-04	3,07E-04	1,22E-03	3,74E-04
	MWaOA	**3,27E-04**	**3,07E-04**	**4,24E-04**	**4,77E-05**
F16	TTAO	-1,03163	-1,03163	-1,03163	1,40E-16
	ZOA	-1,03E+00	-1,03E+00	-1,03E+00	9,52E-11
	SCA	-1,03154	-1,03161	-1,03143	5,99E-05
	ARO	-1,03E+00	-1,03E+00	-1,03E+00	1,72E-16
	SCSO	-1,03E+00	-1,03E+00	-1,03E+00	8,52E-10
	DO	-1,03163	-1,03E+00	-1,03163	1,93E-11
	GWO	-1,03E+00	-1,03E+00	-1,03E+00	5,58E-08
	WaOA	-1,03E+00	-1,03E+00	-1,03E+00	0,00E+00
	MWaOA	**-1,03E+00**	**-1,03E+00**	**-1,03E+00**	**0,00E+00**
F17	TTAO	0,397887	0,397887	0,397887	0,00E+00
	ZOA	3,98E-01	3,98E-01	3,98E-01	5,16E-09
	SCA	0,40029	0,398437	0,402798	1,72E-03
	ARO	3,98E-01	3,98E-01	3,98E-01	0,00E+00
	SCSO	3,98E-01	3,98E-01	3,98E-01	5,20E-08
	DO	0,397887	3,98E-01	0,397887	2,56E-11
	GWO	3,98E-01	3,98E-01	3,98E-01	3,08E-06
	WaOA	3,98E-01	3,98E-01	3,98E-01	0,00E+00
	MWaOA	**3,98E-01**	**3,98E-01**	**3,98E-01**	**0,00E+00**

	TTAO	3	3	3	2,63E-15
	ZOA	3,00E+00	3,00E+00	3,00E+00	1,51E-05
	SCA	3,000196	3,000036	3,000835	3,15E-04
	ARO	3,00E+00	3,00E+00	3,00E+00	2,18E-15
F18	SCSO	3,00E+00	3,00E+00	3,00E+00	4,15E-05
	DO	3	3,00E+00	3	2,85E-08
	GWO	1,65E+01	3,00E+00	8,40E+01	3,31E+01
	WaOA	3,00E+00	3,00E+00	3,00E+00	6,59E-16
	MWaOA	**3,00E+00**	**3,00E+00**	**3,00E+00**	**6,88E-16**
	TTAO	-3,86278	-3,86278	-3,86278	3,44E-16
	ZOA	-3,73E+00	-3,86E+00	-3,09E+00	3,15E-01
	SCA	-3,84944	-3,85468	-3,83556	7,00E-03
	ARO	-3,86E+00	-3,86E+00	-3,86E+00	1,99E-16
F19	SCSO	-3,86E+00	-3,86E+00	-3,86E+00	1,80E-03
	DO	-3,86278	-3,86E+00	-3,86278	2,66E-08
	GWO	-3,86E+00	-3,86E+00	-3,85E+00	3,59E-03
	WaOA	-3,86E+00	-3,86E+00	-3,86E+00	0,00E+00
	MWaOA	**-3,86E+00**	**-3,86E+00**	**-3,86E+00**	**0,00E+00**
	TTAO	-3,3186	-3,322	-3,3032	7,57E-03
	ZOA	-3,30E+00	-3,32E+00	-3,20E+00	4,89E-02
	SCA	-2,87325	-3,00794	-2,24282	3,09E-01
	ARO	-3,28E+00	-3,32E+00	-3,20E+00	6,14E-02
F20	SCSO	-3,20E+00	-3,32E+00	-3,02E+00	1,37E-01
	DO	-3,28236	-3,32E+00	-3,20308	6,14E-02
	GWO	-3,28E+00	-3,32E+00	-3,09E+00	9,28E-02
	WaOA	-3,30E+00	-3,32E+00	-3,20E+00	4,85E-02
	MWaOA	**-3,26E+00**	**-3,32E+00**	**-3,20E+00**	**6,51E-02**
	TTAO	-10,1179	-10,1532	-9,95823	7,85E-02
	ZOA	-9,30E+00	-1,02E+01	-5,06E+00	2,08E+00
	SCA	-1,48882	-2,10484	-0,88072	5,04E-01
	ARO	-1,02E+01	-1,02E+01	-1,02E+01	2,01E-10
F21	SCSO	-5,06E+00	-5,10E+00	-5,06E+00	1,85E-02
	DO	-6,80355	-1,02E+01	-2,63047	3,78E+00
	GWO	-8,90E+00	-1,02E+01	-2,63E+00	3,07E+00
	WaOA	-1,02E+01	-1,02E+01	-1,02E+01	1,59E-15
	MWaOA	**-9,30E+00**	**-1,02E+01**	**-5,06E+00**	**2,08E+00**
	TTAO	-10,3664	-10,4029	-10,2897	5,37E-02
	ZOA	-9,52E+00	-1,04E+01	-5,09E+00	2,17E+00
	SCA	-1,74216	-3,52313	-0,52399	1,16E+00
	ARO	-9,52E+00	-1,04E+01	-5,09E+00	2,17E+00
F22	SCSO	-5,59E+00	-1,04E+01	-2,77E+00	2,54E+00
	DO	-6,74183	-1,04E+01	-2,75193	4,03E+00
	GWO	-9,51E+00	-1,04E+01	-5,09E+00	2,17E+00
	WaOA	-1,04E+01	-1,04E+01	-1,04E+01	0,00E+00
	MWaOA	**-8,63E+00**	**-1,04E+01**	**-5,09E+00**	**2,74E+00**
	TTAO	-10,0412	-10,5364	-8,43827	8,53E-01
	ZOA	-9,64E+00	-1,05E+01	-5,13E+00	2,21E+00
	SCA	-4,19986	-6,94689	-0,94858	1,92E+00
F23	ARO	-1,05E+01	-1,05E+01	-1,05E+01	2,71E-06
	SCSO	-7,83E+00	-1,05E+01	-5,13E+00	2,96E+00
	DO	-6,12043	-1,05E+01	-2,42734	3,61E+00
	GWO	-1,05E+01	-1,05E+01	-1,05E+01	2,57E-03

WaOA	-8,73E+00	-1,05E+01	-5,13E+00	2,79E+00
MWaOA	**-9,64E+00**	**-1,05E+01**	**-5,13E+00**	**2,21E+00**

According to Table III. 5, the proposed MWaOA optimizer outperforms the others in terms of the mean and best values for most of the studied functions. Based on this, compared to the other optimizers, the MWaOA optimizer was able to locate both the best solution and better options on average.

III.7.1.2. Analysis of the convergence curves

The convergence plots of the MWaOA algorithm and other previously documented methods, including SCSO, GWO, DO, TTAO, ARO, ZOA, CDO, and standard WaOA, are shown in Figure III.5.

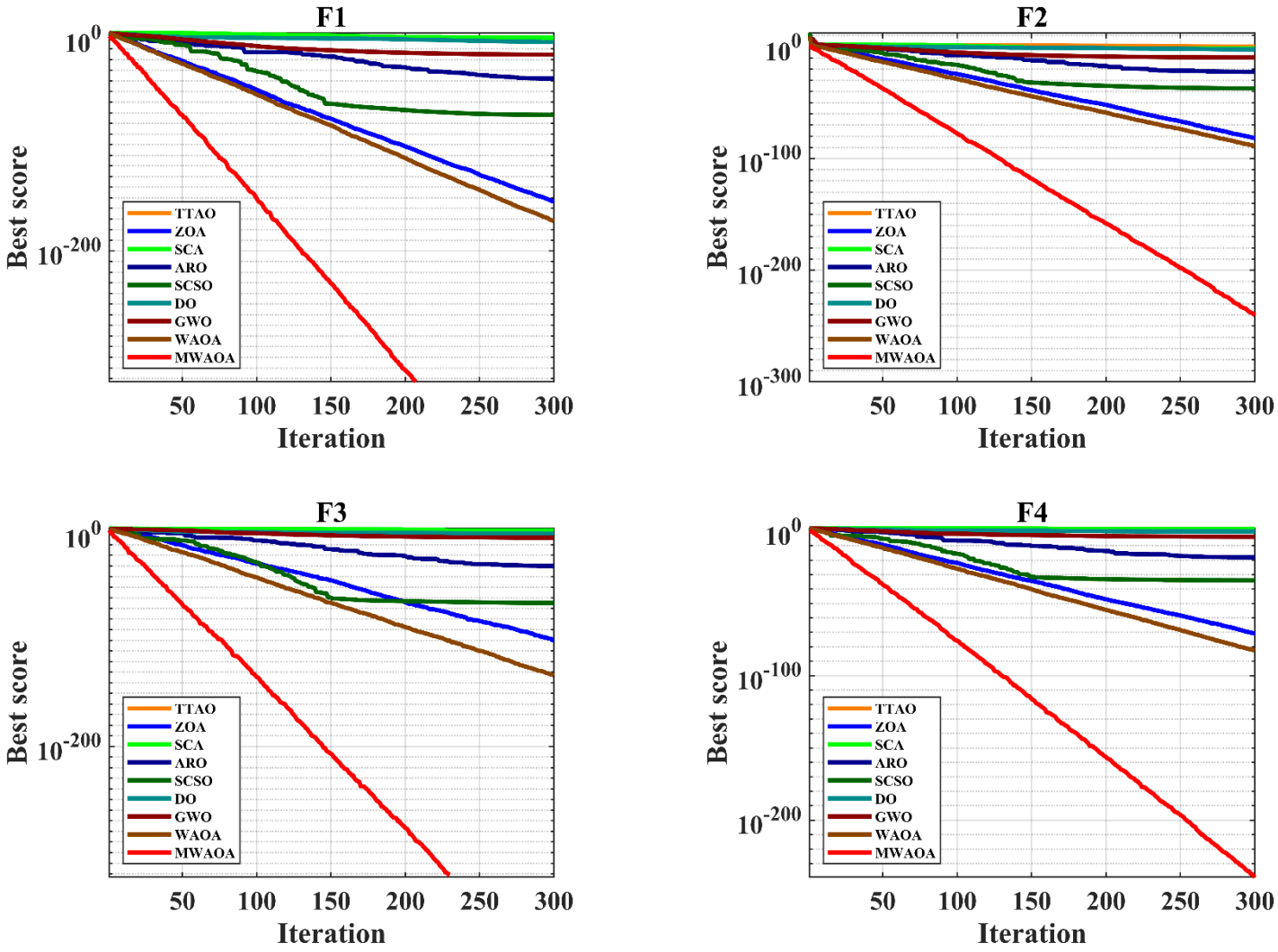

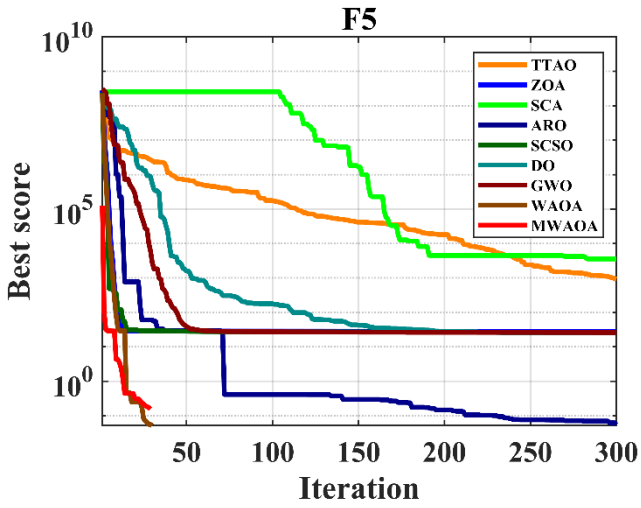
F5
Best score
Iteration
TTAO
ZOA
SCA
ARO
SCSO
DO
GWO
WAOA
MWAOA

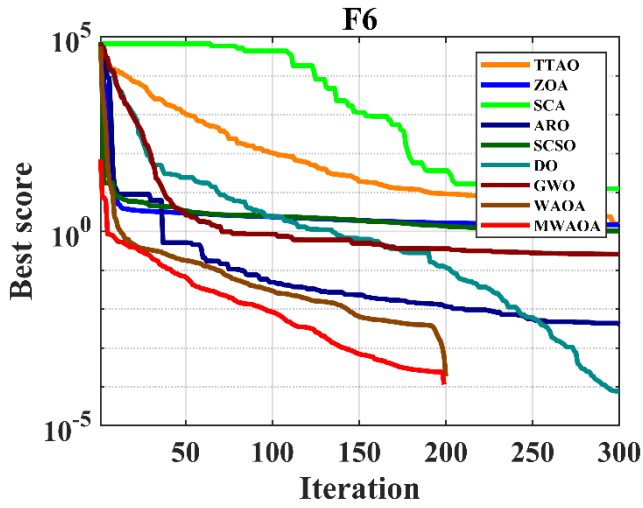
F6
Best score
Iteration
TTAO
ZOA
SCA
ARO
SCSO
DO
GWO
WAOA
MWAOA

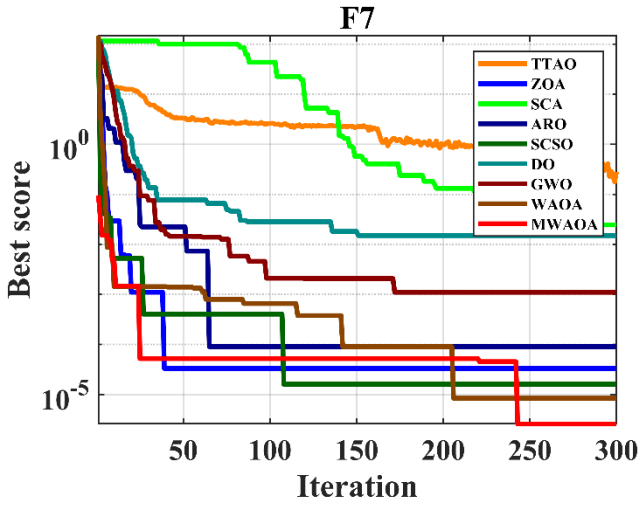
F7
Best score
Iteration
TTAO
ZOA
SCA
ARO
SCSO
DO
GWO
WAOA
MWAOA

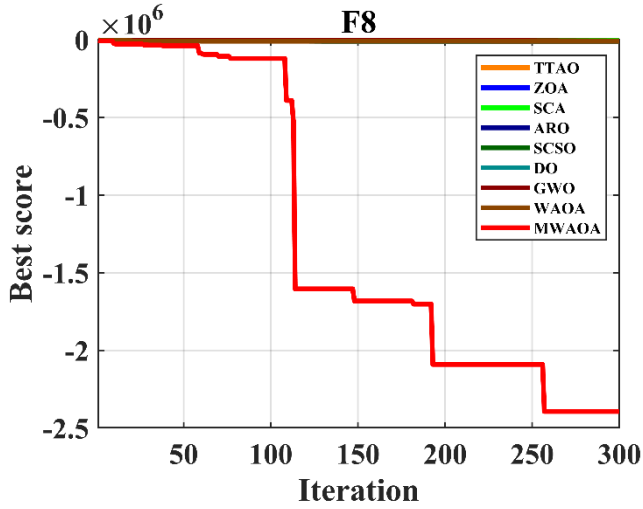
F8
Best score
Iteration
TTAO
ZOA
SCA
ARO
SCSO
DO
GWO
WAOA
MWAOA

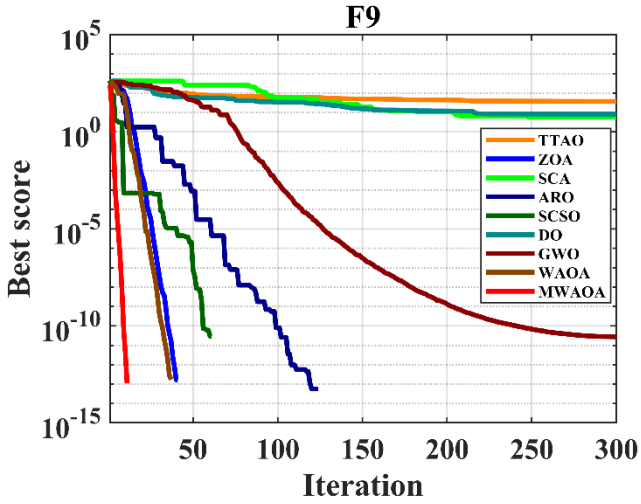
F9
Best score
Iteration
TTAO
ZOA
SCA
ARO
SCSO
DO
GWO
WAOA
MWAOA

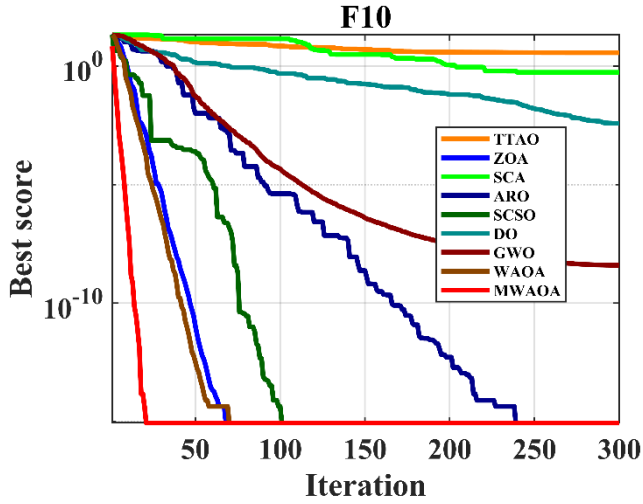
F10
Best score
Iteration
TTAO
ZOA
SCA
ARO
SCSO
DO
GWO
WAOA
MWAOA

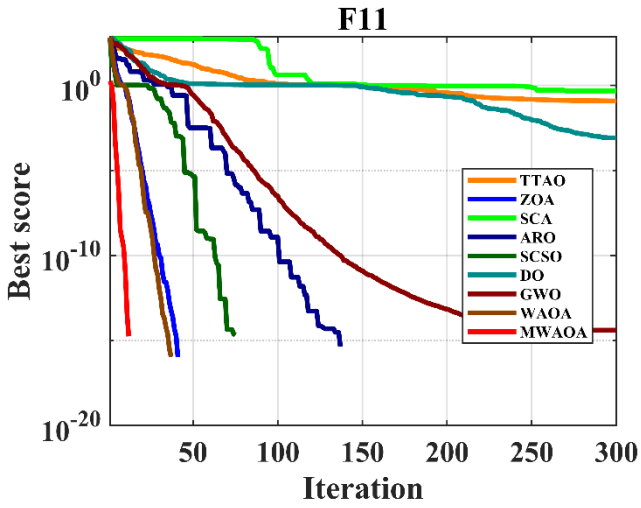
F11
Best score
Iteration
TTAO
ZOA
SCA
ARO
SCSO
DO
GWO
WAOA
MWAOA

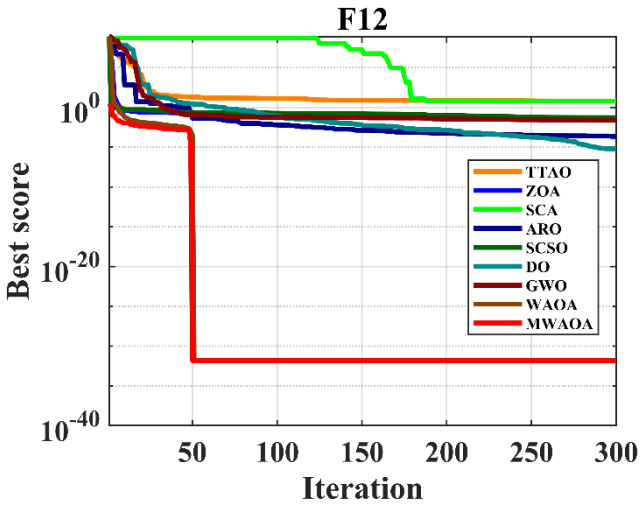
F12
Best score
Iteration
TTAO
ZOA
SCA
ARO
SCSO
DO
GWO
WAOA
MWAOA

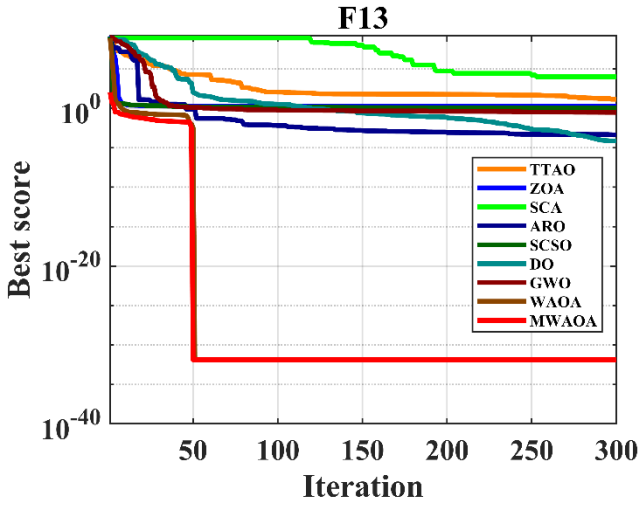
F13
Best score
Iteration
TTAO
ZOA
SCA
ARO
SCSO
DO
GWO
WAOA
MWAOA

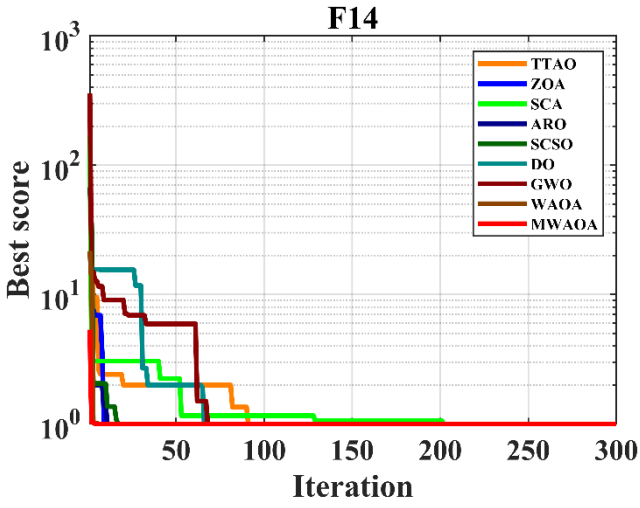
F14
Best score
Iteration
TTAO
ZOA
SCA
ARO
SCSO
DO
GWO
WAOA
MWAOA

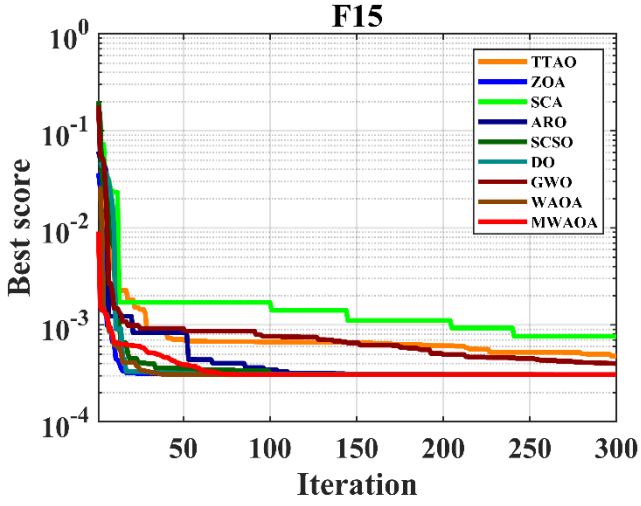
F15
Best score
Iteration
TTAO
ZOA
SCA
ARO
SCSO
DO
GWO
WAOA
MWAOA

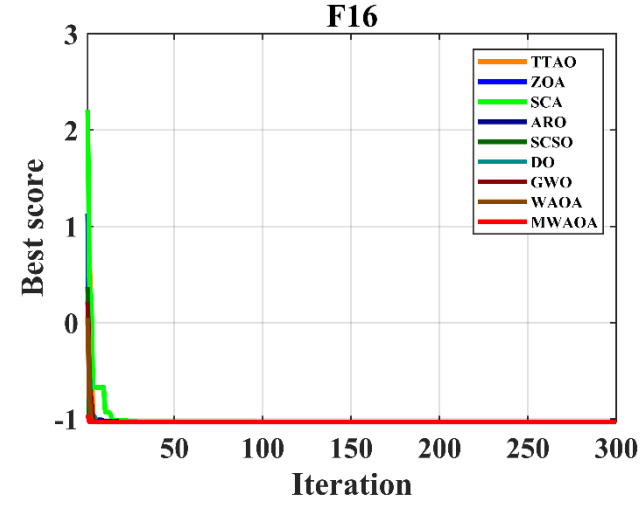
F16
Best score
Iteration
TTAO
ZOA
SCA
ARO
SCSO
DO
GWO
WAOA
MWAOA

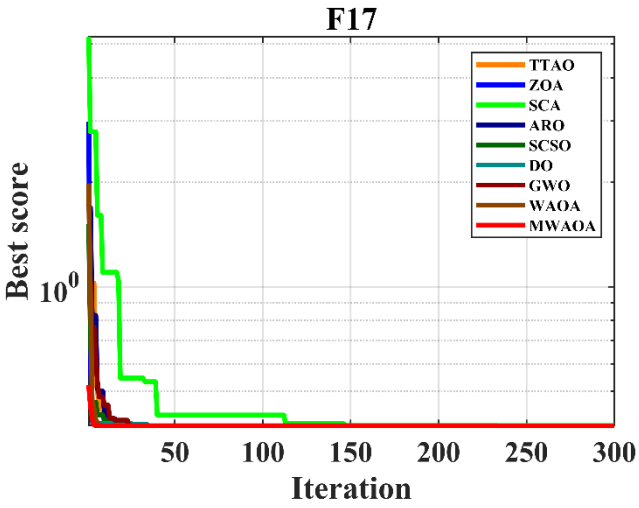
F17
Best score
Iteration
TTAO
ZOA
SCA
ARO
SCSO
DO
GWO
WAOA
MWAOA

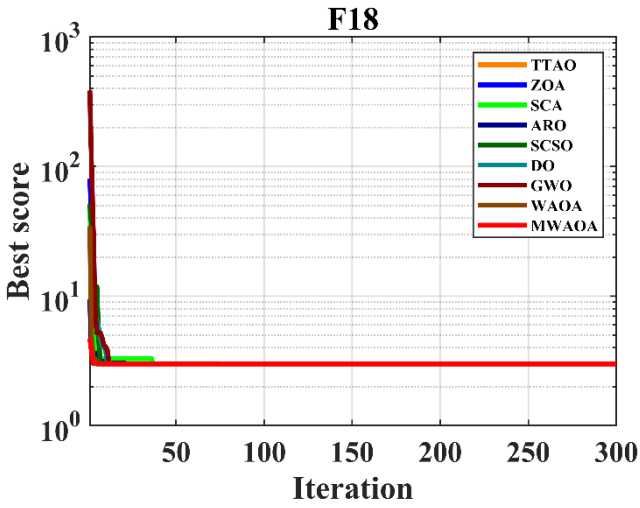
F18
Best score
Iteration
TTAO
ZOA
SCA
ARO
SCSO
DO
GWO
WAOA
MWAOA

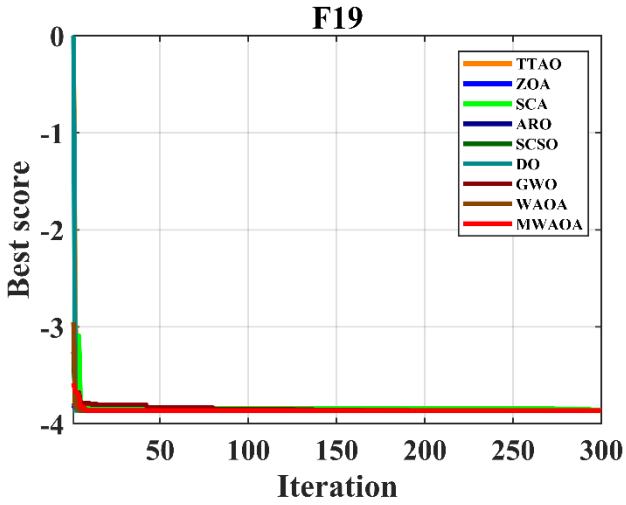
F19
Best score
Iteration
TTAO
ZOA
SCA
ARO
SCSO
DO
GWO
WAOA
MWAOA

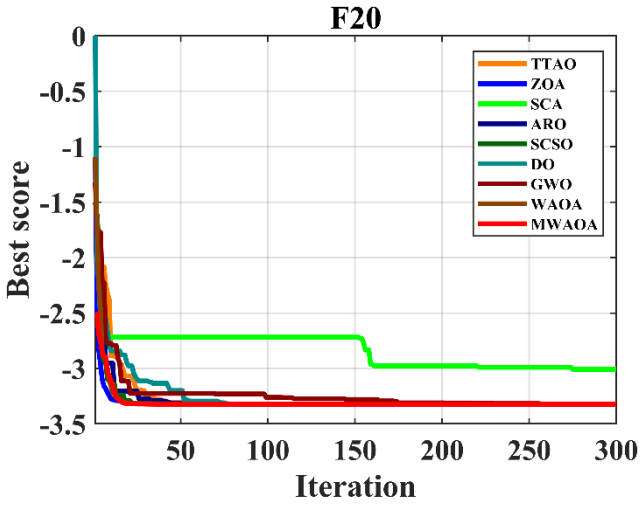
F20
Best score
Iteration
TTAO
ZOA
SCA
ARO
SCSO
DO
GWO
WAOA
MWAOA

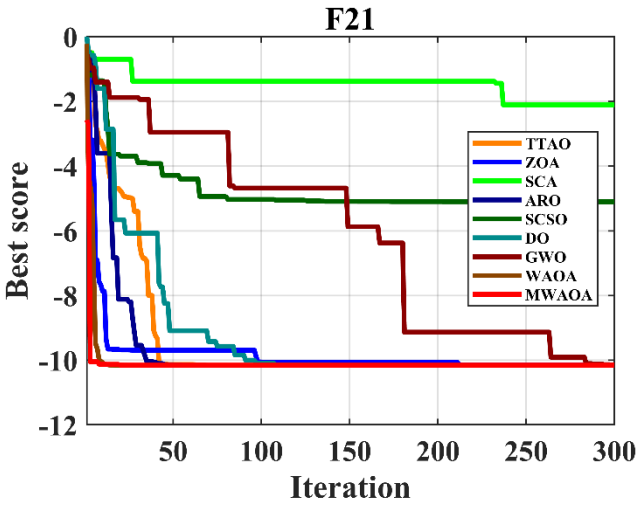
F21
Best score
Iteration
TTAO
ZOA
SCA
ARO
SCSO
DO
GWO
WAOA
MWAOA

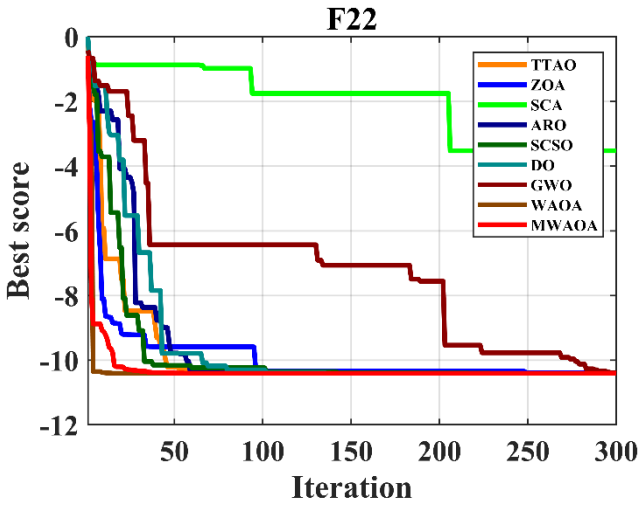
F22
Best score
Iteration
TTAO
ZOA
SCA
ARO
SCSO
DO
GWO
WAOA
MWAOA

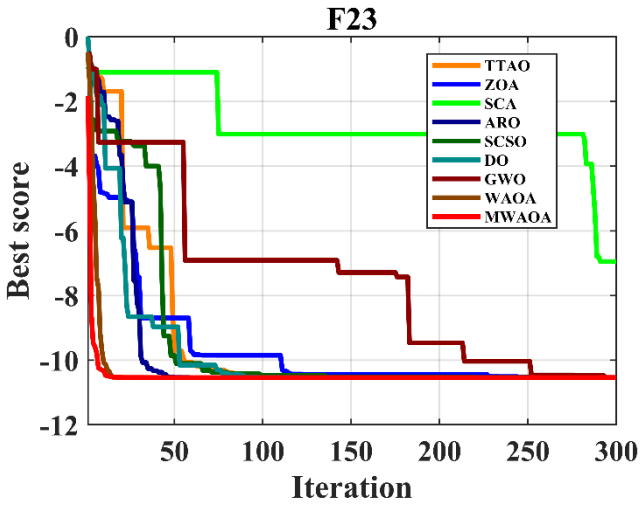

Figure III.5: Convergence analysis of various optimizers on test benchmark functions.

Based on the convergence curves, it was demonstrated that the suggested MWaOA method is quicker and more accurate than previous algorithms. The suggested alteration to the WaOA algorithm improves its exploration stage, enabling it to reach an optimal solution faster than the conventional WaOA method.

III.7.1.3. Examining data using boxplots

Boxplot graphs are a useful tool for examining data distribution characteristics because they efficiently illustrate patterns of data [171]. The boxplots for the suggested MWaOA approach and other known optimization strategies are displayed in Figure III.6. MWaOA's boxplots clearly show a narrower spread than those of the other optimization methods.

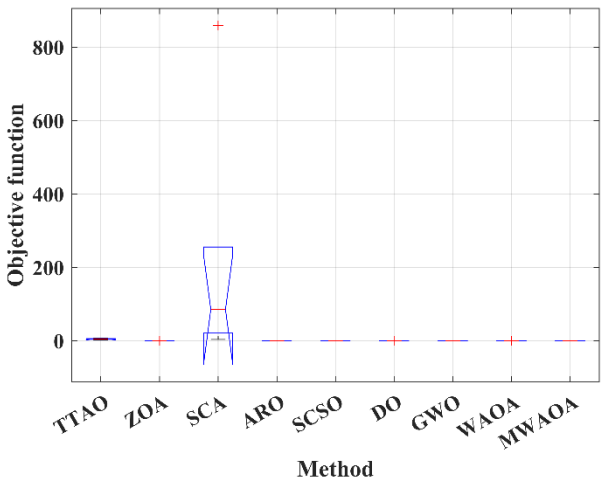

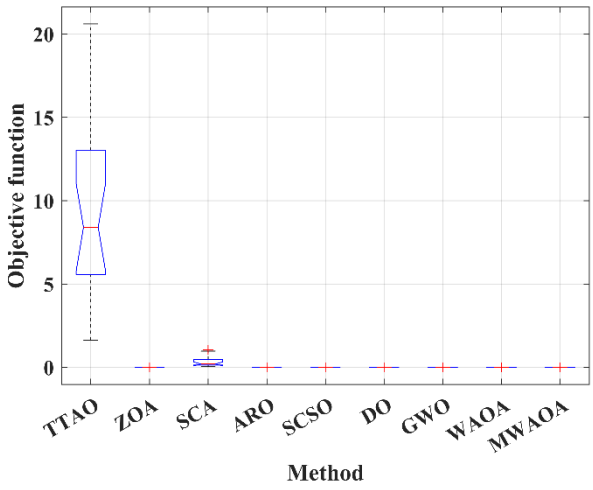

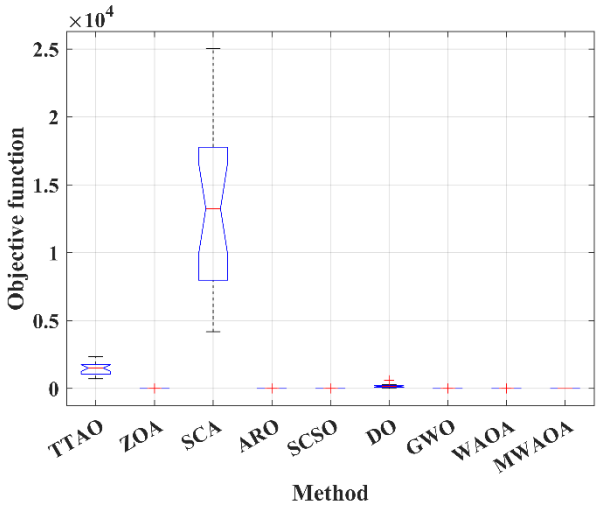
×10^4
Objective function
Method
TTAO
ZOA
SCA
ARO
SCSO
DO
GWO
WAOA
MWAOA

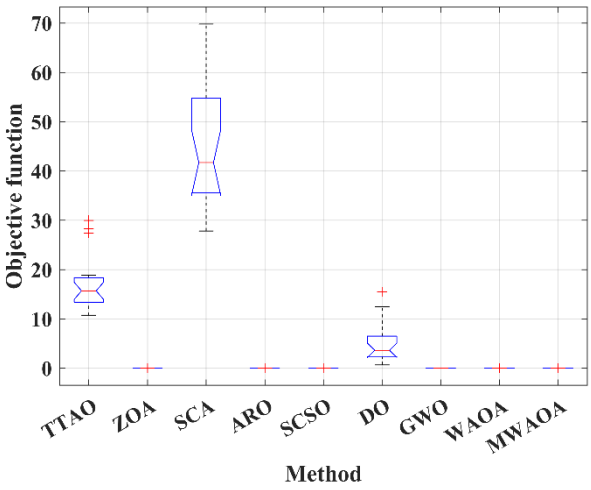
Objective function
Method
TTAO
ZOA
SCA
ARO
SCSO
DO
GWO
WAOA
MWAOA

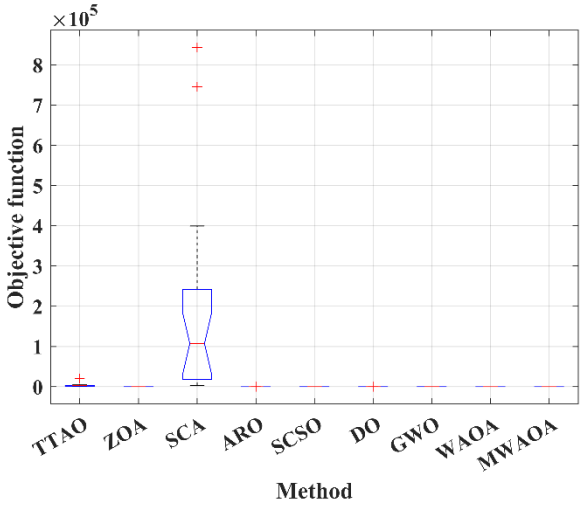
×10^5
Objective function
Method
TTAO
ZOA
SCA
ARO
SCSO
DO
GWO
WAOA
MWAOA

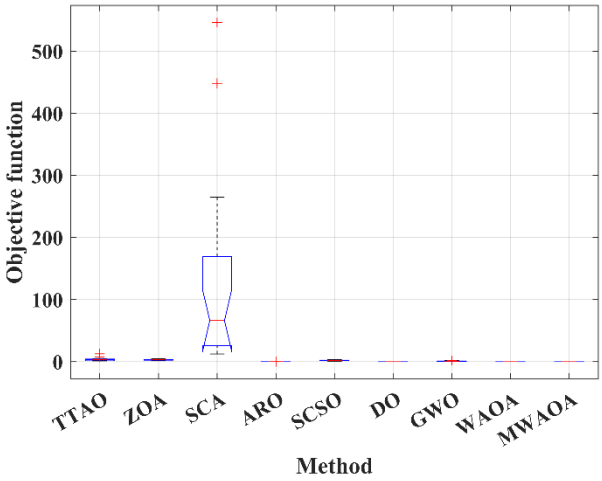
Objective function
Method
TTAO
ZOA
SCA
ARO
SCSO
DO
GWO
WAOA
MWAOA

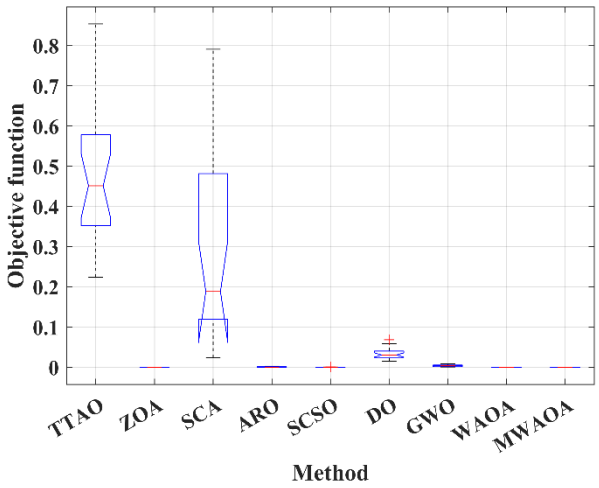
Objective function
Method
TTAO
ZOA
SCA
ARO
SCSO
DO
GWO
WAOA
MWAOA

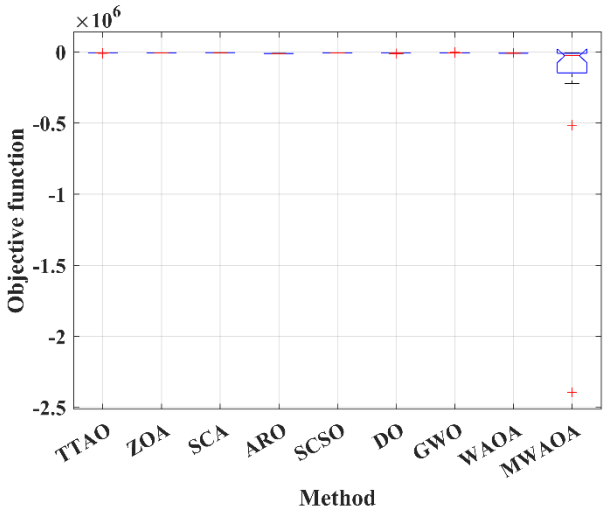
×10^6
Objective function
Method
TTAO
ZOA
SCA
ARO
SCSO
DO
GWO
WAOA
MWAOA

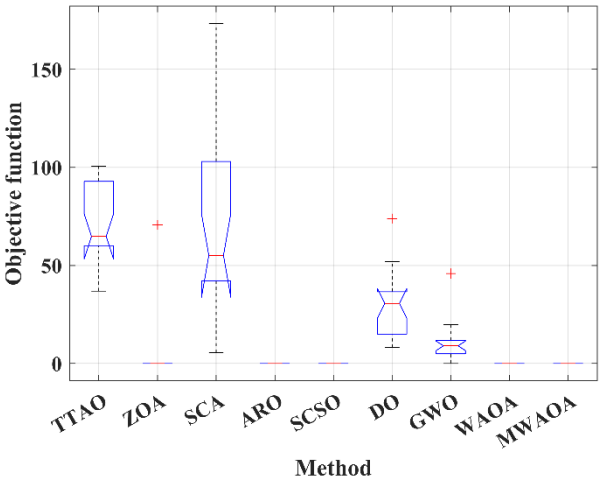
Objective function
150
100
50
0
TTAO
ZOA
SCA
ARO
SCSO
DO
GWO
WAOA
MWAOA
Method

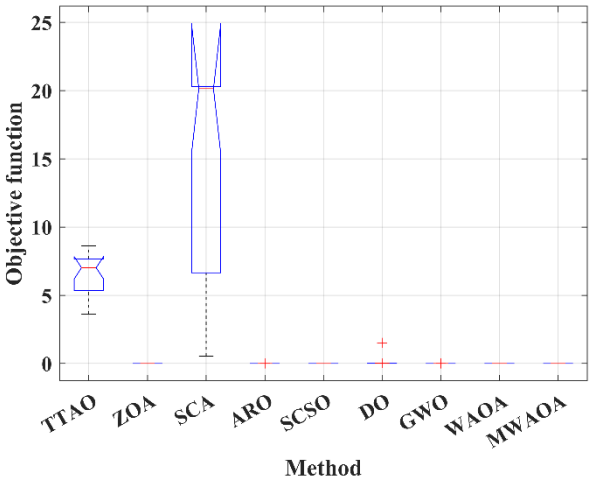
Objective function
25
20
15
10
5
0
TTAO
ZOA
SCA
ARO
SCSO
DO
GWO
WAOA
MWAOA
Method

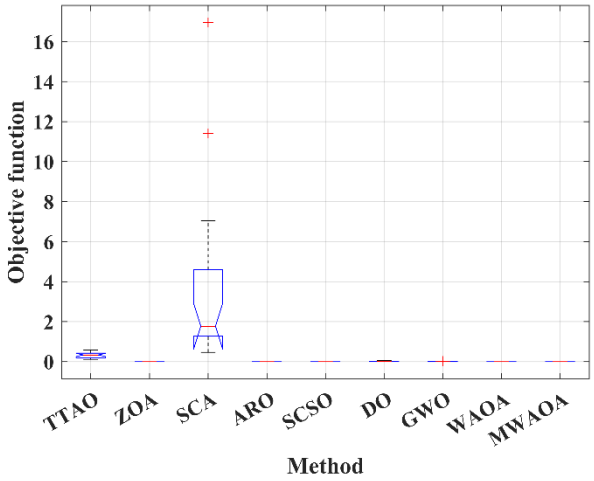
Objective function
16
14
12
10
8
6
4
2
0
TTAO
ZOA
SCA
ARO
SCSO
DO
GWO
WAOA
MWAOA
Method

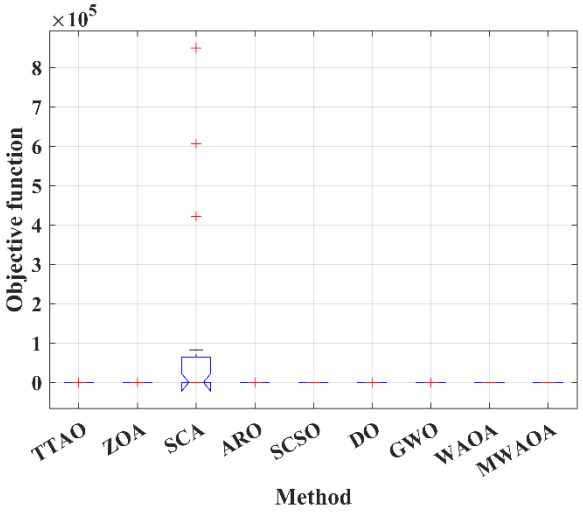
×10^5
Objective function
8
7
6
5
4
3
2
1
0
TTAO
ZOA
SCA
ARO
SCSO
DO
GWO
WAOA
MWAOA
Method

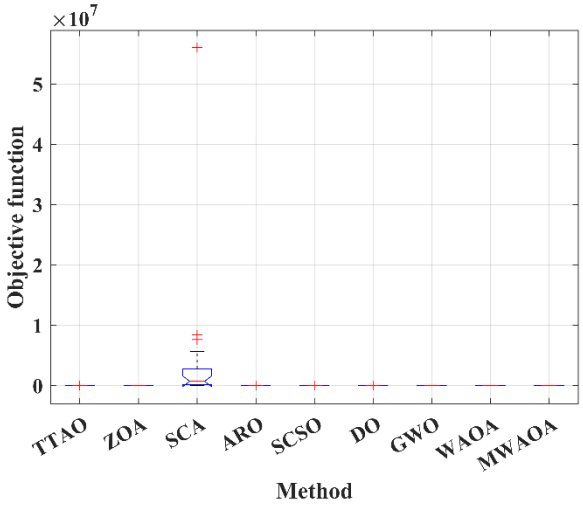
×10^7
Objective function
5
4
3
2
1
0
TTAO
ZOA
SCA
ARO
SCSO
DO
GWO
WAOA
MWAOA
Method

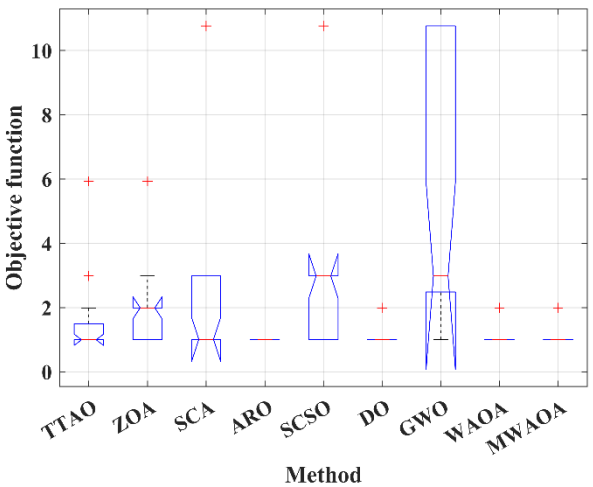
Objective function
10
8
6
4
2
0
TTAO
ZOA
SCA
ARO
SCSO
DO
GWO
WAOA
MWAOA
Method

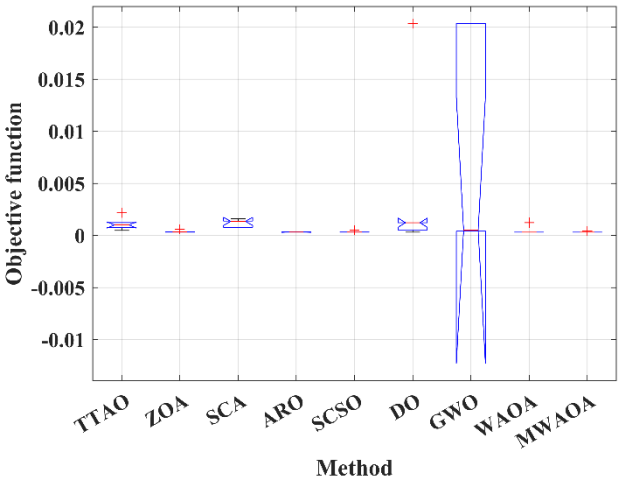
Objective function
0.02
0.015
0.01
0.005
0
-0.005
-0.01
TTAO
ZOA
SCA
ARO
SCSO
DO
GWO
WAOA
MWAOA
Method

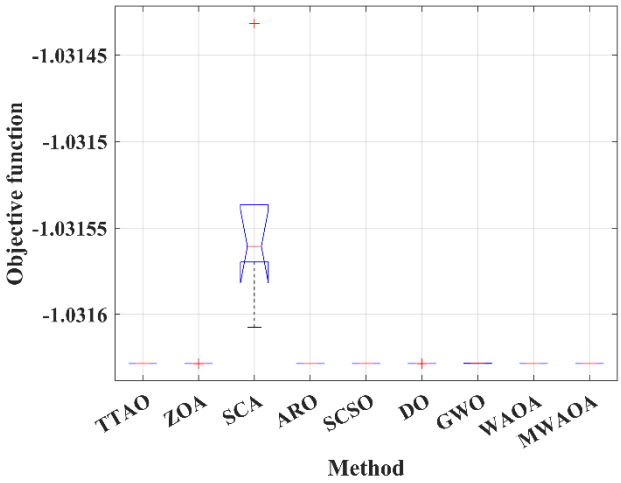
Objective function
-1.03145
-1.0315
-1.03155
-1.0316
TTAO
ZOA
SCA
ARO
SCSO
DO
GWO
WAOA
MWAOA
Method

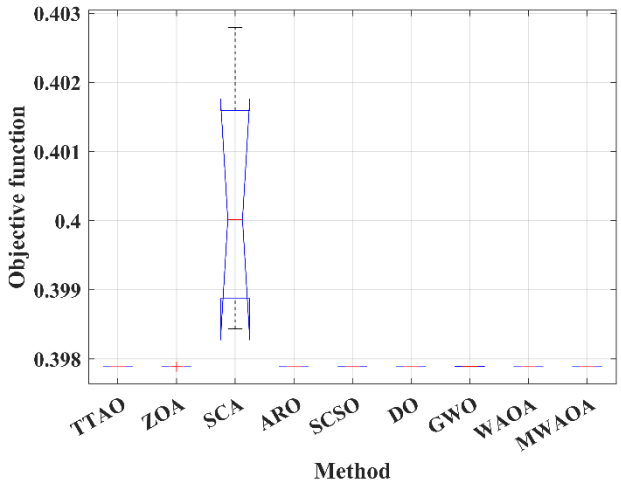
Objective function
0.403
0.402
0.401
0.4
0.399
0.398
TTAO
ZOA
SCA
ARO
SCSO
DO
GWO
WAOA
MWAOA
Method

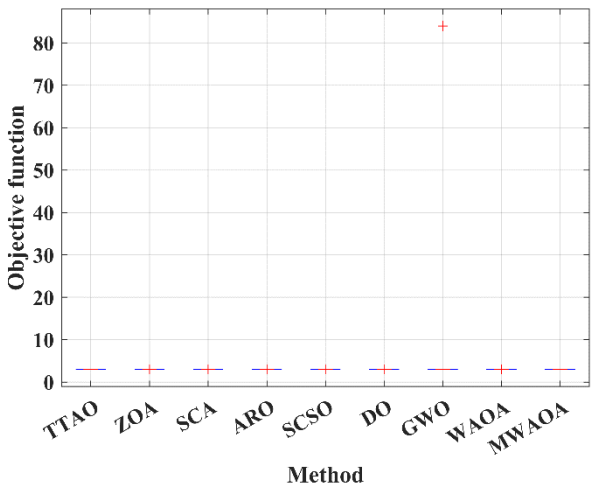
Objective function
80
70
60
50
40
30
20
10
0
TTAO
ZOA
SCA
ARO
SCSO
DO
GWO
WAOA
MWAOA
Method

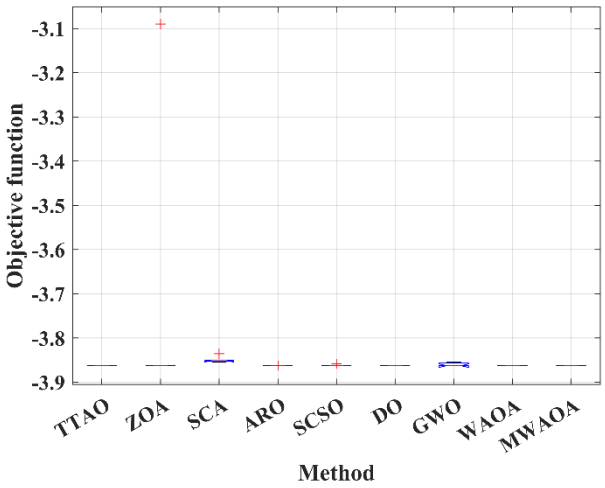
Objective function
-3.1
-3.2
-3.3
-3.4
-3.5
-3.6
-3.7
-3.8
-3.9
TTAO
ZOA
SCA
ARO
SCSO
DO
GWO
WAOA
MWAOA
Method

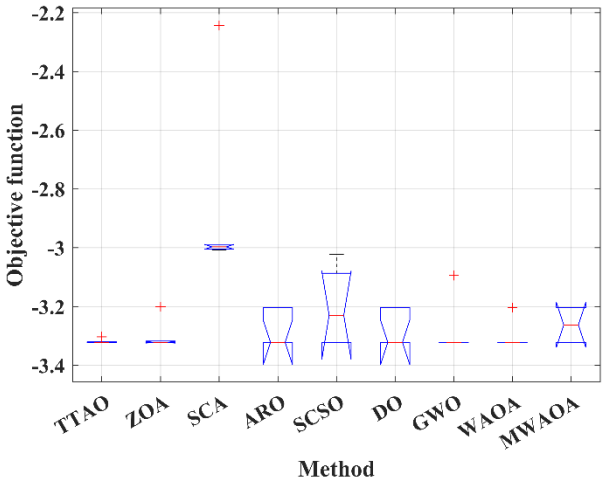
Objective function
-2.2
-2.4
-2.6
-2.8
-3
-3.2
-3.4
TTAO
ZOA
SCA
ARO
SCSO
DO
GWO
WAOA
MWAOA
Method

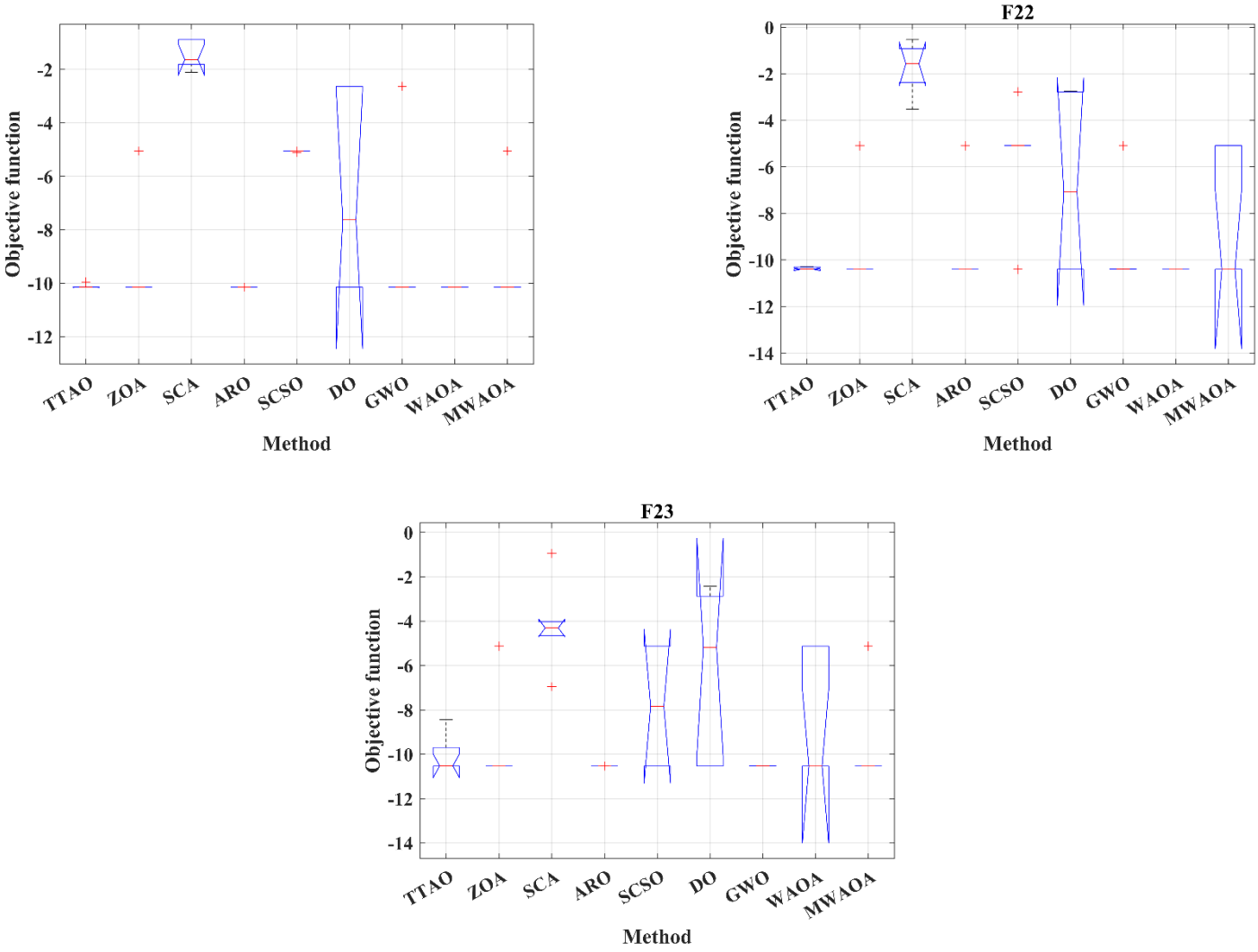

Figure III.6: Boxplot assessment with different techniques applied to test functions.

III.8. Conclusion

This chapter has presented a Modified Walrus Optimization Algorithm (MWaOA) that integrates Levy flight to enhance its capabilies in searching for optimal solution. The performance of MWaOA was evaluated on 23 benchmark functions and compared against several state-of-the-art optimization algorithms including Sand Cat Swarm Optimization (SCSO), Triangulation Topology Aggregation Optimizer (TTAO), Dandelion Optimizer (DO), Gray Wolf Optimization (GWO), Zebra Optimization Algorithm (ZOA), Sine Cosine Algorithm (SCA), Artificial Rabbits Optimization (ARO), and standard walrus behavior (WaOA).The results analysis, including statistical findings, convergence plots, and boxplots, demonstrated MWaOA's superior optimization ability over these existing methods.

Specifically, MWaOA attained better solutions on average and identified optimal solutions with fewer iterations. The modifications made to the standard WaOA's feeding, migration, and predator escape mechanisms allowed more thorough exploration via occasional longer jumps. This facilitated escaping local optima and discovering new promising areas.

Overall, the proposed MWaOA displayed faster convergence and consistently outperformed its competitors across diverse problem landscapes. This affirms the benefits of assimilating Levy flight to amplify the exploration-exploitation balance.

CHAPTER IV

Optimal Distribution Network Operation with Renewable Energy Sources

IV.1. Introduction

This chapter explores the optimal locations and sizes of Renewable Energy Resources in two distinct scenarios. The first scenario assumes the absence of uncertainty, while the second scenario incorporates the presence of uncertainty. The effectiveness of the presented methods is evaluated through testing on various test cases, encompassing standard IEEE EDNs such as IEEE 33-Bus and IEEE 69-Bus. The analyzed cases are comprehensive, including the optimal integration of Photovoltaic (PV) units and wind turbines (WT). The methodologies employed consist of the presented methods and a forward-backward sweep-based power flow algorithm. The implementation of the program code is executed in MATLAB software, with simulations conducted on a PC featuring an i7-3537U CPU operating at 2.5 GHz and 6 GB RAM, using MATLAB 2021a. The ensuing section will presents and will discusses all simulation results for the test cases. The suggested methods have a fixed population size and a maximum iteration count set at 30 and 100, respectively. This chapter is structured to examine applied algorithms for both single and multi-objective functions, encompassing technical and economic objective functions.

IV.2. Case study of a system in the absence of uncertainty (24-hour period)

This case study focuses on a thorough examination of a system operating over a 24-hour period in a controlled environment devoid of uncertainty. By isolating the system from unpredictable factors, our aim is to unravel its inherent behavior and characteristics. This initial exploration lays the foundation for a clearer understanding of the system's dynamics, paving the way for subsequent analyses that will consider the impact of uncertainties on its performance. In Figure IV.1, the day-ahead load demand is depicted, providing a comprehensive view of the anticipated load requirements. Concurrently, Figure IV.2 showcases the market price for energy procurement, offering insights into the economic aspects of the energy market. Furthermore, Figures IV.3, IV.4, and IV.5 delve into critical meteorological factors, presenting the expected wind speed, irradiance, and temperature, respectively. These visualizations contribute to a holistic understanding of the dynamic elements influencing the energy system, aiding in strategic decision-making and resource planning.

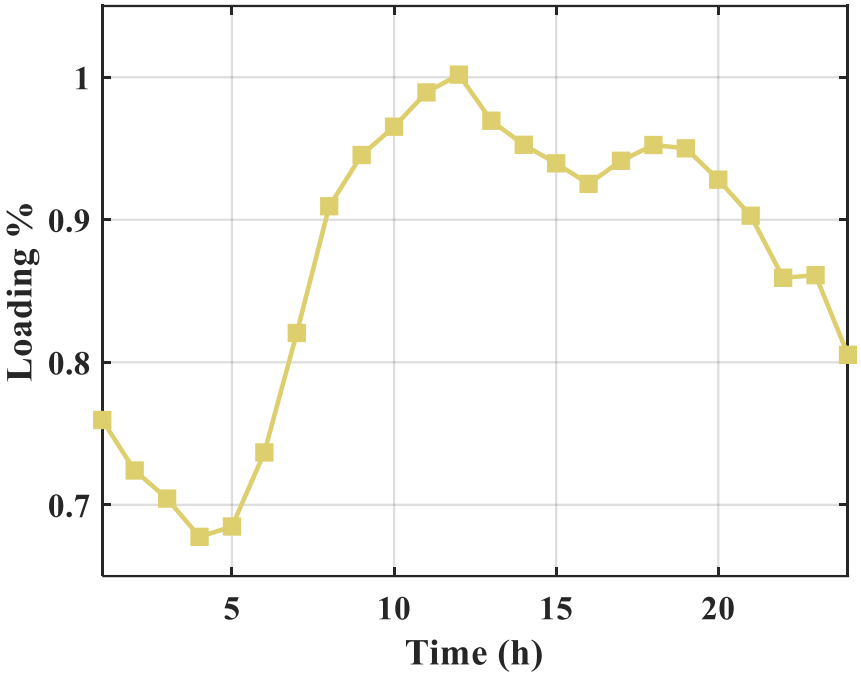

Figure IV.1: The load profile.

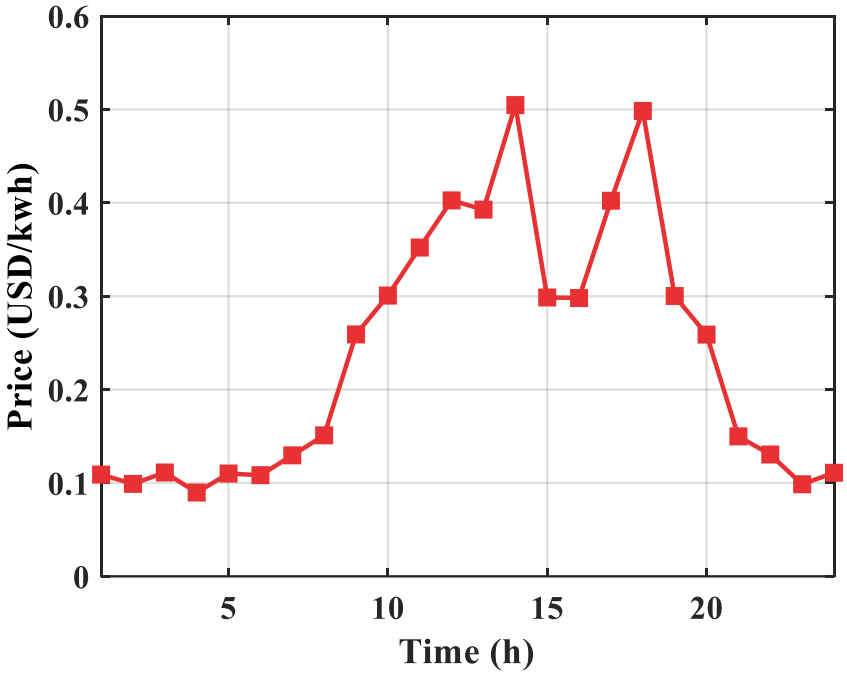

Figure IV.2: The price profile.

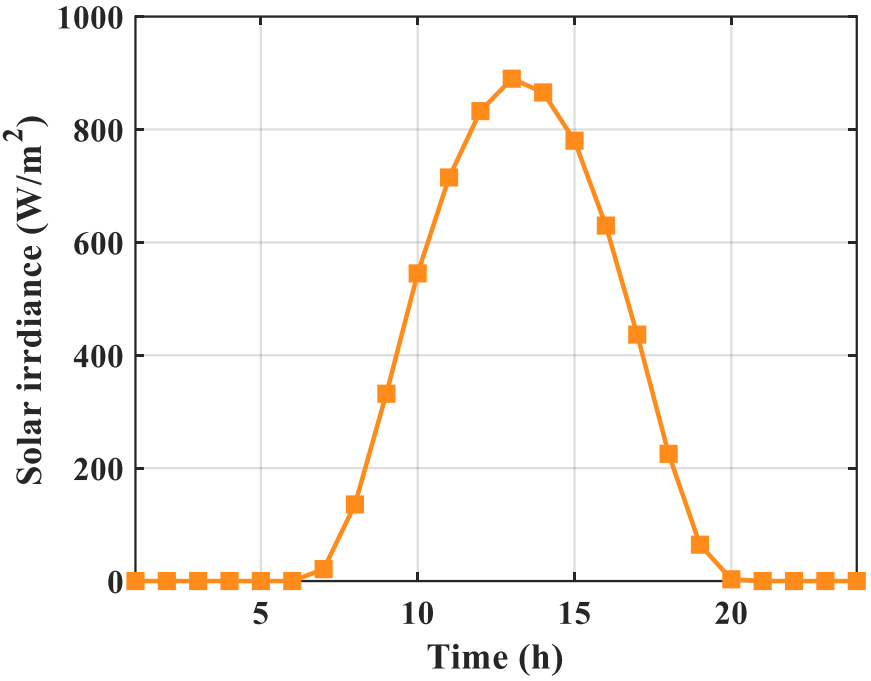

Figure IV.3: The solar irradiance profile.

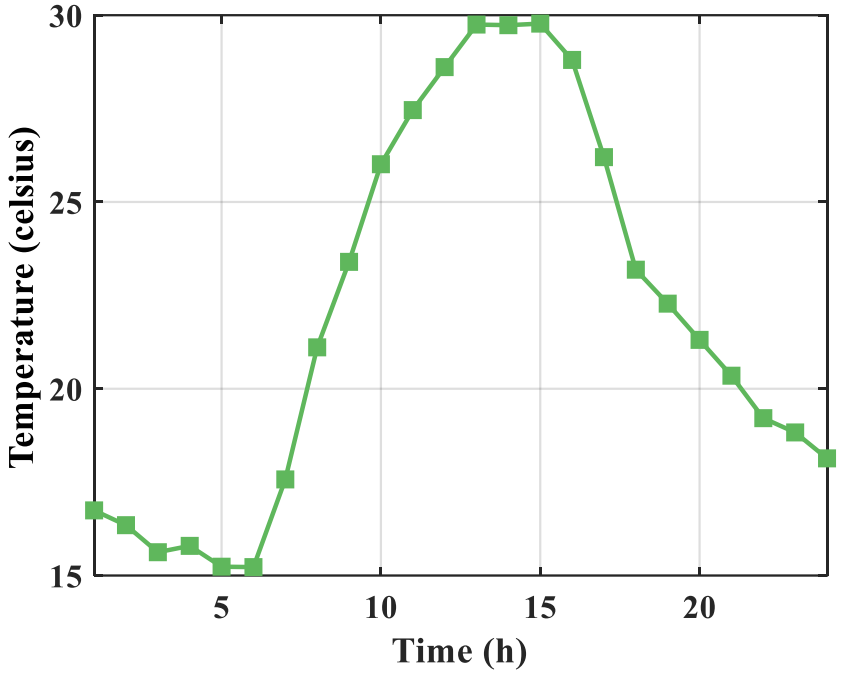

Figure IV.4: The temperature profile.

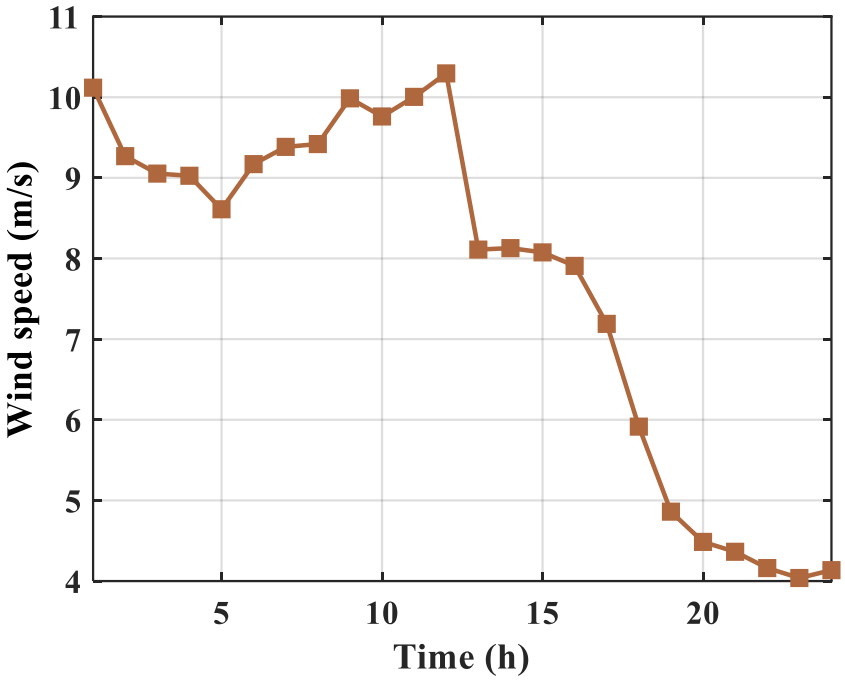

Figure IV.5: The wind speed profile.

IV.2.1. Single objective function

IV.2.1.1. Total real power loss minimization

The computation of total real power losses $TRPL$ in an EDN with NT branches is elucidated through equations [172]:

$$\boldsymbol{f = min}\left(\frac{\boldsymbol{TRPL_{RESs}}}{\boldsymbol{TRPL_{Base}}}\right) \quad \text{(IV.1)}$$

$$TRPL = \sum_{h=1}^{24}\sum_{i=1}^{NT} P_{Loss(i,h)} \quad \text{(IV.2)}$$

$$P_{Loss(i,h)} = \left|I_{(i,h)}\right|^2 R_i = \left(\frac{P_{s(i,h)}^2 + Q_{s(i,h)}^2}{\left|V_{s(i,h)}\right|^2}\right) R_i \quad \text{(IV.3)}$$

where P_s and Q_s are the active and reactive powers flowing through the line, respectively, $|V_s|$ is the voltage magnitude at the sending end bus of the branch, and $|I|$ indicates the amount of branch current. $RESs$ and $Base$ are subscripts refer to with RESs and the base case,

respectively. R is the resistance of the branch.

IV.2.1.2. Inequality and equality constraints

The objective function must satisfy all equality and inequality constraints.

IV.2.1.2.1. Inequality constraints

$$V_{min} \leq V_{(i,h)} \leq V_{max} \tag{IV.4}$$

$$\sum_{i=1}^{Ns} P_{PV\_rated(i,h)} + \sum_{i=1}^{Ns} P_{WT\_rated(i,h)} \leq \sum_{i=1}^{NB} P_{Load(i,h)} \tag{IV.5}$$

$$PF_{min} \leq PF_{(i,h)} \leq PF_{max} \qquad i = 1,2,\dots,Ns \tag{IV.6}$$

$$I_{(i,h)} \leq I_{max,i} \qquad i = 1,2,\dots,NT \tag{IV.7}$$

where the lower and upper voltage limitations are denoted by V_{min} and V_{max}, respectively. P_{Load} represents the real load. The number of buses in the network is specified by NB. I_{max} is the maximum allowable current limit of the line. P_{PV_rated} and P_{WT_rated} are the maximum amount of power that the PV and WT system can generate. The WT power factor has a minimum of PF_{min} and a maximum of PF_{max}. The photovoltaic farms' power factor have to be one. The PV/WT system number is Ns.

IV.2.1.2.2. Equality constraints

$$P_{SS,h} + \sum_{i=1}^{Ns} P_{PV(i,h)} + \sum_{i=1}^{Ns} P_{WT(i,h)} = \sum_{i=1}^{NT} P_{Loss(i,h)} + \sum_{i=1}^{NB} P_{Load(i,h)} \tag{IV.8}$$

$$Q_{SS,h} + \sum_{i=1}^{Ns} Q_{WT(i,h)} = \sum_{i=1}^{NT} Q_{Loss(i,h)} + \sum_{i=1}^{NB} Q_{Load(i,h)} \tag{IV.9}$$

where the main network's hourly reactive and real powers are denoted by $Q_{SS,h}$ and $P_{SS,h}$, respectively. The hourly generated power from the system's WTs and PVs is indicated by the variables $P_{WT(i,h)}$ and $P_{PV(i,h)}$.

IV.2.2. Results of IEEE 33-bus and 69-bus for single objective function

In this study, the proposed MWaOA algorithm was evaluated using EDN of 33-bus and 69-bus under various scenarios for PVs and WTs unit allocation. The IEEE 33-bus EDN, as illustrated in Figure IV.6, consists of 33 buses and 32 branches and was used as a test case. The total load on this radial system is 3715 kW and 2300 kVAR. The IEEE 69-bus EDN, which contains 69 buses and 68 branches, was also used as a test case. This system has a total load of 3802.19 kW and 2694.6 kVAR, as illustrated in Figure IV.7. The maximum number of PVs and WTs that were installed for the test systems was limited to four (two PVs with two WTs). The goal of this study was to locate and optimally size the PVs and WTs with an optimal power factor of WTs by minimizing the total real power loss through the application of the MWaOA and standard WaOA. The lines and buses data of this system are given in Appendix A and Appendix B.

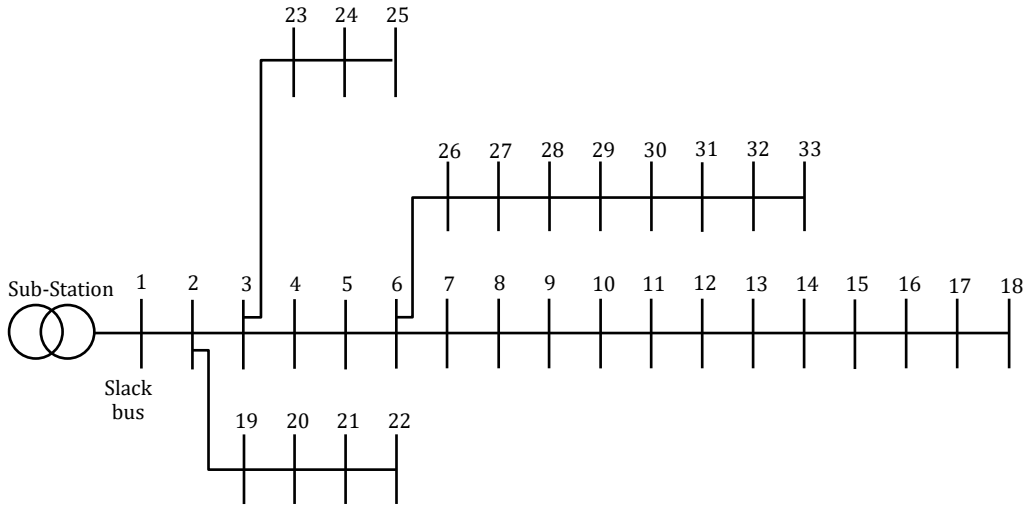

Figure IV.6: Schematic diagram of the IEEE 33-bus EDN.

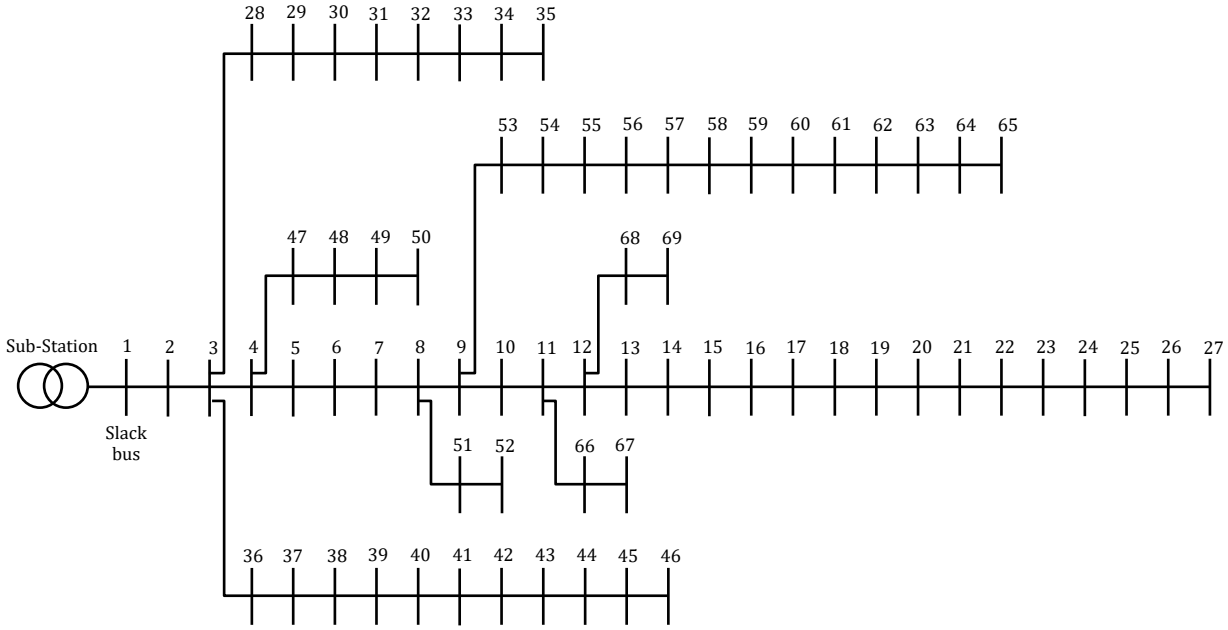

Figure IV.7: Schematic diagram of the IEEE 69-bus EDN.

Table IV.1 shows the selected limits of system voltage, area sizes of the solar PV units, the number of wind units, and the power factor of the generators of the wind turbine.

Table IV.1: Grid and generators constraints.

Generator and grid constraints	**Value**
Bounds of voltage	$0.9\ p.u \leq V \leq 1.05\ p.u$
Area sizes	$0 \leq \text{area} \leq 15000\ \ \text{m}^2$
WT sizes	$0 \leq \text{WT} \leq 16\ \text{turbines}$
PV's power factor	1
WT's power factor	$0.7 \leq PF \leq 1$

Table IV.2 presents the findings from the case studies that were conducted on the 33-bus system. The table shows the effects of integrating WTs and PVs on the system. Over all, it provides information on how PVs and WTs may enhance the functionality of energy-using distribution systems.

Table IV.2: The energy management solutions for the single function of the IEEE 33 EDN.

Item	Without RESs	MWaOA	WaOA
Energy losses (kWh)	3829.200	843.6964	910.0934
Optimal location of PVs	-	7 25	3 6
Optimal location of WTs	-	12 30	30 10
Optimal area of the solar module (m^2)	-	5908.6 8863.7	1147.3 4650.2
Optimal size PVs (kW)		896.8 1345.4	174.17 705.8
Optimal size WTs (kW)	-	1250 1250	1250 1250
Ideal PF for WTs	-	0.8819 0.7026	0.7000 0.8735
Best objective function	1	0.2203	0.2377

The primary objective of this study was to enhance the efficiency of an electrical EDN by minimizing total energy losses through the integration of RESs. The findings underscore the efficacy of the Modified Whale Optimization Algorithm (MWaOA) in achieving a substantial reduction in total energy losses. In the absence of RESs within the EDN, the total energy losses were quantified at 3829.200 kWh. However, through the application of the MWaOA algorithm and strategic allocation of RESs, this value was significantly diminished to 843.6964 kWh. The study pinpointed optimal locations for the deployment of photovoltaic (PV) units, identifying nodes 7 and 25 as strategic points. Similarly, optimal positions for wind turbines (WTs) were determined at nodes 12 and 30. The rated capacities of the WTs were specified as 1250 kW and 1250 kW, respectively. Furthermore, the surface areas allocated for solar modules were measured at 5908.6 m^2 and 8863.7 m^2. These results highlight the pivotal role of the MWaOA algorithm in optimizing the placement and capacities of RESs, leading to a significant reduction in total energy losses within the EDN. The strategic integration of PV units and WTs at identified optimal locations showcases the potential for sustainable energy solutions to enhance the overall performance of the network.

Figures IV.8 and IV.9 show the system voltage profiles with and without RESs. Based on these figures, it can be inferred that the addition of the PV units and WTs has significantly improved the voltage profile. Furthermore, as Figure IV.10 illustrates, there has been a notable reduction in power losses.

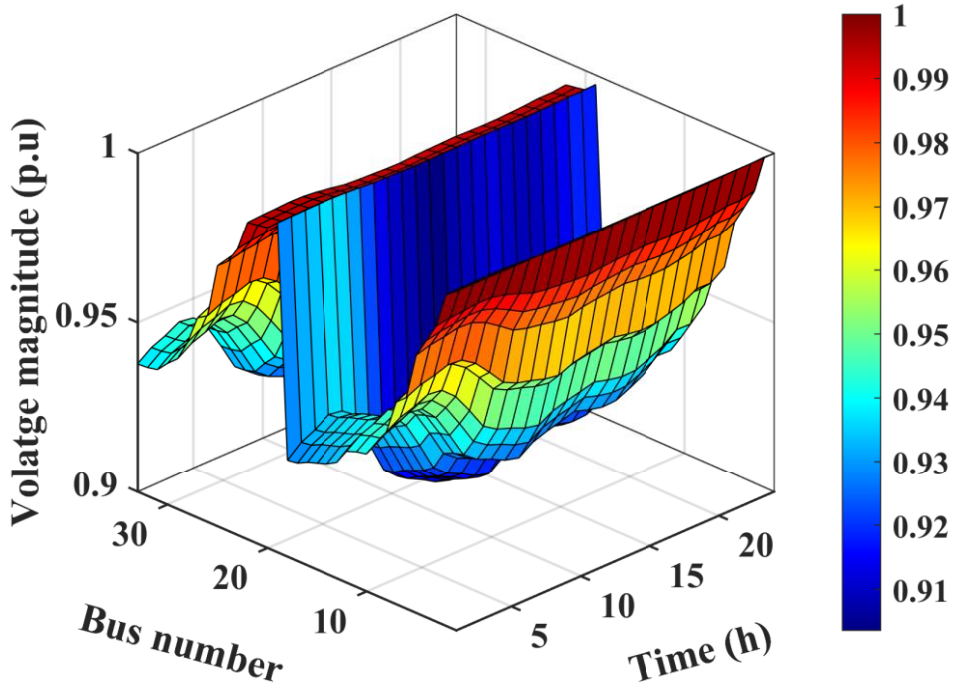

Figure IV.8: The voltage profile for the 33-bus without RESs.

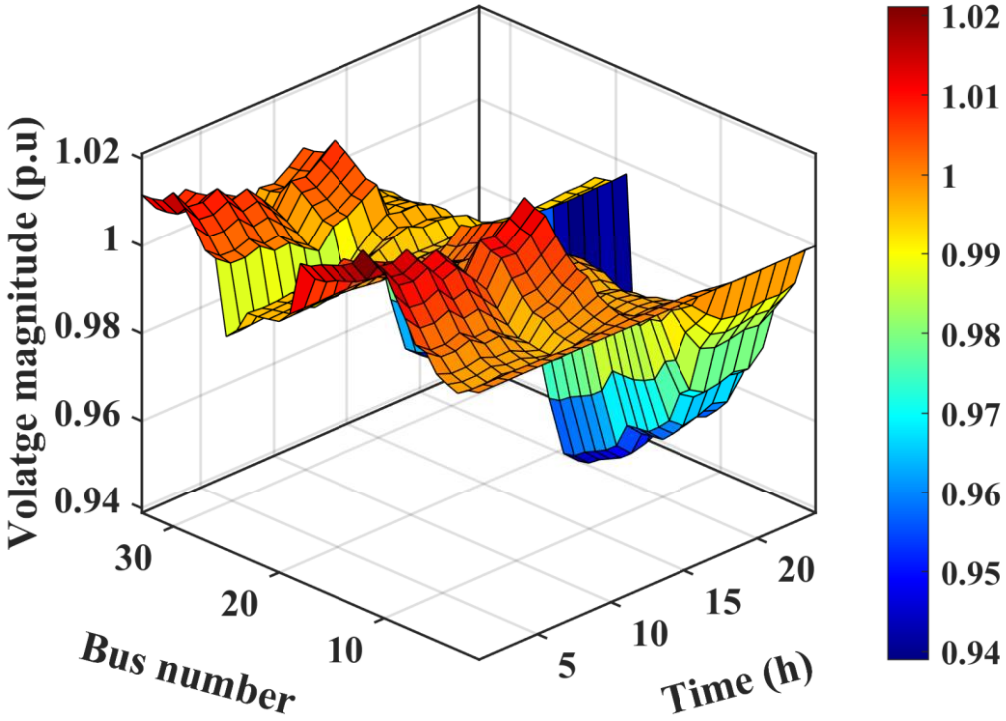

Figure IV.9: The voltage profile for the 33-bus with RESs.

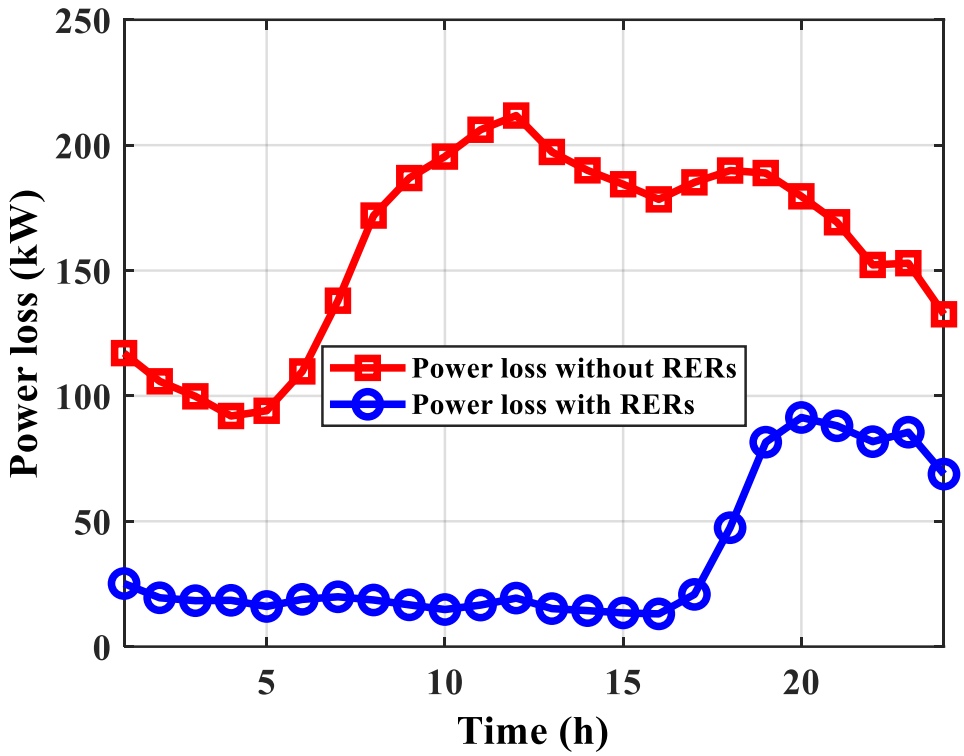

Figure IV.10: Power losses without and with RESs for the 33-bus.

The convergence of the IEEE 33-bus system has been visually depicted in Figure IV.11. This provides a clear picture of the performance of our proposed algorithm compared to the standard one.

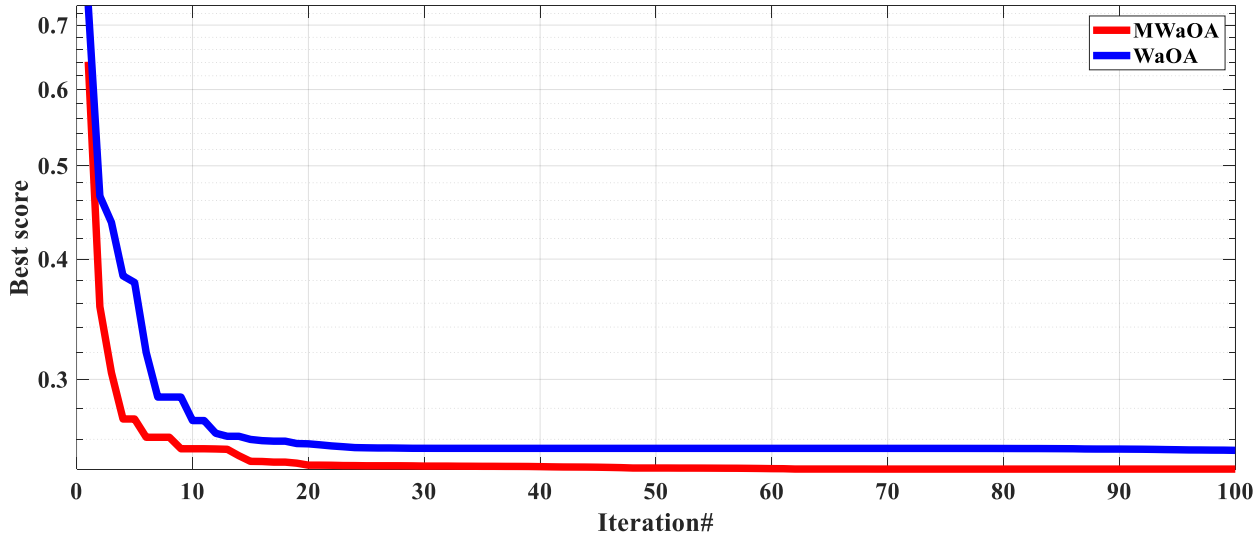

Figure IV.11: Convergence curve of the IEEE 33-bus system.

Based on Figure IV.11, it is noteworthy that the MWaOA algorithm demonstrated faster

convergence and achieved higher solution quality compared to the WaOA algorithme. The MWaOA algorithm converged to solutions with a value of 0.2203, while the WaOA algorithm converged to a slightly higher value of 0.2377 under the same scenarios.

The following table illustrates the results obtained from both the modified algorithm and the conventional algorithm for the IEEE 69-bus electrical network. The comparison provides insights into the performance differences between the two algorithms in optimizing the network.

Table IV.3: The energy management solutions for the single function of the IEEE 69 EDN.

Item	Without RESs	MWaOA	WaOA
Energy losses (kWh)	4075.800	691.0835	715.8867
Optimal location of PVs	-	59 38	40 60
Optimal location of WTs	-	61 21	61 12
Optimal area of the solar module (m^2)	-	6310.10 2158.80	1606.10 5743.90
Optimal size PVs (kW)	-	957.78 327.6750	243.78 871.8
Optimal size WTs (kW)	-	2000 750	1750 1250
Ideal PF for WTs	-	0.7645 0.8521	0.7262 0.8615
Best objective function	1	0.1696	0.1756

From the provided table, the efficiency of the modified algorithm is evident. Through its implementation, we successfully reduced energy losses from 4075.800 to 643.5624 kWh by incorporating PVs at nodes 59 and 38, with optimal areas of 6310.10 m^2 and 2158.80 m^2, respectively. Furthermore, WTs were integrated at nodes 61 and 21, with capacities of 2000 kW and 750 kW, respectively.

The results provided in Figures IV.12 and IV.13 highlight the impact of integrating PV units and WTs on the system voltage profiles. The visual representation suggests a substantial improvement in the voltage profile when RESs are introduced into the system. Moreover, the observation from Figure IV.14 reinforces the positive effect of incorporating PV units and WTs

on the overall network performance. The noticeable reduction in power losses is a significant outcome, emphasizing the potential of renewable energy integration for enhancing system efficiency and reliability.

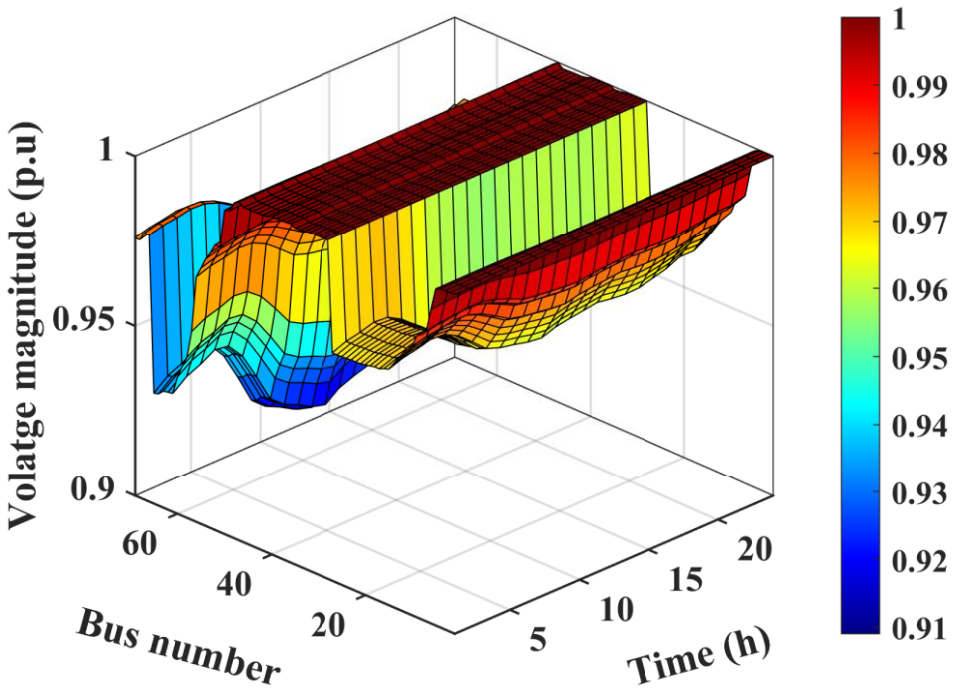

Figure IV.12: The voltage profile for the 69-bus without RESs.

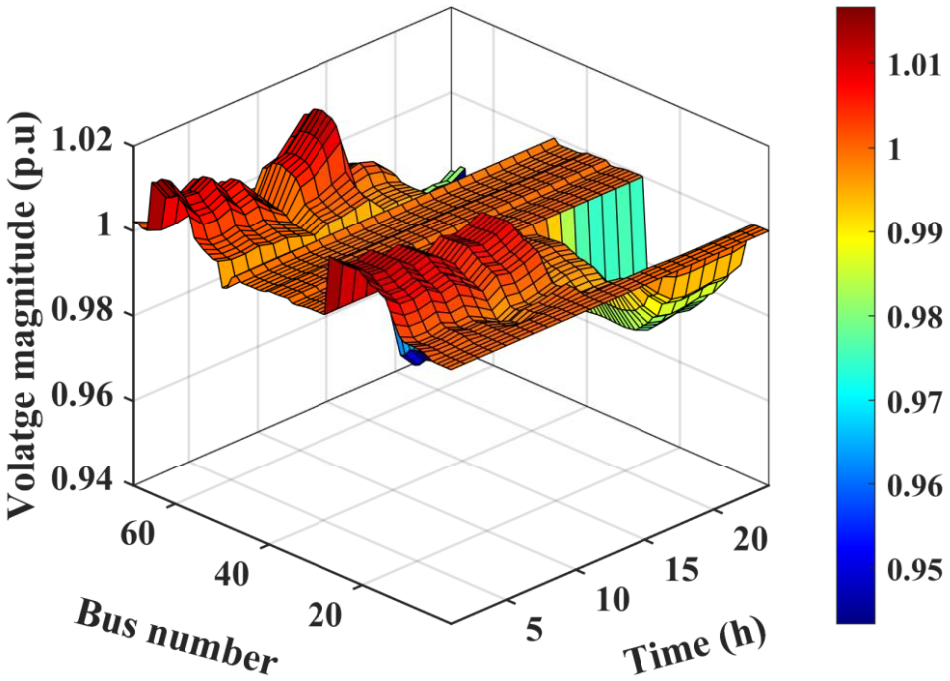

Figure IV.13: The voltage profile for the 69-bus with RESs.

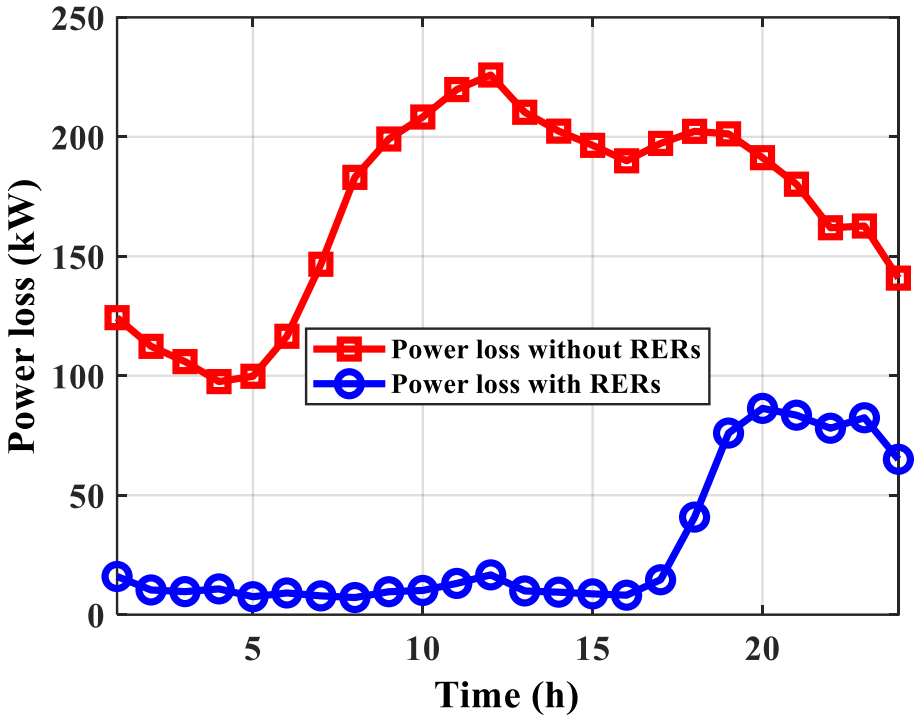

Figure IV.14: Power losses without and with RESs for the 69-bus.

Figure IV.15 visually illustrates the convergence of the IEEE 69-bus system, offering a distinct comparison between the performance of our proposed algorithm and the standard one.

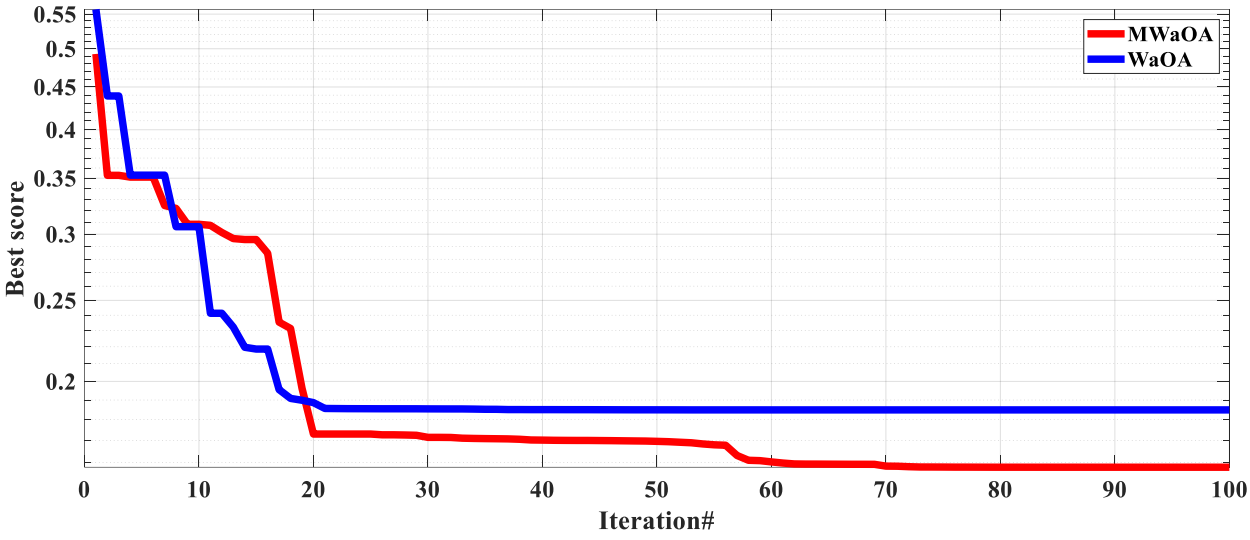

Figure IV.15: Convergence curve of the IEEE 69-bus system.

Observing Figure IV.15, it is significant to highlight that the MWaOA algorithm exhibited quicker convergence and attained superior solution quality when compared to the WaOA algorithm. Specifically, the MWaOA algorithm reached convergence with a solution

value of 0.1696. Conversely, in identical scenarios, the WaOA algorithm achieved convergence at a slightly higher value of 0.1756.

IV.2.3. Multiple objective functions

Multiple objective functions are examined in this study, and they are as follows:

IV.2.3.1. The minimization of costs

The considered objective function includes the cost of WT (C_{WT}), the cost of PV units (C_{PV}), the annual price of energy loss (C_{Loss}), and the price of electricity procured from the grid (C_{Grid}). The total annual price can be written as :

$$C = C_{WT} + C_{PV} + C_{Loss} + C_{Grid} \quad \text{(IV.10)}$$

In which,

$$C_{Grid} = 365 \times \sum_{h=1}^{24} P_{Grid(h)} \times U_{Grid(h)} \quad \text{(IV.11)}$$

where U_{Grid} is the price of buying energy from the network and $P_{Grid(h)}$ is the hourly power taken out of the grid.

$$C_{Loss} = 365 \times U_{Loss} \times \sum_{h=1}^{24} P_{T\_Loss(h)} \quad \text{(IV.12)}$$

where U_{Loss} represents the expenditure associated with energy loss and $P_{T\_Loss(h)}$ indicates the overall power losses during time h.

$$C_{PV} = C_{PV}^{inst} + C_{PV}^{O\&M} \quad \text{(IV.13)}$$

where $C_{PV}^{O\&M}$ denotes the maintenance and operating expenses for the PV unit, while C_{PV}^{inst} represents the installation cost of the PV system.

$$C_{PV}^{O\&M} = 365 \times U_{PV}^{O\&M} \times \sum_{i=1}^{Ns} \sum_{h=1}^{24} P_{PV(i,h)} \quad \text{(IV.14)}$$

$$C_{PV}^{inst.} = CF \times U_{PV} \times P_{rated\_PV} \quad \text{(IV.15)}$$

where P_{rated_PV} is the maximum amount of power that the PV system can generate, and CF is a factor that influences how quickly the cost of the PV system is paid back.

$$C_{WT} = C_{WT}^{inst.} + C_{WT}^{O\&M} \quad \text{(IV.16)}$$

where $C_{WT}^{O\&M}$ is the wind's maintenance and operating costs and $C_{WT}^{inst.}$ is the cost of installing the WT.

$$C_{WT}^{O\&M} = 365 \times U_{WT}^{O\&M} \times \sum_{i=1}^{Ns} \sum_{h=1}^{24} P_{WT(i,h)} \quad \text{(IV.17)}$$

where the maintenance and operating expenses for WTs and PVs are represented by $U_{WT}^{O\&M}$ and $U_{PV}^{O\&M}$. Ns is the number of RESs with the system considered.

$$C_{WT}^{inst.} = CF \times U_{WT} \times P_{rated\_WT} \quad \text{(IV.18)}$$

where U_{WT} and U_{PV} stand for the corresponding purchasing costs of WTs and PVs. The rated generated power of WT is denoted by P_{rated_WT} . $P_{WT(i,h)}$ and $P_{PV(i,h)}$ denote the hourly produced power from WTs and PVs of the ith system.

$$CF = \frac{\beta \times (1+\beta)^{NP}}{(1+\beta)^{NP} - 1} \quad \text{(IV.19)}$$

where NP and β are the system lifetime and interest rate of the PVs or WTs, respectively.

IV.2.3.2. Increasing the voltage level

To ensure that the power grid operates efficiently and reliably, the voltage deviations should be maintained within an allowable range, ideally close to 1 p.u. The definition of the overall voltage deviation is:

$$TVD = \sum_{h=1}^{24} \sum_{i=1}^{NB} \left| \left(V_{(i,h)} - 1 \right) \right| \quad \text{(IV.20)}$$

where $V_{(i,h)}$ represents the hourly voltage of the ith bus and NB represents the number of buses in the network.

IV.2.3.3. Enhanced system stability

The index for voltage stability of the bus j is as follows:

$$TVSI = \sum_{h=1}^{24} \sum_{i=1}^{NT} VSI_{r(i,h)} \quad \text{(IV.21)}$$

$$VSI_{r(i,h)} = \left| V_{s(i,h)} \right|^4 - 4 \left(P_{r(i,h)} X_i - Q_{r(i,h)} R_i \right)^2 - 4 (P_{r(i,h)} R_i + Q_{r(i,h)} X_i)^2 \left| V_{s(i,h)} \right|^2 \quad \text{(IV.22)}$$

where $VSI_{\mathrm{r}(i,h)}$ is the voltage stability index for the receiving end bus of branch i. $P_{r,i}$ and $Q_{r,i}$ define the real and reactive power flow of the branch i , near the receiving end bus, respectively. X_i and R_i represents the reactance and resistance of the transmission line. $V_{s(i,h)}$ is the hourly voltage of the sending end bus of branch i.

IV.2.3.4. Total real power loss minimization

The equation for $TRPL$ was discussed in the previous section.

$$TRPL = \sum_{h=1}^{24} \sum_{i=1}^{NT} P_{Loss(i,h)} \quad \text{(IV.23)}$$

The optimization takes into account the following four goal functions concurrently. To simplify the problem, we transformed the multi-objective function into a single-objective function.

$$\min(F) = \min(\varepsilon_1 F_1 + \varepsilon_2 F_2 + \varepsilon_3 F_3 + \varepsilon_4 F_4) \quad \text{(IV.24)}$$

$$F_1 = \frac{C_{RESs}}{C_{Base}} \quad \text{(IV.25)}$$

$$F_2 = \frac{TVD_{RESs}}{TVD_{Base}} \quad \text{(IV.26)}$$

$$F_3 = \frac{1}{TVSI} \quad \text{(IV.27)}$$

$$F_4 = \frac{TRPL_{RESs}}{TRPL_{Base}} \quad \text{(IV.28)}$$

ε_1, ε_2, $\varepsilon_3$and ε_4 are the weight of each part of objective function that the sum of the values of theses coefficients must be equal to one.

IV.2.4. Results of IEEE 33-bus and 69-bus for multiple objective function

In this section, the MWaOA approach is employed to optimize the operation and identify the optimal locations for four RESs, comprising two PV units and two WT, within the IEEE 33 and 69 EDN. Table IV.4 provides an overview of the operational constraints alongside the pricing variables for RESs.

Table IV.4: The constraints and the cost coefficients.

Parameter	Value
WT cost [173]	
The investment cost (U_{WT})	1400 USD/kW
The maintenance and operation costs ($U_{WT}^{O\&M}$)	0.01 USD/kWh
The interest rate (β_{WT})	10%

The lifetime (NP_{WT})	20
PV cost [74]	
The investment cost (U_{PV})	770 USD/kW
The maintenance and operation costs ($U_{PV}^{O\&M}$)	0.01 USD/kWh
The interest rate (β_{PV})	10%
The lifetime (NP_{PV})	20
Cost coefficients [174]	
The energy loss cost (U_{Loss})	0.06 USD/kWh
Constraints of grid and generators	
Voltage boundaries [175]	$0.9\ p.u \leq V \leq 1.1\ p.u$
Area sizes	$0 \leq \text{area} \leq 15000$ m^2
WT sizes	$0 \leq \text{WT} \leq 15$ turbines
Power factor of the PV	1
Power factor of the WT	$0.7 \leq PF \leq 1$

The results of the case studies conducted on the 33-bus system are shown in Table IV.5. This table illustrates how integrating WTs and PVs affects the system. Overall, it offers insights into how PVs and WTs might enhance the performance of energy-consuming EDNs.

Table IV.5: The energy management solutions for the multiple function of the IEEE 33 EDN

Item	**Without RESs**	**MWaOA**	**WaOA**
Energy losses (kWh)	3829.20	835.6340	936.8425
Optimal location of PVs	-	7 24	29 25
Optimal location of WTs	-	30 13	9 30
Optimal area of the solar module (m^2)	-	8467.20 9584.40	2661.1 9550.80
Optimal size PVs (kW)	-	1285.2 1454.8	403.9 1449.7
Optimal size WTs (kW)	-	1250 1000	1750 1250
Ideal PF for WTs	-	0.7005 0.8726	0.9421 0.7003
$\sum VD(p.u)$	37.3582	10.3878	11.0175
$\sum VSI\ (p.u)$	632.3890	737.0128	742.4466
Total annual cost (USD)	7496.90×10^3	3250.3×10^3	3104.4×10^3
Best objective function	-	0.2328	0.2387

Upon analysis, the proposed MWaOA algorithm demonstrated notable achievements in reducing costs, enhancing voltage stability, minimizing total energy losses, and mitigating voltage deviations. In the absence of Renewable Energy Sources integration into the EDN, the total annual cost stood at 7496.90 USD. However, with the strategic implementation of the MWaOA algorithm and RESs allocation, this cost markedly decreases to 3250.3×10^3 USD. The voltage deviations show a significant reduction from 37.3582 per unit (p.u.) to 10.3878 p.u., accompanied by an increase in the Voltage Stability Index from 632.3890 p.u. to 737.0128 p.u. The total energy losses were reduced from 3829.20 kWh to 835.6340 kWh.

The optimal locations for the systems within the EDN were identified as nodes 7, 24, 30, and 13 respectively. The Wind Turbines (WTs) are rated at 1250 kW and 1000 kW, while the corresponding areas for the solar modules are 8467.20 m² and 9584.40 m².

Figure IV.16 shows the system voltage profiles with RESs in IEEE 33 EDN. Based on this figure, it can be inferred that the addition of the PV units and WTs significantly improved the voltage profile.

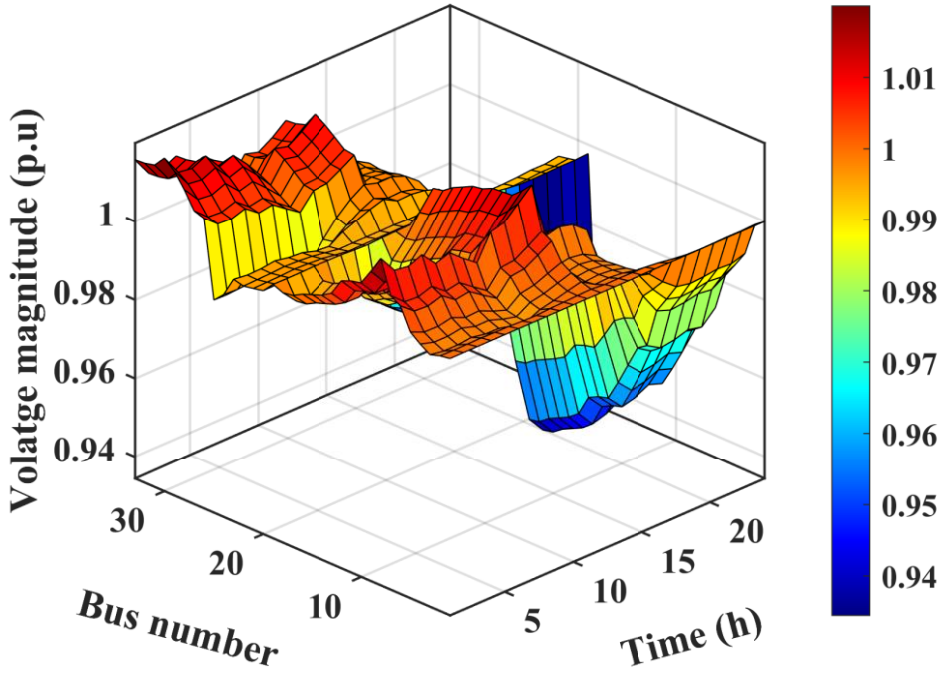

Figure IV.16: The voltage profile for the 33-bus with RESs for multiple objective function.

Figure IV.17 shows a graphical representation of the convergence of the IEEE 33-bus. This provides a clear image of how well our suggested method performs in comparison to the traditional one.

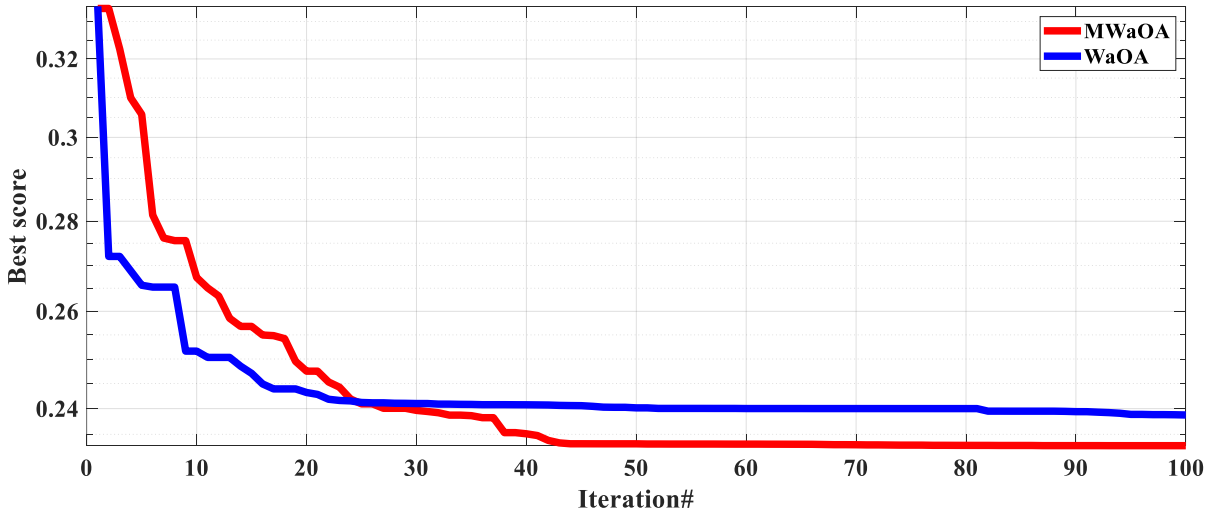

Figure IV.17: Convergence curve of the IEEE 33-bus system for multiple objective function.

Remarkably, based on Figure IV.17, the MWaOA algorithm outperformed the WaOA in terms of convergence speed and solution quality. The answers produced by the MWaOA algorithm have a value of 0.2332. On the other hand, the WaOA algorithm converged to a slightly higher value of 0.2734 under the identical conditions.

The results of the case studies conducted on the 69-bus system are shown in Table IV.6.

Table IV. 6: The energy management solutions for the multiple function of the IEEE 69 EDN

Item	Without RESs	MWaOA	WaOA
Energy losses (kWh)	4075.80	765.8708	869.0485
Optimal location of PVs	-	66 62	14 50
Optimal location of WTs	-	61 13	61 59
Optimal area of the solar module (m^2)	-	8752.80 6249.60	8559.60 6686.40
Optimal size PVs (kW)	-	1328.6 948.6	1299.2 1014.9
Optimal size WTs (kW)	-	1750 1000	1500 1250
Ideal PF for WTs	-	0.7093 0.9234	0.8281 0.7950
$\sum VD(p.u)$	38.0594	10.4854	13.2486
$\sum VSI\ (p.u)$	1490.10	1608.10	1596.60
Total annual cost (USD)	7690.20×10^3	3224.10×10^3	3207.50×10^3

Best objective function	-	0.2208	0.2448

Upon thorough analysis, the MWaOA algorithm showcased significant accomplishments in cost reduction, voltage stability enhancement, minimization of total energy losses minimization, and mitigation of voltage deviations. In the absence of RESs integration into the EDN, the total annual cost amounted to 7690.20×10^3 USD. However, with the strategic implementation of the MWaOA algorithm and allocation of RESs, this cost markedly dropped to 3224.10×10^3 USD. Voltage deviations exhibited a substantial reduction from 38.0594 per unit (p.u.) to 10.4854 p.u., coupled with an increase in the Voltage Stability Index from 1490.10 p.u. to 1608.10 p.u. Additionally, total energy losses were reduced from 4075.80 kWh to 765.8708 kWh. The optimal locations for the systems within the EDN were identified as nodes 66, 62, 61, and 13, respectively. The Wind Turbines (WTs) are rated at 1750 kW and 1000 kW, while the corresponding areas for the solar modules are 8752.80 m² and 6249.60 m².

The system voltage profiles with RESs in the IEEE 69 EDN in the case of multiple objective function are displayed in Figure IV.16. These figures suggest that the voltage profile was greatly enhanced by the installation of the PV units and WTs.

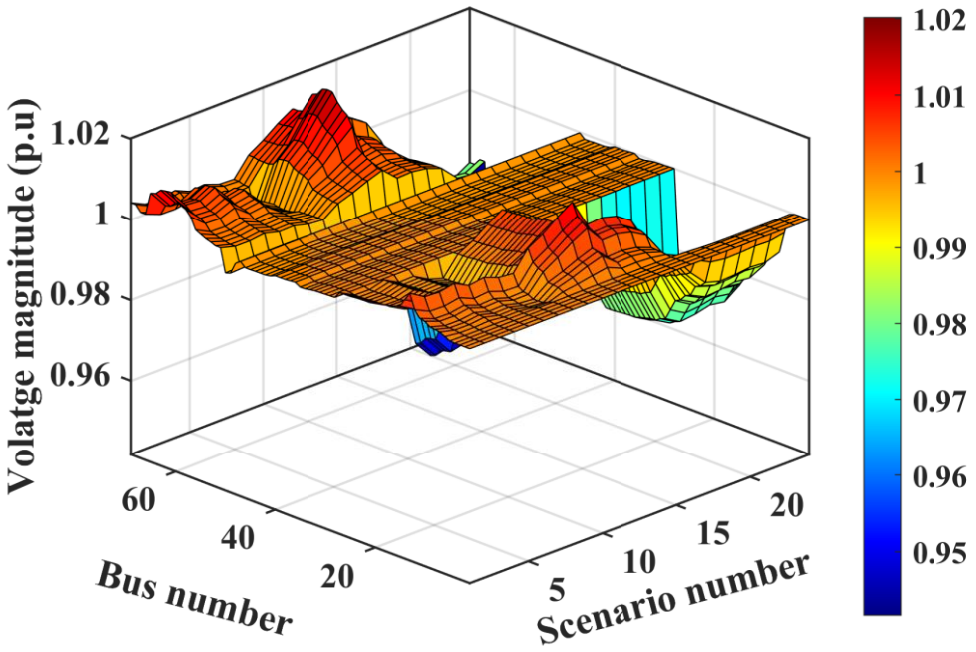

Figure IV.18: The voltage profile for the 69-bus with RESs for multiple objective function.

The convergence of the IEEE 69-bus system has been visually depicted in Figure IV.19

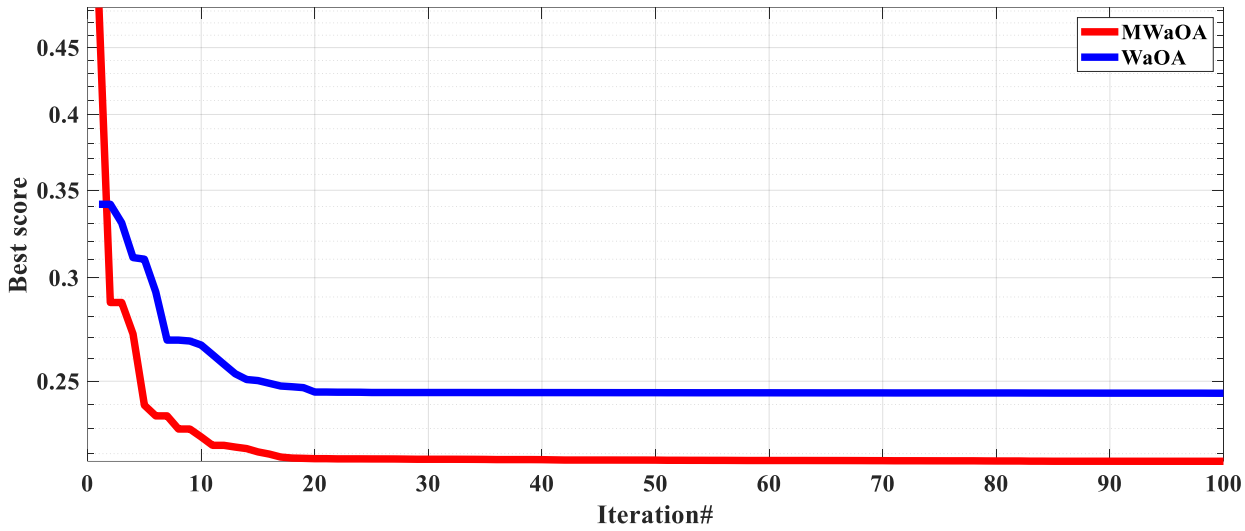

Figure IV.19: Convergence curve of the IEEE 69-bus system for multiple objective function.

Based on Figure IV.19, the MWaOA algorithm outperformed the WaOA in terms of convergence speed and solution quality. The answers produced by the MWaOA algorithm have a value of 0.2208. On the other hand, the WaOA algorithm converged to a slightly higher value of 0.2448 under identical conditions.

IV.3. Case study of a system in the presence of uncertainty

In this section, we will delve into the study of a specific system under the presence of uncertainty, focusing on the analysis of a multi-objective function. This function comprises variables such as expected power losses, expected voltage deviation index, expected voltage stability index, and the total annual expected cost. It is noteworthy that we have selected the 12:00 PM hour to investigate uncertainty for 25 scenarios. This strategic choice allows us to explore the impact of variable factors during this crucial time on the system's performance. We will comprehensively analyze the results to gain a thorough understanding of the system's response under these uncertain conditions, providing insights into both challenges and opportunities that may arise in the context of uncertainty.

Building upon the theoretical underpinnings laid out in the preceding second chapter, where we delved into the intricacies of uncertainty in scenario analysis, we have methodically calculated "The Probability for Each Scenario". This rigorous computational process, grounded in the principles established in our earlier discussions, aims to provide a comprehensive understanding of the likelihood associated with diverse outcomes within the studied system.

This exploration is meticulously designed to unveil the intricacies of the system's behavior under uncertain conditions, thus offering valuable insights into potential variability. The analysis, rooted in the theoretical framework presented in the second chapter, serves as a robust foundation for facilitating informed decision-making based on a nuanced and scientific assessment of probabilities. The forthcoming graph, titled The Probability for Each Scenario, visually represents the outcomes of this detailed calculation, providing a clear perspective for understanding the probabilities associated with each scenario in our analysis.

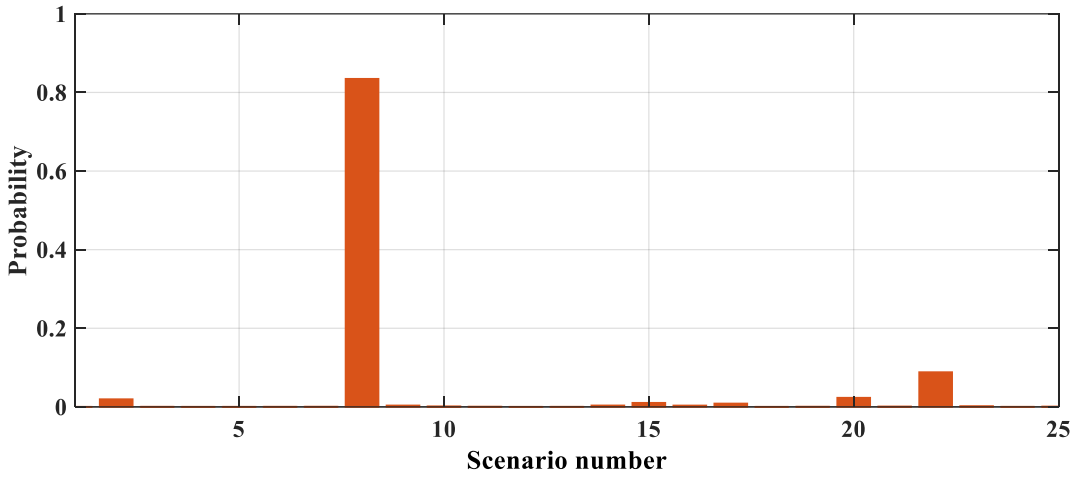

Figure IV.20: The probability for each scenario.

The expected real power loss ($ERPL$) is calculated over all scenarios as:

$$ERPL = \sum_{sc=1}^{Nsc} \pi_S \times P_{Loss(sc)} \quad \text{(IV.29)}$$

Where, the probability of the scenario is π_s and optimized power loss for the scenario is $P_{Loss(sc)}$, π_S is the total number of selected scenarios , and Nsc is the total number of selected scenarios.

The expected voltage deviation index (EVD) is calculated over all scenarios as:

$$EVD = \sum_{sc=1}^{Nsc} \pi_S \times VD_{(sc)} \quad \text{(IV.30)}$$

Where, $VD_{(sc)}$ represent the voltage deviations for all scenarios.

The expected voltage stability index ($EVSI$) is calculated over all scenarios as:

$$EVSI = \sum_{sc=1}^{Nsc} \pi_S \times VSI_{(sc)} \quad \text{(IV.31)}$$

Where, $VSI_{(sc)}$ represent the voltage stability index for all scenarios.

The expected total cost (ETC) is calculated over all scenarios as:

$$ETC = \sum_{sc=1}^{Nsc} \pi_S \times TC_{(sc)} \quad \text{(IV.32)}$$

$$TC_{(sc)} = C_{WT(sc)} + C_{PV(sc)} + C_{Loss(sc)} + C_{Grid(sc)} \quad \text{(IV.33)}$$

Where

$TC_{(sc)}$ represent the total cost for all scenarios.

IV.3.1. Proposed multi-objective function

In this work, the previous objective functions are considered simultaneously. To consider these objective functions concurrently, the weight approach method is utilized. In addition, the objectives should be normalized as follows by dividing them by their base value (without PV or WT). This makes the objective function dimensionless and also prevents any scaling problems. The augmented objective function can be described as follows:

$$\min(F) = \min(\varepsilon_1 F_1 + \varepsilon_2 F_2 + \varepsilon_3 F_3 + \varepsilon_4 F_4) \quad \text{(IV.34)}$$

$$F_1 = \frac{ETC}{ETC_{base}} \quad \text{(IV.35)}$$

$$F_2 = \frac{ERPL}{ERPL_{Base}} \quad \text{(IV.36)}$$

$$F_3 = \frac{1}{EVSI} \quad \text{(IV.37)}$$

$$F_4 = \frac{EVD}{EVD_{Base}} \quad \text{(IV.38)}$$

ε_1, ε_2, $\varepsilon_3$and ε_4 are the weight of each part of objective function that the sum of the values of theses coefficients must be equal to one.

IV.3.2. Results of IEEE 33 and 69-bus in the presence of uncertainty

Table IV.7 presents a comprehensive scenario analysis of a renewable energy system, focusing on key variables such as Irradiance, Wind Speed, Loading, Temperature, Price, and their associated probabilities. This analysis aims to provide insights into the diverse scenarios and their likelihoods within the renewable energy context. Understanding the variability of these critical factors is essential for effective decision-making and optimization in renewable energy systems. The table outlines different scenarios and the probabilities associated with each variable, offering a valuable resource for assessing the potential outcomes in the studied energy system.

Table IV.7: Scenario analysis of renewable energy system: irradiance, wind speed, loading, temperature, price, and their probabilities.

Scenario	Irradiance	Wind speed	Loading	Temperature	Price	Probability
1	938.7843	10.1545	128.4257	52.5136	0.6092	3.1501e-07
2	782.2679	9.7595	108.5169	38.0553	0.2240	0.01928
3	828.4465	12.9875	67.8419	5.5934	0.3594	0.000195
4	771.1289	3.6944	95.4883	15.6500	0.1263	5.18420e-05
5	725.6597	13.9540	80.3517	10.3786	0.6272	5.91013e-05

6	691.9552	5.8095	101.5747	13.0398	0.5773	0.0002019
7	900.0048	11.4920	122.0901	49.9261	0.2538	0.0003544
8	877.0543	7.7262	92.5312	28.9917	0.3017	0.83449090
9	867.1604	8.4857	85.6306	46.1728	0.1605	0.00343155
10	816.1006	6.1276	106.4735	59.1866	0.4690	0.00115592
11	883.6181	15.5953	124.0334	21.6456	0.2386	0.00044662
12	757.2879	6.5869	119.3793	11.7061	0.6719	9.94777e-06
13	750.5067	15.8908	78.1681	39.7900	0.4257	0.0001381
14	929.1977	14.2393	103.4249	35.7767	0.5499	0.0035007
15	908.5089	5.2964	111.3525	17.0690	0.3903	0.0101417
16	797.7770	15.0159	98.2883	48.2786	0.3776	0.0033557
17	704.5893	7.0918	88.9044	19.0790	0.5039	0.00839149
18	735.1714	4.5401	73.4625	7.5436	0.5282	1.0942e-05
19	668.8223	13.3805	117.2540	27.0788	0.5948	0.00035865
20	805.5916	9.2807	131.3822	31.8530	0.2725	0.02306291
21	836.3865	12.6094	71.8253	43.4857	0.1829	0.000792032
22	851.6024	10.6532	125.9276	34.1851	0.4436	0.08810812
23	917.8632	3.9739	115.2961	25.1533	0.4044	0.00168401
24	659.2595	4.8888	83.2013	41.1698	0.3221	0.00010274
25	712.8600	12.2650	75.2402	23.8062	0.1968	0.00066697

Table IV.8 showcases the expected values for individual scenarios, taking into account the optimal integration of RESs within the IEEE 33-bus network. As highlighted in Table IV.8, the summation of expected values, including $ERPL$, EVD, EVSI, and ETC has been enhanced to 53.9342 kW, 0.6121 p.u, 30.8922 p.u, and 7.5431e+06 USD, respectively.

Table IV.8: The expected values for each scenario of IEEE 33-bus system.

Scenario	π_S	$ERPL$	**EVD**	**EVSI**	**ETC**
S1	3.1501e-07	3.18241e-05	2.6105386e-07	9.08199e-06	4.8827457
S2	0.01928	1.255146	0.0105708	0.5761273655	90988.91705
S3	0.000195	0.0110427	0.00010719	0.0066640632	140.8427203
S4	5.18420e-05	0.0038015	3.326388e-05	0.0015302432	138.7112323
S5	5.91013e-05	0.00242315	1.6787551e-05	0.001931457	270.5541891
S6	0.0002019	0.01466084	0.00013503	0.00593976	2267.335700

S7	0.0003544	0.02848121	0.000225657	0.010469813	2139.555136
S8	0.83449090	44.0781401	0.239917641	25.75965123	3631282.888
S9	0.00343155	0.14251820	0.000796634	0.106866013	8104.5857146
S10	0.00115592	0.097242976	0.00097683	0.033259508	12414.895642
S11	0.00044662	0.03562958	0.00021342	0.013460673	2325.1344341
S12	9.94777e-06	0.00102087	8.5079056e-06	0.000285826	158.77117398
S13	0.0001381	0.00461330	3.4748149e-05	0.00447578	510.11144981
S14	0.0035007	0.1900703	0.00098272	0.109727200	27344.350361
S15	0.0101417	0.9351948	0.00695210	0.297688719	81674.562405
S16	0.0033557	0.1495929	0.0008992751	0.104162589	19692.369659
S17	0.00839149	0.40335830	0.00314542	0.25618231	61781.608994
S18	1.094254e-05	0.00047094	2.3100948e-06	0.000341301	56.831852190
S19	0.00035865	0.0251000	0.00020928	0.01066604	4619.8422995
S20	0.02306291	2.6314569	0.02152503	0.65618280	176625.77406
S21	0.000792032	0.02903024	0.00026492	0.026153548	1085.5510348
S22	0.08810812	8.04002755	0.06281520	2.57761725	937609.70412
S23	0.00168401	0.1863375	0.001492585	0.04819530	15999.507366
S24	0.00010274	0.00506313	5.77407683e-05	0.003063522	559.99211619
S25	0.00066697	0.0237293	0.000187961	0.02183903	1125.883781
Summation	**1**	**58.2941**	**0.35157**	**30.6324**	**5.07892×10^{6}**

Figure IV.21 illustrates the voltage profile for the generated scenarios. As depicted in the figure, it is evident that the voltage magnitudes for all scenarios fall within the permissible limits, with no instances of violation observed.

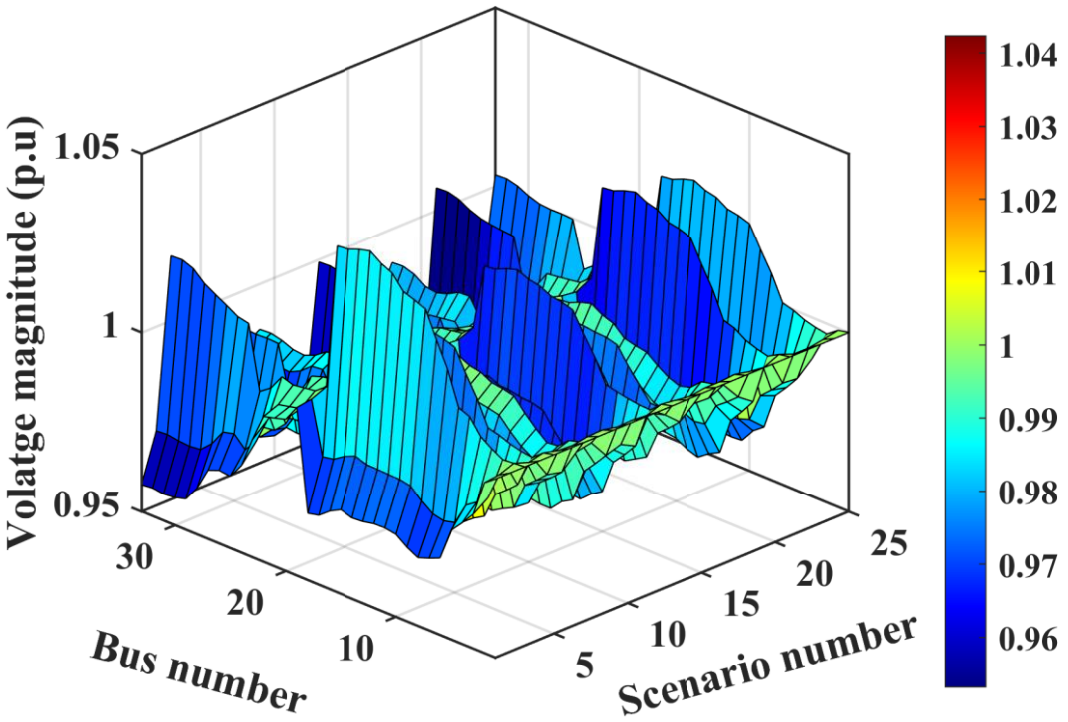

Figure IV.21: The voltage profile for the 33-bus with RESs for 25 scenarios.

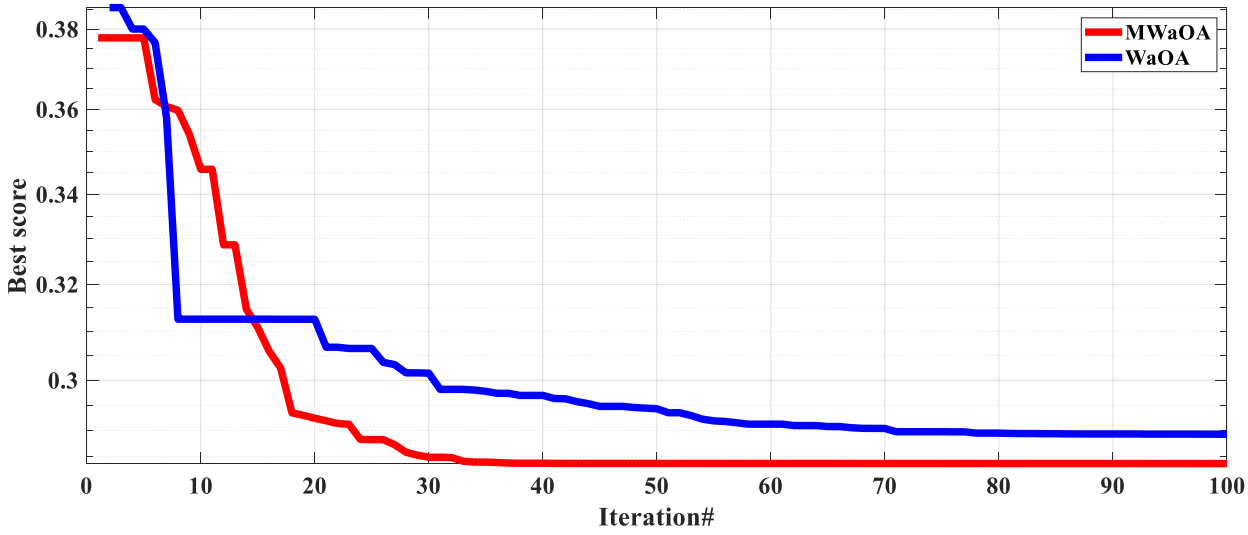

Figure IV.22: Convergence curve of the IEEE 33-bus system for 25 scenarios.

Observing Figure IV.22, it is notable that the MWaOA algorithm exhibited accelerated convergence and attained superior solution quality when compared to the WaOA. The MWaOA algorithm converged to solutions with a value of 0.2836. In contrast, under identical scenarios, the WaOA algorithm converged to a slightly higher value of 0.2893.

Now, we embark on an analysis of the IEEE 69-bus network in the presence of

uncertainty. In this examination, we explore various scenarios, considering the optimal integration of RESs, as highlighted in Table IV.9. The summation of expected values, encompassing $ERPL$, EVD, EVSI, and ETC, has been enhanced to 40.7454 kW, 0.6254 p.u, 65.9976 p.u, and 7.4745e+06 USD, respectively. This analysis aims to provide valuable insights into the network's performance under uncertain conditions, shedding light on the robustness and efficiency of the proposed integration strategies.

Table IV.9: The expected values for each scenario of IEEE 69-bus system.

Scenario	π_S	$ERPL$	EVD	EVSI	ETC
S1	3.1501e-07	4,03982e-05	2,695477e-07	2,0389719e-05	5,04098439
S2	0.01928	1,59988469	0,0109424510	1,269562799	93856,515719
S3	0.000195	0,01164180	0,0001089994	0,0137390808	145,2146412
S4	5.18420e-05	0,00343030	3,880493e-05	0,00337408128	140,4262235
S5	5.91013e-05	0,00316242	2,322008e-05	0,00406819850	281,64432800
S6	0.0002019	0,01452709	0,0001491267	0,013149864	2309,2195314
S7	0.0003544	0,03994147	0,0002404127	0,023232423	2220,2667890
S8	0.83449090	43,8291338	0,2751281614	55,6585716	3697214,0770
S9	0.00343155	0,15649134	0,001059790	0,230157360	8296,0040421
S10	0.00115592	0,10372808	0,00104387	0,0745797563	12696,865158
S11	0.00044662	0,04762871	0,00026935	0,0295420737	2408,6892479
S12	9.94777e-06	0,00104530	9,252224e-06	0,00064077007	162,00230760
S13	0.0001381	0,00701468	6,014150e-05	0,00947736616	533,8273445
S14	0.0035007	0,25699569	0,001693232	0,23603755	28333,7274444
S15	0.0101417	0,86463955	0,007968059	0,658628565	82782,063824
S16	0.0033557	0,24123510	0,001830562	0,225475458	20533,973608
S17	0.00839149	0,41333102	0,003492359	0,556881783	63013,286289
S18	1.0942e-05	0,000407222	3,121399e-06	0,00073169715	57,18810110
S19	0.00035865	0,039450360	0,000246938	0,0236114164	4814,539989
S20	0.02306291	3,16219960	0,022475567	1,48242637	181961,56492
S21	0.000792032	0,038769365	0,0003176130	0,0548200345	1133,8156542
S22	0.08810812	10,3357236	0,064665107	5,74313603	968521,74346
S23	0.00168401	0,171651516	0,001695150	0,107976610	16211,185427
S24	0.00010274	0,004973402	6,394930e-05	0,0067364807	570,27724509
S25	0.00066697	0,03318135	0,000274109	0,045977959	1175,7518822

Summation	**1**	**61.3802**	**0.3938**	**66.4726**	**5.1894×10^{6}**

The voltage profiles for the generated scenarios are shown in Figure IV.23. As seen in the drawing, all of the scenarios' voltage magnitudes are clearly within the acceptable ranges, and no violations are shown.

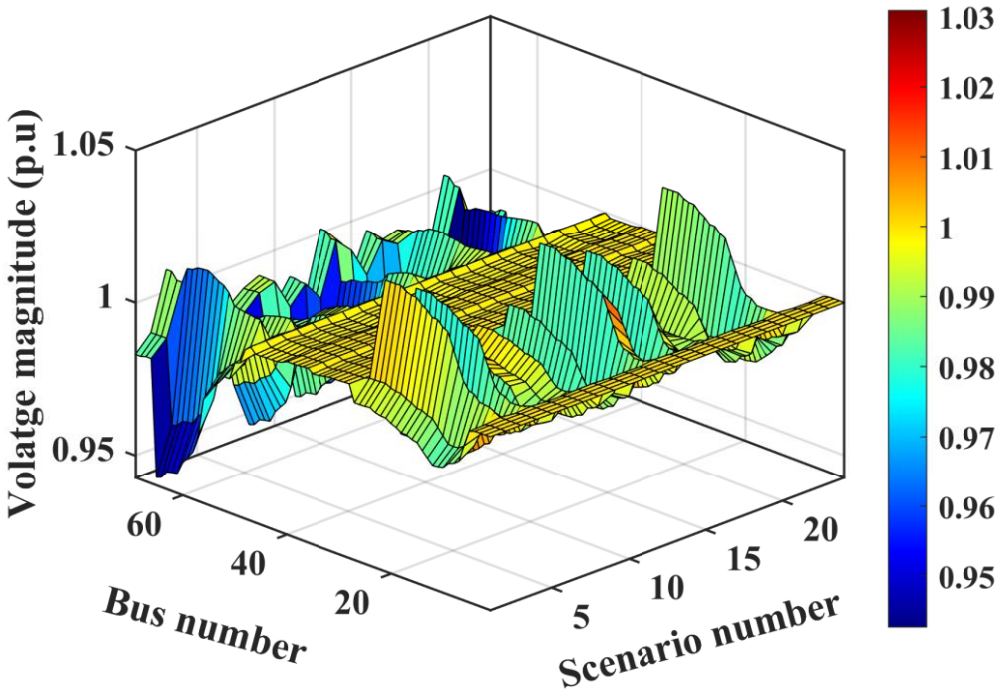

Figure IV.23: The voltage profile for the 69-bus with RESs for 25 scenarios.

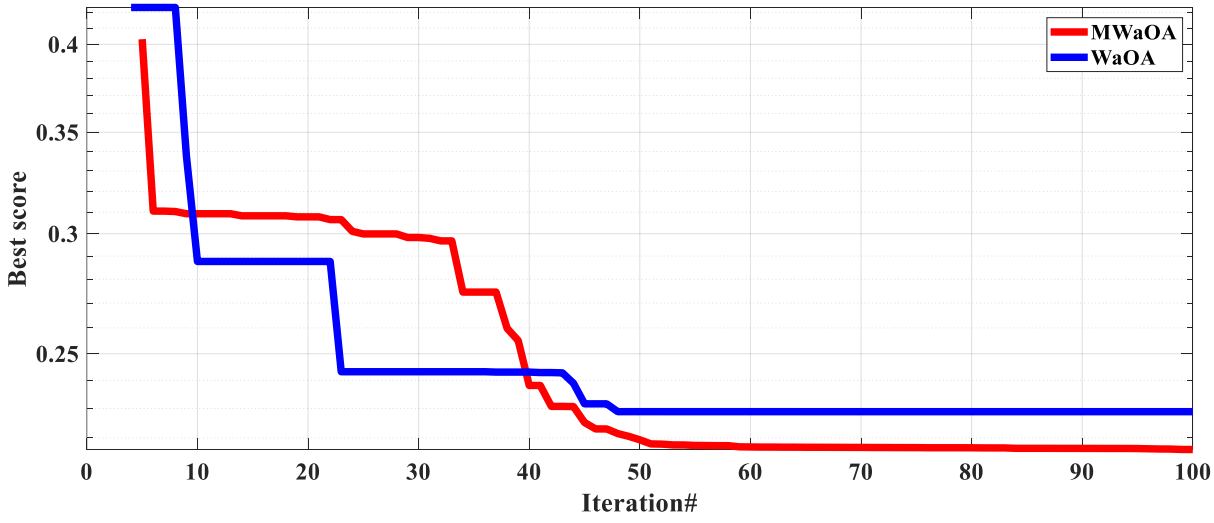

Figure IV. 24: Convergence curve of the IEEE 69-bus system for 25 scenarios.

Observing Figure IV.24, it is notable that the MWaOA algorithm exhibited accelerated convergence and attained superior solution quality when compared to the WaOA. The MWaOA algorithm converged to solutions with a value of 0.2431. In contrast, under identical scenarios, the WaOA algorithm converged to a slightly higher value of 0.2638.

IV.4. Conclusion

This chapter presented a comprehensive analysis and comparison of the proposed Modified Walrus Optimization Algorithm (MWaOA) against the standard Walrus Optimization Algorithm (WaOA) for the optimal placement and sizing of renewable distributed generators in distribution systems. The results demonstrate that the MWaOA significantly outperforms the WaOA in terms of convergence speed and solution quality for the single objective of minimizing real power losses, as well as for multi-objective formulations considering cost, voltage deviations, and stability. Superior technical and economic optimization is achieved for both the IEEE 33-bus and 69-bus test systems. A detailed investigation into system operation under uncertainty further proves the efficacy of the MWaOA in enhancing expected performance across numerous scenarios covering variability in irradiance, wind speeds, loading, temperatures and pricing. The voltage profile analysis validates resilient operation within limits across all cases.

In summary, the MWaOA provides an excellent optimization tool for sustainable and reliable integration of renewable DG units in modern distribution grids. By leveraging this algorithm, notable improvements can be attained in loss reduction, cost savings, voltage regulation and overall network efficiency and robustness. The approach thereby enables smart planning and operation paradigms for present and future power systems alike.

General conclusion

General conclusion

Due to the continuous increase in energy consumption, distribution networks have received considerable attention in terms of optimization. Distributed generation is an exceptional solution that can play a key role in minimizing power losses and voltage drops. In this context, we addressed in this work the problem of planning and optimal integration of distributed generation based on renewable sources into radial electrical distribution networks of various sizes and complexities. This work is carried out by optimizing various technical and economic parameters, based on single and multi-objective functions, using a new modified algorithm called the Modified Walrus Optimization Algorithm. We identified the best locations and sizes for photovoltaic and wind sources to integrate them optimally into IEEE standard distribution networks. This was done by studying the impact of these sources on the technical and economic parameters of the networks studied, which include active power losses, voltage, as well as the total system cost and enhanced system stability. Additionally, we studied the uncertainty associated with renewable energies to ensure their reliable integration into distribution networks. Uncertainty analysis in this thesis involved comprehensive examination of factors such as variation in solar radiation, wind speed fluctuations, and the unpredictability of demand to develop robust renewable energy integration strategies.

In the first chapter, we have presented a state-of-the-art review on distributed generation based on renewable energies, including their definition, classification, and their impact on distribution networks. We have also discussed the modeling of photovoltaic (PV) and modules as well as the modeling of wind turbines (WT). Lastly, in this chapter, we have highlighted an efficient power flow calculation method known as the Backward/Forward Sweep algorithm.

In the second chapter, we have extensively discussed models for handling parameter uncertainty in modern power systems, covering aspects such as load demand, renewable generation, and electricity prices. Monte Carlo simulation was highlighted as a key technique due to its user-friendly nature, effectiveness in addressing complex problems, and compatibility with probability distributions. We have emphasized the practical significance of Monte Carlo simulation in generating hourly scenarios for critical parameters. Additionally, we have discussed scenario-based reduction as a method to enhance computational efficiency while maintaining accuracy, introducing tools such as probability distribution and optimal hourly

scenario for assessing scenario likelihoods and identifying optimal conditions. These findings will help guide our study of uncertainty in the final chapter.

In Chapter 3, we have introduced the Modified Walrus Optimization Algorithm (MWaOA), which incorporates Levy flight to enhance its capabilities in searching for optimal solutions. We evaluated the performance of MWaOA on 23 benchmark functions and compared it against several state-of-the-art optimization algorithms, including Sand Cat Swarm Optimization SCSO, TTAO, DO, GWO,ZOA, SCA, ARO, and WaOA. The analysis of results, including statistical findings, convergence plots, and boxplots, demonstrated MWaOA's superior optimization ability over these existing methods. Specifically, MWaOA achieved better solutions on average and identified optimal solutions with fewer iterations.

In Chapter 4, serving as the culmination of our work, we have conducted a comprehensive examination and comparison between the proposed Modified Walrus Optimization Algorithm (MWaOA) and the standard Walrus Optimization Algorithm (WaOA) to determine optimal locations and sizes for distributed renewable energy sources in distribution networks. Our findings demonstrate that the MWaOA significantly outperforms the WaOA in terms of convergence speed and solution quality, both for multi-objective formulations considering cost, voltage variations, and stability, as well as for the single objective of reducing actual power losses. We have achieved efficient and superior technical optimization for the IEEE 33-bus and 69-bus test systems. Furthermore, we have illustrated the effectiveness of the MWaOA in enhancing predicted performance across various scenarios, encompassing variations in irradiance, wind speeds, loads, temperatures, and prices, through a comprehensive examination of system behavior under uncertainty.

This research work leads to various promising topics for future investigations. The following recommendations are made for future research:

1. Applying the latest optimization techniques for solving the allocation problem of the RESs considering the uncertainty.

2. Solving the optimal RESs allocation with the presence of charging stations for electric vehicles and Considering the uncertainty of electric vehicles (EVs), Electricity price uncertainty, Load growth uncertainty.

3. Improving the searching capabilities of optimization techniques: based on enhancing the explorations and exploitations phases to solve the RESs optimal allocation problem efficiently

4. Improving different uncertainty methods to model the uncertainties and compare these techniques.

5. Studying the impact of RESs on distribution system security must be evaluated such as, Power quality issues like frequency balance, voltage stabilization, and reactive power regulations should be addressed carefully.

6. Applying of different methods to study the environmental effects of optimal integration of RESs in the distributed system for reducing the carbon dioxide emissions.

Scientific works

Publications

1. **Hachemi, A. T**., Sadaoui, F., Arif, S., Saim, A., Ebeed, M., Kamel, S., & Mohamed, E. A. (2023). Modified reptile search algorithm for optimal integration of renewable energy sources in distribution networks. Energy Science & Engineering, 11(12), 4635-4665.
2. **Hachemi, A. T**., Sadaoui, F., Saim, A., Ebeed, M., Abbou, H. E., & Arif, S. (2023). Optimal Operation of Distribution Networks Considering Renewable Energy Sources Integration and Demand Side Response. Sustainability, 15(24), 16707.

International conferences

1. **Hachemi, A. T.**, Sadaoui, F., & Arif, S. Analysis of Grid Connected Photovoltaic System in Different Scenarios. International Conference on Innovative Academic Studies on 10-13 September in 2022 at Konya/Turkey.
2. **Hachemi, A. T**., Sadaoui, F., & Arif, S. The impacts of solar photovoltaic unit on distribution network losses and voltage profile. International Conference on Engineering and Applied Natural Sciences on 15-18 October in 2022 at Konya/Turkey.
3. **Hachemi, A**., Sadaoui, F., & Arif, S. (2022, November). Optimal location and sizing of capacitor banks in distribution systems using grey wolf optimization algorithm. In International Conference on Artificial Intelligence in Renewable Energetic Systems (pp. 719-728). Cham: Springer International Publishing.
4. **Hachemi, A. T**., Sadaoui, A., Abbou, H. E., & Arif, S Optimal DG of wind turbine Placement and sizing based on Minimization of Power Losses. International Conference on Solar Energy and Hybrid Systems (ICSEHS'22), Laghouat, Algeria, 28-29 Nov.2022

National conferences

1. **Hachemi, A. T**., Sadaoui, F., & Arif, S. Optimal Location and Size for Distributed Generation Using Harris Hawk's Leader Optimization. National Conference on Materials Sciences and Engineering (MSE'22), June 28 & 29th, 2022.
2. **Hachemi, A**. T., Sadaoui, F., & Arif, S. Mitigating Overloading in Electrical Distribution Networks through Effective Integration of Dispersed Generation Using DE

Algorithm. National Conference on Applied Physics & Chemistry (3rdNCAPC23) held on March 12th &13th, 2023 in Laghouat

References

[1] D. Tran Khanh Viet, "Interconnexion des sources d'énergie renouvelable au réseau de distribution électrique," PhD Thesis. Université du Québec à Trois-Rivières, 2009.

[2] N. KETFI, "Contribution à la gestion des réseaux de distribution en présence de génération d'énergie dispersée," PhD Thesis. Université de Batna 2, 2014.

[3] C. Ammari, D. Belatrache, B. Touhami, and S. Makhloufi, "Sizing, optimization, control and energy management of hybrid renewable energy system—A review," *Energy and Built Environment*, vol. 3, no. 4, pp. 399-411, 2022.

[4] M. Mosbah, "Optimal sizing and placement of distributed generation in transmission systems," in *ICREGA-2016*, 2016, pp. 8-10.

[5] A. Hachemi, F. Sadaoui, and S. Arif, "Optimal Location and Sizing of Capacitor Banks in Distribution Systems Using Grey Wolf Optimization Algorithm," in *International Conference on Artificial Intelligence in Renewable Energetic Systems*, 2022: Springer, pp. 719-728.

[6] O. Sadeghian, M. Nazari-Heris, M. Abapour, S. S. Taheri, and K. Zare, "Improving reliability of distribution networks using plug-in electric vehicles and demand response," *Journal of Modern Power Systems and Clean Energy*, vol. 7, no. 5, pp. 1189-1199, 2019.

[7] I. Ortega-Romero, X. Serrano-Guerrero, A. Barragán-Escandón, and C. Ochoa-Malhaber, "Optimal Integration of Distributed Generation in Long Medium-Voltage Electrical Networks," *Energy Reports*, vol. 10, pp. 2865-2879, 2023.

[8] R. Viral and D. K. Khatod, "Optimal planning of distributed generation systems in distribution system: A review," *Renewable and sustainable energy Reviews*, vol. 16, no. 7, pp. 5146-5165, 2012.

[9] A. Omri, "Analyse de la transition vers les énergies renouvelables en Tunisie: Risques, enjeux et stratégies à adopter," PhD Thesis.Université Côte d'Azur; Université de Sfax (Tunisie). Faculté des Sciences …, 2016.

[10] M. Telidjane, "Modélisation des panneaux photovoltaïques et adaptation de la cyclostationnarité pour le diagnostic," PhD Thesis. Université de Lyon, 2017.

[11] X.-L. Dang, "Contribution à l'étude des système Photovoltaïque/Stockage distribués. Impact de leur intégration à un réseau fragile," PhD Thesis. Ecole Doctorale Sciences Pratiques de Cachan, 2014.

[12] S. Ruin and G. Sidén, *Small-Scale Renewable Energy Systems: Independent Electricity for Community, Business and Home*. CRC Press, 2019.

[13] N. Goudarzi and W. Zhu, "A review of the development of wind turbine generators across the world," in *ASME International Mechanical Engineering Congress and Exposition*, 2012, vol. 45202: American Society of Mechanical Engineers, pp. 1257-1265.

[14] A. Bartle, "Hydropower potential and development activities," *Energy policy*, vol. 30, no. 14, pp. 1231-1239, 2002.

[15] E. Barbier, "Geothermal energy technology and current status: an overview," *Renewable and sustainable energy reviews*, vol. 6, no. 1-2, pp. 3-65, 2002.

[16] G. J. Herbert and A. U. Krishnan, "Quantifying environmental performance of biomass energy," *Renewable and Sustainable Energy Reviews*, vol. 59, pp. 292-308, 2016.

[17] R.-H. Liang and J.-H. Liao, "A fuzzy-optimization approach for generation scheduling with wind and solar energy systems," *IEEE transactions on power systems*, vol. 22, no. 4, pp. 1665-1674, 2007.

[18] S. S. Reddy, P. Bijwe, and A. R. Abhyankar, "Real-time economic dispatch considering renewable power generation variability and uncertainty over scheduling period," *IEEE Systems journal*, vol. 9, no. 4, pp. 1440-1451, 2014.

[19] E. Ali, S. Abd Elazim, and A. Abdelaziz, "Ant Lion Optimization Algorithm for optimal location and sizing of renewable distributed generations," *Renewable Energy*, vol. 101, pp. 1311-1324, 2017.

[20] P. Kayal and C. Chanda, "Placement of wind and solar based DGs in distribution system for power loss minimization and voltage stability improvement," *International Journal of Electrical Power & Energy Systems*, vol. 53, pp. 795-809, 2013.

[21] M. S. Rawat and S. Vadhera, "Impact of photovoltaic penetration on static voltage stability of distribution networks: a probabilistic approach," *Asian Journal of Water, Environment and Pollution*, vol. 15, no. 3, pp. 51-62, 2018.

[22] M. F. Mostafa, S. H. A. Aleem, and A. M. Ibrahim, "Using solar photovoltaic at Egyptian airports: Opportunities and challenges," in *2016 eighteenth international middle east power systems conference (MEPCON)*, 2016: IEEE, pp. 73-80.

[23] S. Roy, "Market constrained optimal planning for wind energy conversion systems over multiple installation sites," *IEEE transactions on energy conversion*, vol. 17, no. 1, pp. 124-129, 2002.

[24] J. Hetzer, C. Y. David, and K. Bhattarai, "An economic dispatch model incorporating wind power," *IEEE Transactions on energy conversion*, vol. 23, no. 2, pp. 603-611, 2008.

[25] M. H. Amrollahi and S. M. T. Bathaee, "Techno-economic optimization of hybrid photovoltaic/wind generation together with energy storage system in a stand-alone micro-grid subjected to demand response," *Applied energy*, vol. 202, pp. 66-77, 2017.

[26] R. Pallabazzer, "Evaluation of wind-generator potentiality," *Solar energy*, vol. 55, no. 1, pp. 49-59, 1995.

[27] A. R. Jordehi, "Allocation of distributed generation units in electric power systems: A review," *Renewable and Sustainable Energy Reviews*, vol. 56, pp. 893-905, 2016.

[28] U. Agarwal and N. Jain, "Distributed energy resources and supportive methodologies for their optimal planning under modern distribution network: a review," *Technology and Economics of Smart Grids and Sustainable Energy*, vol. 4, pp. 1-21, 2019.

[29] S. S. Kola, "A review on optimal allocation and sizing techniques for DG in distribution systems," *International Journal of Renewable Energy Research (IJRER)*, vol. 8, no. 3, pp. 1236-1256, 2018.

[30] A. R. Gupta and A. Kumar, "Optimal placement of D-STATCOM using sensitivity approaches in mesh distribution system with time variant load models under load growth," *Ain Shams Engineering Journal*, vol. 9, no. 4, pp. 783-799, 2018.

[31] M. P. HA, P. D. Huy, and V. K. Ramachandaramurthy, "A review of the optimal allocation of distributed generation: Objectives, constraints, methods, and algorithms," *Renewable and Sustainable Energy Reviews*, vol. 75, pp. 293-312, 2017.

[32] F. S. Abu-Mouti and M. El-Hawary, "Optimal distributed generation allocation and sizing in distribution systems via artificial bee colony algorithm," *IEEE transactions on power delivery*, vol. 26, no. 4, pp. 2090-2101, 2011.

[33] T. P. Nguyen, T. T. Tran, and D. N. Vo, "Improved stochastic fractal search algorithm with chaos for optimal determination of location, size, and quantity of distributed generators in distribution systems," *Neural Computing and Applications*, vol. 31, pp. 7707-7732, 2019.

[34] C. Ma, J. Dasenbrock, J.-C. Töbermann, and M. Braun, "A novel indicator for evaluation of the impact of distributed generations on the energy losses of low voltage distribution grids," *Applied Energy*, vol. 242, pp. 674-683, 2019.

[35] D. Q. Hung, N. Mithulananthan, and K. Y. Lee, "Optimal placement of dispatchable and nondispatchable renewable DG units in distribution networks for minimizing energy loss," *International Journal of Electrical Power & Energy Systems*, vol. 55, pp. 179-186, 2014.

[36] S. Sultana and P. K. Roy, "Krill herd algorithm for optimal location of distributed generator in radial distribution system," *Applied Soft Computing*, vol. 40, pp. 391-404, 2016.

[37] B. Mohanty and S. Tripathy, "A teaching learning based optimization technique for optimal location and size of DG in distribution network," *journal of electrical systems and information technology*, vol. 3, no. 1, pp. 33-44, 2016.

[38] M. Natarajan, R. Balamurugan, and L. Lakshminarasimman, "Optimal placement and sizing of DGs in the distribution system for loss minimization and voltage stability improvement using CABC," *International Journal on Electrical Engineering and Informatics*, vol. 7, no. 4, p. 679, 2015.

[39] A. S. Hassan, Y. Sun, and Z. Wang, "Multi-objective for optimal placement and sizing DG units in reducing loss of power and enhancing voltage profile using BPSO-SLFA," *Energy Reports*, vol. 6, pp. 1581-1589, 2020.

[40] P. Prakash and D. K. Khatod, "Optimal sizing and siting techniques for distributed generation in distribution systems: A review," *Renewable and sustainable energy reviews,* vol. 57, pp. 111-130, 2016.

[41] Z. Abdmouleh, A. Gastli, L. Ben-Brahim, M. Haouari, and N. A. Al-Emadi, "Review of optimization techniques applied for the integration of distributed generation from renewable energy sources," *Renewable Energy,* vol. 113, pp. 266-280, 2017.

[42] A. M. Hemeida *et al.*, "Multi-objective multi-verse optimization of renewable energy sources-based micro-grid system: Real case," *Ain Shams Engineering Journal,* vol. 13, no. 1, p. 101543, 2022.

[43] M. M. Sayed, M. Y. Mahdy, S. H. Abdel Aleem, H. K. Youssef, and T. A. Boghdady, "Simultaneous Distribution Network Reconfiguration and Optimal Allocation of Renewable-Based Distributed Generators and Shunt Capacitors under Uncertain Conditions," *Energies,* vol. 15, no. 6, p. 2299, 2022.

[44] N. Rezaei, Y. Pezhmani, and A. Khazali, "Economic-environmental risk-averse optimal heat and power energy management of a grid-connected multi microgrid system considering demand response and bidding strategy," *Energy,* vol. 240, p. 122844, 2022.

[45] Q. Yan, M. Zhang, H. Lin, and W. Li, "Two-stage adjustable robust optimal dispatching model for multi-energy virtual power plant considering multiple uncertainties and carbon trading," *Journal of Cleaner Production,* vol. 336, p. 130400, 2022.

[46] Z. M. Ali, S. H. A. Aleem, A. I. Omar, and B. S. Mahmoud, "Economical-environmental-technical operation of power networks with high penetration of renewable energy systems using multi-objective coronavirus herd immunity algorithm," *Mathematics,* vol. 10, no. 7, p. 1201, 2022.

[47] M. S. Abid, H. J. Apon, K. A. Morshed, and A. Ahmed, "Optimal planning of multiple renewable energy-integrated distribution system with uncertainties using artificial hummingbird algorithm," *IEEE Access,* vol. 10, pp. 40716-40730, 2022.

[48] E. S. Bakhtiar, A. Naeimi, A. Behbahaninia, and G. Pignatta, "Size Optimization of a Grid-Connected Solar–Wind Hybrid System in Net Zero Energy Buildings: A Case Study," *Environmental Sciences Proceedings,* vol. 12, no. 1, p. 12, 2022.

[49] C. Venkatesan, R. Kannadasan, M. H. Alsharif, M.-K. Kim, and J. Nebhen, "A novel multiobjective hybrid technique for siting and sizing of distributed generation and capacitor banks in radial distribution systems," *Sustainability,* vol. 13, no. 6, p. 3308, 2021.

[50] N. Mansouri, A. Lashab, J. M. Guerrero, and A. Cherif, "Photovoltaic power plants in electrical distribution networks: A review on their impact and solutions," *IET Renewable Power Generation,* vol. 14, no. 12, pp. 2114-2125, 2020.

[51] J. Martins, S. Spataru, D. Sera, D.-I. Stroe, and A. Lashab, "Comparative study of ramp-rate control algorithms for PV with energy storage systems," *Energies,* vol. 12, no. 7, p. 1342, 2019.

[52] N. Mansouri, A. Lashab, D. Sera, J. M. Guerrero, and A. Cherif, "Large photovoltaic power plants integration: A review of challenges and solutions," *Energies,* vol. 12, no. 19, p. 3798, 2019.

[53] S. K. SUDABATTULA and K. MUNISWAMY, "Optimal Allocation of Different Types of Distributed Generators in Distribution System," *Gazi University Journal of Science,* vol. 32, no. 1, pp. 186-203, 2019.

[54] S. R. Biswal and G. Shankar, "Simultaneous optimal allocation and sizing of DGs and capacitors in radial distribution systems using SPEA2 considering load uncertainty," *IET Generation, Transmission & Distribution,* vol. 14, no. 3, pp. 494-505, 2020.

[55] P. P. Biswas, P. N. Suganthan, R. Mallipeddi, and G. A. Amaratunga, "Optimal reactive power dispatch with uncertainties in load demand and renewable energy sources adopting scenario-based approach," *Applied Soft Computing,* vol. 75, pp. 616-632, 2019.

[56] A. K. Pandey and S. Kirmani, "Multi-objective optimal location and sizing of hybrid photovoltaic system in distribution systems using crow search algorithm," *International Journal of Renewable Energy Research,* vol. 9, no. 4, pp. 1681-1693, 2019.

[57] M. Saric, J. Hivziefendic, and M. Tesanovic, "Optimal DG allocation for power loss reduction considering load and generation uncertainties," in *2019 11th International Symposium on Advanced Topics in Electrical Engineering (ATEE)*, 2019: IEEE, pp. 1-6.

[58] S. Abdel-Fatah, M. Ebeed, and S. Kamel, "Optimal reactive power dispatch using modified sine cosine algorithm," in *2019 International Conference on Innovative Trends in Computer Engineering (ITCE)*, 2019: IEEE, pp. 510-514.

[59] M. J. Hadidian-Moghaddam, S. Arabi-Nowdeh, M. Bigdeli, and D. Azizian, "A multi-objective optimal sizing and siting of distributed generation using ant lion optimization technique," *Ain shams engineering journal,* vol. 9, no. 4, pp. 2101-2109, 2018.

[60] S. K. Sudabattula, M. Kowsalya, S. Velamuri, and R. K. Melimi, "Optimal allocation of renewable distributed generators and capacitors in distribution system using dragonfly algorithm," in *2018 International Conference on Intelligent Circuits and Systems (ICICS)*, 2018: IEEE, pp. 393-396.

[61] M. Saric, J. Hivziefendic, T. Konjic, and A. Ktena, "Distributed generation allocation considering uncertainties," *International Transactions on Electrical Energy Systems,* vol. 28, no. 9, p. e2585, 2018.

[62] W. S. Sakr, R. A. El-Sehiemy, and A. M. Azmy, "Adaptive differential evolution algorithm for efficient reactive power management," *Applied Soft Computing,* vol. 53, pp. 336-351, 2017.

[63] Y. Gao, J. Liu, J. Yang, H. Liang, and J. Zhang, "Multi-objective planning of multi-type distributed generation considering timing characteristics and environmental benefits," *Energies,* vol. 7, no. 10, pp. 6242-6257, 2014.

[64] M. F. Shaaban and E. El-Saadany, "Accommodating high penetrations of PEVs and renewable DG considering uncertainties in distribution systems," *IEEE transactions on power systems,* vol. 29, no. 1, pp. 259-270, 2013.

[65] B. Kroposki, P. K. Sen, and K. Malmedal, "Optimum sizing and placement of distributed and renewable energy sources in electric power distribution systems," *IEEE Transactions on Industry Applications,* vol. 49, no. 6, pp. 2741-2752, 2013.

[66] Z. Liu, F. Wen, and G. Ledwich, "Optimal siting and sizing of distributed generators in distribution systems considering uncertainties," *IEEE Transactions on power delivery,* vol. 26, no. 4, pp. 2541-2551, 2011.

[67] N. Belbachir, M. Zellagui, A. Lasmari, C. Z. El-Bayeh, and B. Bekkouche, "Optimal integration of photovoltaic distributed generation in electrical distribution network using hybrid modified PSO algorithms," *Indonesian Journal of Electrical Engineering and Computer Science,* vol. 24, no. 1, pp. 50-60, 2021.

[68] D. R. Prabha and T. Jayabarathi, "Optimal placement and sizing of multiple distributed generating units in distribution networks by invasive weed optimization algorithm," *Ain Shams Engineering Journal,* vol. 7, no. 2, pp. 683-694, 2016.

[69] M. Suresh and E. J. Belwin, "Optimal DG placement for benefit maximization in distribution networks by using Dragonfly algorithm," *Renewables: Wind, Water, and Solar,* vol. 5, no. 1, pp. 1-8, 2018.

[70] B. N. Rao, A. Abhyankar, and N. Senroy, "Optimal placement of distributed generator using monte carlo simulation," in *2014 Eighteenth National Power Systems Conference (NPSC)*, 2014: IEEE, pp. 1-6.

[71] M. Esmaeili, M. Sedighizadeh, and M. Esmaili, "Multi-objective optimal reconfiguration and DG (Distributed Generation) power allocation in distribution networks using Big Bang-Big Crunch algorithm considering load uncertainty," *Energy,* vol. 103, pp. 86-99, 2016.

[72] S. F. Santos *et al.*, "Novel multi-stage stochastic DG investment planning with recourse," *IEEE Transactions on Sustainable Energy,* vol. 8, no. 1, pp. 164-178, 2016.

[73] H. Baghaee, M. Mirsalim, G. Gharehpetian, and H. Talebi, "Reliability/cost-based multi-objective Pareto optimal design of stand-alone wind/PV/FC generation microgrid system," *Energy,* vol. 115, pp. 1022-1041, 2016.

[74] S. R. Gampa and D. Das, "Optimum placement and sizing of DGs considering average hourly variations of load," *International Journal of Electrical Power & Energy Systems,* vol. 66, pp. 25-40, 2015.

[75] X. Peng, L. Lin, W. Zheng, and Y. Liu, "Crisscross optimization algorithm and Monte Carlo simulation for solving optimal distributed generation allocation problem," *Energies,* vol. 8, no. 12, pp. 13641-13659, 2015.

[76] K. Gnanambal and S. Suriya, "Optimal Sizing Of Distributed Generation For Voltage Profile Improvement Considering Maximum Loadability Limit," *International Journal of Innovative Research in Science, Engineering and Technology,* vol. 3, no. 3, pp. 304-309, 2014.

[77] B. Zeng, J. Zhang, Y. Zhang, X. Yang, J. Dong, and W. Liu, "Active distribution system planning for low-carbon objective using cuckoo search algorithm," *Journal of Electrical Engineering and Technology,* vol. 9, no. 2, pp. 433-440, 2014.

[78] S. Ganguly and D. Samajpati, "Distributed generation allocation with on-load tap changer on radial distribution networks using adaptive genetic algorithm," *Applied Soft Computing,* vol. 59, pp. 45-67, 2017.

[79] T. P. Nguyen and D. N. Vo, "Optimal number, location, and size of distributed generators in distribution systems by symbiotic organism search based method," *Advances in Electrical and Electronic Engineering,* vol. 15, no. 5, pp. 724-735, 2018.

[80] S. K. Sudabattula and M. Kowsalya, "Optimal allocation of solar based distributed generators in distribution system using Bat algorithm," *Perspectives in Science,* vol. 8, pp. 270-272, 2016.

[81] O. A. Saleh, M. Elshahed, and M. Elsayed, "Enhancement of radial distribution network with distributed generation and system reconfiguration," *Journal of Electrical Systems,* vol. 14, no. 3, pp. 36-50, 2018.

[82] V. Y. de Oliveira, R. M. de Oliveira, and C. M. Affonso, "Cuckoo Search approach enhanced with genetic replacement of abandoned nests applied to optimal allocation of distributed generation units," *IET Generation, Transmission & Distribution,* vol. 12, no. 13, pp. 3353-3362, 2018.

[83] L. F. Grisales-Noreña, D. Gonzalez Montoya, and C. A. Ramos-Paja, "Optimal sizing and location of distributed generators based on PBIL and PSO techniques," *Energies,* vol. 11, no. 4, p. 1018, 2018.

[84] V. R. VC, "Ant Lion optimization algorithm for optimal sizing of renewable energy resources for loss reduction in distribution systems," *Journal of Electrical Systems and Information Technology,* vol. 5, no. 3, pp. 663-680, 2018.

[85] K. S. Sambaiah and T. Jayabarathi, "Optimal allocation of renewable distributed generation and capacitor banks in distribution systems using salp swarm algorithm," *Int. J. Renew. Energy Res,* vol. 9, no. 1, pp. 96-107, 2019.

[86] G. Deb, K. Chakraborty, and S. Deb, "Spider monkey optimization technique–based allocation of distributed generation for demand side management," *International Transactions on Electrical Energy Systems,* vol. 29, no. 5, p. e12009, 2019.

[87] Z. A. Kamaruzzaman, A. Mohamed, and R. Mohamed, "Optimal placement of grid-connected photovoltaic generators in a power system for voltage stability enhancement," *Indones. J. Electr. Eng. Comput. Sci*, vol. 13, p. 339, 2019.

[88] M. Abdelbadea, T. A. Boghdady, and D. K. Ibrahim, "Enhancing active radial distribution networks by optimal sizing and placement of DGs using modified crow search algorithm," *Indonesian Journal of Electrical Engineering and Computer Science (IJEECS)*, vol. 16, no. 13, pp. 1179-1188, 2019.

[89] S. Settoul, R. Chenni, H. A. Hasan, M. Zellagui, and M. N. Kraimia, "MFO algorithm for optimal location and sizing of multiple photovoltaic distributed generations units for loss reduction in distribution systems," in *2019 7th International renewable and sustainable energy conference (IRSEC)*, 2019: IEEE, pp. 1-6.

[90] M. H. Moradi and M. Abedini, "A combination of genetic algorithm and particle swarm optimization for optimal DG location and sizing in distribution systems," *International Journal of Electrical Power & Energy Systems*, vol. 34, no. 1, pp. 66-74, 2012.

[91] H. Manafi, N. Ghadimi, M. Ojaroudi, and P. Farhadi, "Optimal placement of distributed generations in radial distribution systems using various PSO and DE algorithms," *Elektronika ir Elektrotechnika*, vol. 19, no. 10, pp. 53-57, 2013.

[92] E. Mohamed, A.-A. A. Mohamed, and Y. Mitani, "Genetic-moth swarm algorithm for optimal placement and capacity of renewable DG sources in distribution systems," 2019.

[93] A. Uniyal and S. Sarangi, "Optimal network reconfiguration and DG allocation using adaptive modified whale optimization algorithm considering probabilistic load flow," *Electric Power Systems Research*, vol. 192, p. 106909, 2021.

[94] C. H. Prasad, K. Subbaramaiah, and P. Sujatha, "Cost–benefit analysis for optimal DG placement in distribution systems by using elephant herding optimization algorithm," *Renewables: Wind, Water, and Solar*, vol. 6, no. 1, pp. 1-12, 2019.

[95] E. Karunarathne, J. Pasupuleti, J. Ekanayake, and D. Almeida, "Network loss reduction and voltage improvement by optimal placement and sizing of distributed generators with active and reactive power injection using fine-tuned PSO," *Indones. J. Electr. Eng. Comput. Sci*, vol. 21, pp. 647-656, 2021.

[96] T. D. Pham, T. T. Nguyen, and B. H. Dinh, "Find optimal capacity and location of distributed generation units in radial distribution networks by using enhanced coyote optimization algorithm," *Neural Computing and Applications*, vol. 33, pp. 4343-4371, 2021.

[97] G. Manikanta, A. Mani, H. P. Singh, and D. K. Chaturvedi, "Effect of voltage dependent load model on placement and sizing of distributed generator in large scale distribution system," *Majlesi Journal of Electrical Engineering*, vol. 14, no. 4, pp. 97-121, 2020.

[98] U. Raut and S. Mishra, "A new Pareto multi-objective sine cosine algorithm for performance enhancement of radial distribution network by optimal allocation of distributed generators," *Evolutionary Intelligence*, vol. 14, no. 4, pp. 1635-1656, 2021.

[99] W. F. Tinney and C. E. Hart, "Power flow solution by Newton's method," *IEEE Transactions on Power Apparatus and systems*, no. 11, pp. 1449-1460, 1967.

[100] H.-D. Chiang, "A decoupled load flow method for distribution power networks: algorithms, analysis and convergence study," *International Journal of Electrical Power & Energy Systems*, vol. 13, no. 3, pp. 130-138, 1991.

[101] B. Stott and O. Alsac, "Fast decoupled load flow," *IEEE transactions on power apparatus and systems*, no. 3, pp. 859-869, 1974.

[102] A. Semlyen and F. De León, "Quasi-Newton power flow using partial Jacobian updates," *IEEE Transactions on Power Systems*, vol. 16, no. 3, pp. 332-339, 2001.

[103] K. V. Kumar and M. Selvan, "A simplified approach for load flow analysis of radial distribution network," *International Journal of Computer, Information, and Systems Science, and Engineering*, vol. 2, p. 4, 2008.

[104] S. Singh and T. Ghose, "Improved radial load flow method," *International Journal of Electrical Power & Energy Systems*, vol. 44, no. 1, pp. 721-727, 2013.

[105] A. R. Abul'Wafa, "A network-topology-based load flow for radial distribution networks with composite and exponential load," *Electric Power Systems Research*, vol. 91, pp. 37-43, 2012.

[106] J.-P. Chiou, C.-F. Chang, and C.-T. Su, "Ant direction hybrid differential evolution for solving large capacitor placement problems," *IEEE Transactions on power systems*, vol. 19, no. 4, pp. 1794-1800, 2004.

[107] V. Reddy and M. Sydulu, "2Index and GA based optimal location and sizing of distribution system capacitors," in *2007 IEEE Power Engineering Society General Meeting*, 2007: IEEE, pp. 1-4.

[108] G. J. Duncan, M. S. Sarma, and T. J. Overbye, *Power system analysis and design*. Cengage Learning, 2012.

[109] D. Singh, D. Singh, and K. Verma, "Multiobjective optimization for DG planning with load models," *IEEE transactions on power systems*, vol. 24, no. 1, pp. 427-436, 2009.

[110] K. D. Singh and S. Ghosh, "A new efficient method for load-flow solution for radial distribution networks," *Electrical Review, pe. org. pl/articles/2011/12a*, pp. 66-73, 2011.

[111] M. Srinivas, "Distribution load flows: a brief review," in *2000 IEEE Power Engineering Society Winter Meeting. Conference Proceedings (Cat. No. 00CH37077)*, 2000, vol. 2: IEEE, pp. 942-945.

[112] U. Eminoglu and M. H. Hocaoglu, "Distribution systems forward/backward sweep-based power flow algorithms: a review and comparison study," *Electric Power Components and Systems*, vol. 37, no. 1, pp. 91-110, 2008.

[113] A. G. Expósito and E. R. Ramos, "Reliable load flow technique for radial distribution networks," *IEEE Transactions on Power Systems*, vol. 14, no. 3, pp. 1063-1069, 1999.

[114] U. Eminoglu and M. H. Hocaoglu, "A new power flow method for radial distribution systems including voltage dependent load models," *Electric power systems research*, vol. 76, no. 1-3, pp. 106-114, 2005.

[115] G. Chang, S. Chu, and H. Wang, "An improved backward/forward sweep load flow algorithm for radial distribution systems," *IEEE Transactions on power systems*, vol. 22, no. 2, pp. 882-884, 2007.

[116] J. Liu, M. Salama, and R. Mansour, "An efficient power flow algorithm for distribution systems with polynomial load," *International Journal of Electrical Engineering Education*, vol. 39, no. 4, pp. 371-386, 2002.

[117] A. Alsaadi and B. Gholami, "An effective approach for distribution system power flow solution," *International Journal of Electrical and Computer Engineering*, vol. 3, no. 1, pp. 1-5, 2009.

[118] P. M. De Oliveira-De Jesus, "The Standard Backward/Forward Sweep Power Flow."

[119] S. M. Ismael, S. H. A. Aleem, A. Y. Abdelaziz, and A. F. Zobaa, "State-of-the-art of hosting capacity in modern power systems with distributed generation," *Renewable energy*, vol. 130, pp. 1002-1020, 2019.

[120] A. F. Zobaa, S. A. Aleem, and A. Y. Abdelaziz, *Classical and recent aspects of power system optimization*. Academic Press, 2018.

[121] M. Ebeed and S. H. A. Aleem, "Overview of uncertainties in modern power systems: Uncertainty models and methods," in *Uncertainties in Modern Power Systems*: Elsevier, 2021, pp. 1-34.

[122] M. Aien, A. Hajebrahimi, and M. Fotuhi-Firuzabad, "A comprehensive review on uncertainty modeling techniques in power system studies," *Renewable and Sustainable Energy Reviews*, vol. 57, pp. 1077-1089, 2016.

[123] V. Singh, T. Moger, and D. Jena, "Uncertainty handling techniques in power systems: A critical review," *Electric Power Systems Research*, vol. 203, p. 107633, 2022.

[124] M. Aien, M. Rashidinejad, and M. Fotuhi-Firuzabad, "On possibilistic and probabilistic uncertainty assessment of power flow problem: A review and a new approach," *Renewable and Sustainable energy reviews*, vol. 37, pp. 883-895, 2014.

[125] Q. Dong, Q. Sun, Y. Huang, Z. Li, and C. Cheng, "Hybrid possibilistic-probabilistic energy flow assessment for multi-energy carrier systems," *IEEE access,* vol. 7, pp. 176115-176126, 2019.

[126] Y. Ben-Haim, *Info-gap decision theory: decisions under severe uncertainty*. Elsevier, 2006.

[127] A. E. Lim, J. G. Shanthikumar, and Z. M. Shen, "Model uncertainty, robust optimization, and learning," in *Models, Methods, and Applications for Innovative Decision Making*: INFORMS, 2006, pp. 66-94.

[128] W. Gao, C. Song, and F. Tin-Loi, "Probabilistic interval analysis for structures with uncertainty," *Structural Safety,* vol. 32, no. 3, pp. 191-199, 2010.

[129] W. J. Brattin, T. M. Barry, and N. Chiu, "Monte Carlo modeling with uncertain probability density functions," *Human and Ecological Risk Assessment: An International Journal,* vol. 2, no. 4, pp. 820-840, 1996.

[130] A. Soroudi, M. Aien, and M. Ehsan, "A probabilistic modeling of photo voltaic modules and wind power generation impact on distribution networks," *IEEE Systems Journal*, vol. 6, no. 2, pp. 254-259, 2011.

[131] Y. Atwa, E. El-Saadany, M. Salama, and R. Seethapathy, "Optimal renewable resources mix for distribution system energy loss minimization," *IEEE transactions on power systems,* vol. 25, no. 1, pp. 360-370, 2009.

[132] S. Karaki, R. Chedid, and R. Ramadan, "Probabilistic performance assessment of autonomous solar-wind energy conversion systems," *IEEE Transactions on energy conversion,* vol. 14, no. 3, pp. 766-772, 1999.

[133] A. Rabiee, A. Soroudi, B. Mohammadi-Ivatloo, and M. Parniani, "Corrective voltage control scheme considering demand response and stochastic wind power," *IEEE Transactions on Power Systems,* vol. 29, no. 6, pp. 2965-2973, 2014.

[134] A. Zangeneh, S. Jadid, and A. Rahimi-Kian, "Uncertainty based distributed generation expansion planning in electricity markets," *Electrical Engineering,* vol. 91, pp. 369-382, 2010.

[135] S. Shojaabadi, S. Abapour, M. Abapour, and A. Nahavandi, "Simultaneous planning of plug-in hybrid electric vehicle charging stations and wind power generation in distribution networks considering uncertainties," *Renewable energy,* vol. 99, pp. 237-252, 2016.

[136] A. T. Hachemi, F. Sadaoui, A. Saim, M. Ebeed, H. E. Abbou, and S. Arif, "Optimal Operation of Distribution Networks Considering Renewable Energy Sources Integration and Demand Side Response," *Sustainability,* vol. 15, no. 24, p. 16707, 2023.

[137] A. T. Hachemi *et al.*, "Modified reptile search algorithm for optimal integration of renewable energy sources in distribution networks," *Energy Science & Engineering,* vol. 11, no. 12, pp. 4635-4665, 2023.

[138] M. Basil and A. Jamieson, "Uncertainty of complex systems by Monte Carlo simulation," *measurement and control*, vol. 32, no. 1, pp. 16-20, 1999.

[139] D.-G. Chen and J. D. Chen, *Monte-Carlo simulation-based statistical modeling*. Springer, 2017.

[140] J. Smid, D. Verloo, G. Barker, and A. Havelaar, "Strengths and weaknesses of Monte Carlo simulation models and Bayesian belief networks in microbial risk assessment," *International Journal of Food Microbiology*, vol. 139, pp. S57-S63, 2010.

[141] A. J. Conejo, M. Carrión, and J. M. Morales, *Decision making under uncertainty in electricity markets*. Springer, 2010.

[142] M. Ebeed *et al.*, "Optimal integrating inverter-based PVs with inherent DSTATCOM functionality for reliability and security improvement at seasonal uncertainty," *Solar Energy*, vol. 267, p. 112200, 2024.

[143] A. Ramadan, M. Ebeed, S. Kamel, A. M. Agwa, and M. Tostado-Véliz, "The probabilistic optimal integration of renewable distributed generators considering the time-varying load based on an artificial gorilla troops optimizer," *Energies*, vol. 15, no. 4, p. 1302, 2022.

[144] K. P. Bennett and E. Parrado-Hernández, "The interplay of optimization and machine learning research," *The Journal of Machine Learning Research*, vol. 7, pp. 1265-1281, 2006.

[145] S. Balan, "Metaheuristics in optimization: Algorithmic perspective," *OR-MS-Tomorrow (2020)*, 2021.

[146] F. Héliodore, A. Nakib, B. Ismail, S. Ouchraa, and L. Schmitt, *Metaheuristics for intelligent electrical networks*. John Wiley & Sons, 2017.

[147] O. HaJJI, "Contribution au développement de méthodes d'optimisation stochastiques. Application à la conception des dispositifs électrotechniques," *Mémoire de thèse de Doctorat, Université des sciences et technologies de Lille*, 2003.

[148] F. S. Gharehchopogh and H. Gholizadeh, "A comprehensive survey: Whale Optimization Algorithm and its applications," *Swarm and Evolutionary Computation*, vol. 48, pp. 1-24, 2019.

[149] M. N. Ab Wahab, S. Nefti-Meziani, and A. Atyabi, "A comprehensive review of swarm optimization algorithms," *PloS one*, vol. 10, no. 5, p. e0122827, 2015.

[150] P. Sheth and A. Umbarkar, "Constrained optimization problems solving using evolutionary algorithms: A review," in *2015 International Conference on Computational Intelligence and Communication Networks (CICN)*, 2015: IEEE, pp. 1251-1257.

[151] A. Bourzami, "Contribution à l'étude de la stabilité des grands réseaux électriques dans un marché de l'électricité dérégulé en présence des sources d'énergie renouvelable par la logique floue," 2019.

[152] L. Slimani, "Contribution à l'application de l'optimisation par des méthodes métaheuristiques à l'écoulement de puissance optimal dans un environnement de l'électricité dérégulé," Université de Batna 2, 2009.

[153] S. Kiranyaz, T. Ince, M. Gabbouj, S. Kiranyaz, T. Ince, and M. Gabbouj, "Optimization techniques: an overview," *Multidimensional particle swarm optimization for machine learning and pattern recognition*, pp. 13-44, 2014.

[154] R. H. Zubo, G. Mokryani, H.-S. Rajamani, J. Aghaei, T. Niknam, and P. Pillai, "Operation and planning of distribution networks with integration of renewable distributed generators considering uncertainties: A review," *Renewable and Sustainable Energy Reviews*, vol. 72, pp. 1177-1198, 2017.

[155] K. Sorensen, M. Sevaux, and F. Glover, "A history of metaheuristics," *arXiv preprint arXiv:1704.00853*, 2017.

[156] M. R. Djamel, "Visualisation de l'Information par le Développement d'Interfaces Graphiques pour la Conduite des Réseaux Electriques," PhD Thesis.Université Amar Telidji de Laghouat, Département Electrotec, 2016.

[157] P. Trojovský and M. Dehghani, "A new bio-inspired metaheuristic algorithm for solving optimization problems based on walruses behavior," *Scientific Reports*, vol. 13, no. 1, p. 8775, 2023.

[158] A. F. Kamaruzaman, A. M. Zain, S. M. Yusuf, and A. Udin, "Levy flight algorithm for optimization problems-a literature review," *Applied mechanics and materials*, vol. 421, pp. 496-501, 2013.

[159] M. Chawla and M. Duhan, "Levy flights in metaheuristics optimization algorithms–a review," *Applied Artificial Intelligence*, vol. 32, no. 9-10, pp. 802-821, 2018.

[160] S. Roy and S. S. Chaudhuri, "Cuckoo search algorithm using Lévy flight: a review," *international journal of Modern Education and Computer Science*, vol. 5, no. 12, p. 10, 2013.

[161] A. Seyyedabbasi and F. Kiani, "Sand Cat swarm optimization: A nature-inspired algorithm to solve global optimization problems," *Engineering with Computers*, pp. 1-25, 2022.

[162] W. Zhao, L. Wang, and S. Mirjalili, "Artificial hummingbird algorithm: A new bio-inspired optimizer with its engineering applications," *Computer Methods in Applied Mechanics and Engineering*, vol. 388, p. 114194, 2022.

[163] A. Faramarzi, M. Heidarinejad, B. Stephens, and S. Mirjalili, "Equilibrium optimizer: A novel optimization algorithm," *Knowledge-based systems*, vol. 191, p. 105190, 2020.

[164] Z. W. Geem, J. H. Kim, and G. V. Loganathan, "A new heuristic optimization algorithm: harmony search," *simulation*, vol. 76, no. 2, pp. 60-68, 2001.

[165] H. A. Shehadeh, "Chernobyl disaster optimizer (CDO): a novel meta-heuristic method for global optimization," *Neural Computing and Applications*, vol. 35, no. 15, pp. 10733-10749, 2023.

[166] L. Wang, Q. Cao, Z. Zhang, S. Mirjalili, and W. Zhao, "Artificial rabbits optimization: A new bio-inspired meta-heuristic algorithm for solving engineering optimization problems," *Engineering Applications of Artificial Intelligence*, vol. 114, p. 105082, 2022.

[167] S. Zhao, T. Zhang, S. Ma, and M. Chen, "Dandelion Optimizer: A nature-inspired metaheuristic algorithm for engineering applications," *Engineering Applications of Artificial Intelligence,* vol. 114, p. 105075, 2022.

[168] M. Jamil and X.-S. Yang, "A literature survey of benchmark functions for global optimisation problems," *International Journal of Mathematical Modelling and Numerical Optimisation,* vol. 4, no. 2, pp. 150-194, 2013.

[169] M. Molga and C. Smutnicki, "Test functions for optimization needs," *Test functions for optimization needs,* vol. 101, p. 48, 2005.

[170] S. Mohapatra and P. Mohapatra, "American zebra optimization algorithm for global optimization problems," *Scientific Reports,* vol. 13, no. 1, p. 5211, 2023.

[171] C. K. Goh, K. C. Tan, D. Liu, and S. C. Chiam, "A competitive and cooperative co-evolutionary approach to multi-objective particle swarm optimization algorithm design," *European Journal of Operational Research,* vol. 202, no. 1, pp. 42-54, 2010.

[172] M. H. Ali, S. Kamel, M. H. Hassan, M. Tostado-Véliz, and H. M. J. E. R. Zawbaa, "An improved wild horse optimization algorithm for reliability based optimal DG planning of radial distribution networks," vol. 8, pp. 582-604, 2022.

[173] N. Augustine, S. Suresh, P. Moghe, and K. Sheikh, "Economic dispatch for a microgrid considering renewable energy cost functions," in *2012 IEEE PES Innovative Smart Grid Technologies (ISGT)*, 2012: IEEE, pp. 1-7.

[174] S. Sultana and P. K. Roy, "Optimal capacitor placement in radial distribution systems using teaching learning based optimization," *International Journal of Electrical Power & Energy Systems,* vol. 54, pp. 387-398, 2014.

[175] A. El-Fergany, "Optimal allocation of multi-type distributed generators using backtracking search optimization algorithm," *International Journal of Electrical Power & Energy Systems,* vol. 64, pp. 1197-1205, 2015.

Appendixes

For 33-bus EDN, the active and reactive load demands are given in Table A.1 and the line data of the system is given in Table A.2.

Appendix A

Table A.1: Bus data for 33-bus test system.

Bus No.	P_L **(MW)**	Q_L **(MVar)**	P_g **(MW)**	Q_g **(MVar)**
1	0	0	0	0
2	100	60	0	0
3	90	40	0	0
4	120	80	0	0
5	60	30	0	0
6	60	20	0	0
7	200	100	0	0
8	200	100	0	0
9	60	20	0	0
10	60	20	0	0
11	45	30	0	0
12	60	35	0	0
13	60	35	0	0
14	120	80	0	0
15	60	10	0	0
16	60	20	0	0
17	60	20	0	0
18	90	40	0	0
19	90	40	0	0
20	90	40	0	0
21	90	40	0	0
22	90	40	0	0
23	90	50	0	0
24	420	200	0	0
25	420	200	0	0
26	60	25	0	0
27	60	25	0	0
28	60	20	0	0
29	120	70	0	0
30	200	600	0	0
31	150	70	0	0
32	210	100	0	0
33	60	40	0	0

Table A.2: Transmission line data for 33-bus test system.

Line Number	From bus	To bus	Impedance	
			R (ohm)	X (ohm)
1	1	2	0.0922	0.0470
2	2	3	0.4930	0.2511
3	3	4	0.3660	0.1864
4	4	5	0.3811	0.1941
5	5	6	0.8190	0.7070
6	6	7	0.1872	0.6188
7	7	8	1.7114	1.2351
8	8	9	1.0300	0.7400
9	9	10	1.0440	0.7400
10	10	11	0.1966	0.0650
11	11	12	0.3744	0.1238
12	12	13	1.4680	1.1550
13	13	14	0.5416	0.7129
14	14	15	0.5910	0.5260
15	15	16	0.7463	0.5450
16	16	17	1.2890	1.7210
17	17	18	0.7320	0.5740
18	2	19	0.1640	0.1565
19	19	20	1.5042	1.3554
20	20	21	0.4095	0.4784
21	21	22	0.7089	0.9373
22	3	23	0.4512	0.3083
23	23	24	0.8980	0.7091
24	24	25	0.8960	0.7011
25	6	26	0.2030	0.1034
26	26	27	0.2842	0.1447
27	27	28	1.0590	0.9337
28	28	29	0.8042	0.7006
29	29	30	0.5075	0.2585
30	30	31	0.9744	0.9630
31	31	32	0.3105	0.3619
32	32	33	0.3410	0.5302

Appendix B

For 69-bus EDN, the active and reactive load demands are given in Table B.1 and the line data of the system is given in Table B.2

Table B.1: Bus data for 69-bus test system.

Bus No.	P_L **(MW)**	Q_L **(MVar)**	P_g **(MW)**	Q_g **(MVar)**
1	0	0	0	0
2	0	0	0	0
3	0	0	0	0
4	0	0	0	0
5	0	0	0	0
6	2.60	2.20	0	0
7	40.40	30	0	0
8	75	54	0	0
9	30	22	0	0
10	28	19	0	0
11	145	104	0	0
12	145	104	0	0
13	8	5.50	0	0
14	8	5.50	0	0
15	0	0	0	0
16	45.5	30	0	0
17	60	35	0	0
18	60	35	0	0
19	0	0	0	0
20	1	0.6	0	0
21	114	81	0	0
22	5.3	3.5	0	0
23	0	0	0	0
24	28	20	0	0
25	0	0	0	0
26	14	10	0	0
27	14	10	0	0
28	26	18.6	0	0
29	26	18.6	0	0
30	0	0	0	0
31	0	0	0	0
32	0	0	0	0
33	14	10	0	0
34	19.5	14	0	0
35	6	4	0	0
36	26	18.55	0	0
37	26	18.55	0	0
38	0	0	0	0

39	24	17	0	0
40	24	17	0	0
41	1.2	1	0	0
42	0	0	0	0
43	6	4.3	0	0
44	0	0	0	0
45	39.22	26.3	0	0
46	39.22	26.3	0	0
47	0	0	0	0
48	79	56.4	0	0
49	384.7	274.5	0	0
50	384.7	274.5	0	0
51	40.5	28.3	0	0
52	3.6	2.7	0	0
53	4.35	3.5	0	0
54	26.4	19	0	0
55	24	17.2	0	0
56	0	0	0	0
57	0	0	0	0
58	0	0	0	0
59	100	72	0	0
60	0	0	0	0
61	1244	888	0	0
62	32	23	0	0
63	0	0	0	0
64	227	162	0	0
65	59	42	0	0
66	18	13	0	0
67	18	13	0	0
68	28	20	0	0
69	28	20	0	0

Table B.2: Transmission line data for 69-bus test system

Line Number	**From bus**	**To bus**	**Impedance**	
			R (ohm)	**X (ohm)**
1	1	2	0.0005	0.0012
2	2	3	0.0005	0.0012
3	3	4	0.0015	0.0036
4	4	5	0.0251	0.0294
5	5	6	0.3660	0.1864
6	6	7	0.3811	0.1941
7	7	8	0.0922	0.0470
8	8	9	0.0493	0.0251
9	9	10	0.8190	0.2707
10	10	11	0.1872	0.0691
11	11	12	0.7114	0.2351
12	12	13	1.03	0.34
13	13	14	1.044	0.345

14	14	15	1.058	0.3496
15	15	16	0.1966	0.0650
16	16	17	0.3744	0.1238
17	17	18	0.0047	0.0016
18	18	19	0.3276	0.1083
19	19	20	0.2106	0.0690
20	20	21	0.3416	0.1129
21	21	22	0.0140	0.0046
22	22	23	0.1591	0.0526
23	23	24	0.3463	0.1145
24	24	25	0.7488	0.2745
25	25	26	0.3089	0.1021
26	26	27	0.1732	0.0572
27	3	28	0.0044	0.0108
28	28	29	0.0640	0.1565
29	29	30	0.3978	0.1315
30	30	31	0.0702	0.0232
31	31	32	0.3510	0.1160
32	32	33	0.8390	0.2816
33	33	34	1.7080	0.5646
34	34	35	1.4740	0.4673
35	3	36	0.0044	0.0108
36	36	37	0.0640	0.1565
37	37	38	0.1053	0.1230
38	38	39	0.0304	0.0355
39	39	40	0.0018	0.0021
40	40	41	0.7283	0.8509
41	41	42	0.31	0.3623
42	42	43	0.0410	0.0478
43	43	44	0.0092	0.0116
44	44	45	0.1089	0.1373
45	45	46	0.0009	0.0012
46	4	47	0.0034	0.0084
47	47	48	0.0851	0.2088
48	48	49	0.2898	0.7091
49	49	50	0.0822	0.2011
50	8	51	0.0928	0.0473
51	51	52	0.3319	0.1114
52	9	53	0.1740	0.0886
53	53	54	0.2030	0.1034
54	54	55	0.2842	0.1447
55	55	56	0.2813	0.1433
56	56	57	1.59	0.5337
57	57	58	0.7837	0.2630
58	58	59	0.3042	0.1006
59	59	60	0.3861	0.1172
60	60	61	0.5075	0.2585
61	61	62	0.0974	0.0496

62	62	63	0.1450	0.0738
63	63	64	0.7105	0.3619
64	64	65	1.0410	0.5302
65	11	66	0.2012	0.0611
66	66	67	0.0047	0.0014
67	12	68	0.7394	0.2444
68	68	69	0.0047	0.0016